NASA Technical Paper 3414

December 1994

In-Flight Lift-Drag Characteristics for a Forward-Swept Wing Aircraft (and Comparisions With Contemporary Aircraft)

Edwin J. Saltzman and
John W. Hicks

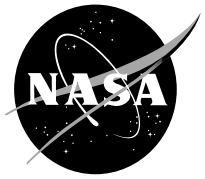

NASA
Technical
Paper
3414

1994

In-Flight Lift-Drag Characteristics for a Forward-Swept Wing Aircraft (and Comparisions With Contemporary Aircraft)

Edwin J. Saltzman
PRC Inc.
Edwards, California

John W. Hicks
Dryden Flight Research Center
Edwards, California

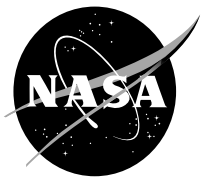

National Aeronautics and
Space Administration

Office of Management

Scientific and Technical
Information Program

ABSTRACT

Lift (L) and drag (D) characteristics have been obtained in flight for the X-29A airplane (a forward-swept-wing demonstrator) for Mach numbers (M) from 0.4 to 1.3. Most of the data were obtained near an altitude of 30,000 ft. A representative Reynolds number, for M = 0.9 and a pressure altitude of 30,000 ft, is 18.6×10^6 based on the mean aerodynamic chord. The X-29A data (forward-swept wing) are compared with three high-performance fighter aircraft—the F-15C, F-16C, and F/A-18. The lifting efficiency of the X-29A, as defined by the Oswald lifting efficiency factor, e, is about average for a cantilevered monoplane for M = 0.6 and angles of attack up to those required for maximum L/D. At M = 0.6 the level of L/D and e, as a function of load factor, for the X-29A was about the same as for the contemporary aircraft. The X-29A and its contemporaries have high transonic wave drag and equivalent parasite area compared with aircraft of the 1940s through 1960s.

NOMENCLATURE

Acronyms and Initialisms

ACC	(wing flaperon) automatic camber control
BIR	buffet intensity rise, as defined in reference 61
DARPA	Defense Advanced Research Projects Agency
LE	leading edge
MAC	mean aerodynamic chord
MCC	(wing flaperon) manual camber control
NACA	National Advisory Committee for Aeronautics
NASA	National Aeronautics and Space Administration
PLA	power lever angle
TED	trailing edge down
TEU	trailing edge up

Symbols

A	aspect ratio, $\frac{b^2}{S}$
A'	aspect ratio based on alternative reference area, $\frac{b^2}{S'}$
A_c	maximum cross-sectional area of complete configuration
A_w	wetted area
a_z	acceleration along aircraft z-axis, g
b	wing span
C_D	drag coefficient, $\frac{D}{\bar{q} \cdot S}$
C_{D_0}	drag coefficient at zero lift
$C_{D_{min}}$	minimum value of drag coefficient for a given polar, not necessarily C_{D_0}
$C_{D_{wave}}$	transonic wave drag coefficient, reference area = A_c (in fig. 14, reference area = S)
C_{F_e}	equivalent average skin-friction coefficient for turbulent flow
C_L	lift coefficient, $\frac{L}{\bar{q} \cdot S}$
C_{L_α}	lift-curve slope, $\frac{\Delta C_L}{\Delta \alpha}$, deg^{-1} or rad^{-1}
$C_{L_{min}}$	value of C_L at corresponding $C_{D_{min}}$ for given polar
c_l	section lift coefficient
D	drag force along flightpath
d	equivalent diameter

e	airplane lifting efficiency factor, $\frac{1}{\pi A} \Big/ \frac{\Delta C_D}{\Delta C_L^2}$, unless otherwise defined in text or figures
f	equivalent parasite area, $C_{D_0} \cdot S$
g	acceleration of gravity
h	pressure altitude
K	drag-due-to-lift factor, $\frac{\Delta C_D}{\Delta C_L^2}$
K'	ratio of lift angle (rad) to K, $\frac{\Delta \alpha}{\Delta C_L} \Big/ \frac{\Delta C_D}{\Delta C_L^2}$
L	lift force, normal to flightpath
l	length
M	Mach number
M_{DR}	drag-rise Mach number, where $\frac{\Delta C_D}{\Delta M} = 0.1$
P	ambient pressure
$\bar{q}$	dynamic pressure, $0.7M^2P$
S	wing reference area assigned by airframe builder
S'	alternative reference area
t	maximum wing thickness
t/c	wing thickness-to-chord ratio, maximum value averaged over the span
α	angle of attack, deg or rad
α_0	angle of attack at zero lift, deg
$\frac{\Delta \alpha}{\Delta C_L}$	lift angle, rad
δ	deflection angle, deg
δ_c	canard deflection angle, deg
δ_f	wing flap or wing flaperon deflection, deg
δ_s	strake flap deflection, deg
Λ	wing leading-edge sweep angle, deg
Λ /4	sweep angle of quarter chord, deg
θ_{twist}	wing twist angle with respect to fuselage reference line, deg
η	semispan fraction, in decimal form
η_a	aerodynamic efficiency at zero-lift, subsonic, based on reference C_{F_e} value of 0.003
$\eta_{\bar{a}}$	aerodynamic efficiency at zero-lift, subsonic, based on calculated C_{F_e} reference value for flat plate turbulent flow for applicable wetted area and Reynolds number
$\eta_{\hat{a}}$	aerodynamic efficiency at zero-lift, subsonic, based on calculated C_{F_e} reference value for applicable Reynolds number and wetted area, including form factor to account for three-dimensional effects

INTRODUCTION

In his National Advisory Committee for Aeronautics (NACA) Technical Note published in 1924, Max Munk said, “Sweep back was used in some of the early airplanes in order to obtain lateral stability” (ref. 1). Though most of the aircraft of the 1920s and 1930s did not use wing sweep, some early tailless gliders and airplanes employed sweep (refs. 2 and 3). Reference 2 refers to four experimenters who employed forward sweep over part or all of the span from 1911 to 1928.

Interest in forward-swept wings increased when some wind-tunnel tests in 1931 showed that 20° of forward sweep provided a greater useful angle-of-attack range than did a corresponding amount of aft sweep (ref. 4). Later, as airplane wings began to experience the effects of local shock waves, A. Busemann and R.T.

Jones independently recommended sweepback as a means of reducing transonic and supersonic drag (refs. 5–7).

It was only natural, then, to consider using forward sweep for high-performance aircraft, because forward sweep offered the dual benefits of reducing compressibility effects at transonic speeds and providing high-lift advantages at lower speeds as indicated by reference 4. This may have been a consideration in the design of the Junkers prototype bomber, the Ju-287, which flew briefly in early 1945 (refs. 8–10). The German-built Ju-287 had about 15° of forward, leading-edge sweep.

Subsequently, interest in forward-swept wings increased in the United States during the years following World War II. References 11 through 27 are a representative, but incomplete, listing of tests of forward sweep before 1960. It may be of interest, especially to persons aware of the earliest flights to supersonic speeds, that the fuselage and empennage of the quarter scale X-1 model were tested with both swept-back and swept-forward wings (ref. 17). Later, during the 1960s, moderate amounts of forward sweep were used in two subsonic airplane designs in Germany, apparently for advantageous positioning of the main spar (ref. 28).

Because of a warning from reference 16, published in 1948, concerning aeroelastic structural divergence for forward-swept wings, designers of high-speed aircraft were reluctant to employ forward sweep for more than two decades. To avoid this problem, that is, to achieve sufficient structural stiffness, conventional metal wing construction would have resulted in substantial weight penalties. Through the development of advanced composite materials and using specially oriented laminates, the aeroelastic divergence problem was alleviated (ref. 29). Now the forward-sweep concept could be applied to high-performance airplanes; consequently several feasibility studies were initiated (refs. 30–33). These and other studies were either sponsored or encouraged by the Defense Advanced Research Projects Agency (DARPA) and supported by the United States Air Force and the National Aeronautics and Space Administration (NASA). DARPA then contracted with three airframe companies to conduct analytical studies for comparing forward- and aft-sweep designs for transonic military applications (ref. 34).

The results of those studies revealed the potential for higher lift-to-drag ratios in maneuvering flight, lower trim drag, and improved low-speed handling qualities. These findings provided justification for building a flight demonstrator vehicle, and it was decided that it should be manned rather than a remotely piloted vehicle (ref. 35). Further analytical and wind-tunnel studies verified the earlier indications of lower drag and in addition found that lift-related drag and wave drag may also be reduced with forward sweep (refs. 36 and 37).

As a result of these studies, DARPA sponsored a contract with Grumman Aerospace Corporation (Bethpage, New York) to design and build a forward-swept-wing flight demonstrator (refs. 38 and 39). This airplane was to incorporate several advanced technologies in addition to the forward-swept wing. By the early 1980s, interest in forward sweep had grown enough that an international symposium was devoted to the subject (ref. 40).

The airplane that was designed and built by Grumman was designated the X-29A. The Wright-Patterson Air Force Base X-29A Advanced Program Office provided overall program management. The NASA Dryden Flight Research Center was the responsible test organization and the Air Force Flight Test Center was the participating test organization. More detailed information about the test organization and the flight test program is given in references 41 through 43.

The X-29A airplane represents the integration of several advanced technology features. The thin supercritical forward-swept wing is the most obvious of these (the complete list of advanced technologies will be given later). As indicated in references 41 through 43, one major objective of the flight program was to define the lift and drag characteristics of the X-29A airplane. The purpose of this paper is to report these results.

Because the X-29A was a technology demonstrator, it did not undergo thorough aerodynamic design optimization. Components from other aircraft (for example, forebody and canopy) were used, and it had exposed hinges and large actuator fairings beneath the wing. Consequently, the X-29A lift and drag results should not be interpreted as definitive for a more optimized high-performance, forward-swept wing aircraft that could be built.

The X-29A (number 1) was first flown by the builder on December 14, 1984. There were four contractor-builder acceptance flights, and the first NASA flight was made on April 2, 1985. This paper contains results

from the dedicated performance flight research phase of the flight program, which followed the initial envelope expansion work. In the flight phase from August to December 1987, a highly instrumented, thrust-calibrated engine was installed. This, along with other aircraft instrumentation improvements, qualified the airplane for flight lift-drag research.

The definition of both the zero-lift drag coefficients and the lift-induced drag factors was achieved over the Mach-number (M) range from 0.4 to approximately 1.3. The altitude range varied from 5,000 to 42,000 ft with particular attention given to altitudes near 30,000 ft. Mach numbers of 0.9 and 1.2 at 30,000 ft represented the two primary design conditions (ref. 41); and the dynamic-pressure and Reynolds-number ranges (based on the mean aerodynamic chord (MAC)) for these test points varied from about 200 to 800 lb/ft^2 and 11 million to 34 million, respectively. For the analysis considered here the maximum lift coefficient was near 1.6 and the corresponding angle of attack was about 16°. Thus the low-speed, very high angle-of-attack research that was conducted using the X-29A (number 2) is not included in this paper (refs. 44–46).

Lift and drag data were obtained during pushover-pullup and windup turn maneuvers using the well-known accelerometer method (see Method and Procedures section). This paper will not address the relationship of full-scale flight data with predictions based upon wind-tunnel model tests. Comparisons will be made, however, between X-29A flight lift and drag characteristics and flight results from three other contemporary high-performance aircraft that were optimized for transonic maneuverability.

AIRCRAFT DESCRIPTION

The X-29A demonstrator aircraft, figure 1, was a single-seat fighter-type aircraft that integrated several advanced technologies intended to provide aircraft aero-performance and maneuverability improvements, especially in transonic flight. Though the most obvious feature of the airplane was its forward-swept wing, several other advance technology factors were significant. These were, from references 39, 40, 42, and 47,

- Thin supercritical airfoil
- Aeroelastically tailored composite wing structure
- Close coupled, variable incidence canards
- Relaxed static stability
- Triply redundant digital fly-by-wire control system
- Automatic variable wing camber control
- Three-surface longitudinal control

Figure 1(a) shows a three-view layout of the aircraft with major geometrical characteristics, and important dimensional data are given in table 1.

Table 1. X-29A general information.

Wing	
Reference area, S	185.0 ft^2
Exposed area	188.84 ft^2
Mean aerodynamic chord	7.22 ft
Aspect ratio (A)	4.0
Leading-edge sweep (Λ)	–29.27°
1/4-chord sweep	–33.73°
Taper ratio	0.4
Dihedral angle	0°
Flaperon area	14.32 ft^2
Flaperon deflection (δ_f)	10° TEU (–) 24.75° TED (+)
Strake-flap area	5.21 ft^2
Strake-flap deflection (δ_s)	30° TEU (–) 30° TED (+)
Canard	
Reference area	37.0 ft^2
Exposed area	35.96 ft^2
Aspect ratio	1.47
Leading-edge sweep	42.0°
1/4-chord sweep	23.06°
Taper ratio	0.318
Deflection (δ_c)	58° TEU (–) 32° TED (+)
Vertical tail	
Reference area	33.75 ft^2
Exposed area	32.51 ft^2
Aspect ratio	2.64
Leading-edge sweep	47.0°
1/4-chord sweep	41.06°
Taper ratio	0.306
Rudder area	7.31 ft^2

Table 1. Concluded.

Rudder deflection	30° TE left (+) 30° TE right (–)
Engine	F404-GE-400
Power setting	
Ground idle	18° PLA
Flight idle	31° PLA
Intermediate	87° PLA
Maximum afterburner	130° PLA
Engine inlet	
Capture area	650 in^2
Throat area	473.5 in^2
Fuel	JP-5
Zero fuel weight and balance	
Gross weight	13,906 lb
Center of gravity range	–14.4% to –7.0% of MAC
Fuel tank capacities	
Feed tank	1,830 lb
Forward tank	1,810 lb
Strake tank	340 lb
Total fuel capacity	3,980 lb
Maximum takeoff weight	17,800 lb

Wing Characteristics

The wing profile was a supercritical section of Grumman designation, with an average wing thickness ratio *t/c* of approximately 5 percent and a MAC of 86.6 in. A built-in wing leading-edge root-to-tip twist was designed to optimize transonic performance at $M = 0.9$ and an altitude of 30,000 ft. Figure 2 illustrates the distribution of the twist for two flight conditions adapted from reference 48.

The design limit load factors for symmetric maneuvers were 8 *g* for subsonic and 6.5 *g* for supersonic speeds. Flight limits were defined as 80 percent of the design values. Leading-edge sweep was –29.3° from $\eta = 0.39$ to the tip. From $\eta = 0.39$ to the root the leading-edge was swept back about 29°. The wing had no leading-edge devices but did have variable trailing-edge camber control throughout almost the entire span. Figure 3 shows a cross-section view of this control device (flaperon).

Because the actuator components used were designed for other aircraft, two rather large (nonoptimum) external fairings were located under each wing to house hydraulic actuators for the flaperons. In addition, each wing had five other lower surface protuberances caused by flaperon actuators and hinges. The estimated extra drag caused by these fairings and hinges will be discussed in a later section. The design lift coefficient at $M = 0.90$ was 0.92.

Control Surfaces

The three longitudinal control surfaces were the variable-incidence canards, the wing flaperons, and the aft-mounted strake flaps. The exposed area of the canards was about 20 percent of the exposed wing area. The maximum canard deflection range was from 32° trailing edge down (TED) to 58° trailing edge up (TEU) at rates up to 100°/sec. The canards had sharp leading and trailing edges, a symmetric airfoil section, and no twist. There was no provision for asymmetric canard deflections.

The aft-wing mounted flaperon chord length was 25 percent of the total (swept-forward) wing chord. The maximum deflection range was from 10° TEU to 24.75° TED, and the maximum commanded deflection rate was 68°/sec. Symmetric flaperon deflection provided pitch control while asymmetric deflection of the flaperons, coordinated with rudder control-assist through an aileron to rudder interconnect, provided roll control.

The strake flaps had a deflection range of ±30°. Figure 4 shows the permissible range of travel between the maximum limits as influenced by angle of attack or Mach number for all three longitudinal control surfaces (ref. 47).

Flight Control System

The X-29A flight control system was a triplex fly-by-wire with two digital modes—a primary and a back up—and an analog mode. All flight research results reported here were performed in the primary mode. Two longitudinal control loop features scheduled the

wing flaperon camber. The primary control loop was the continuously variable automatic camber control (ACC) mode. This was the primary mode for obtaining the lift and drag data of this report. A manual camber control (MCC) mode allowed the pilot to set fixed flaperon positions. Brief examples of lift and drag data will be shown for the MCC mode at –5°, 0°, and 5° flaperon settings. Reference 49 shows a block diagram for the longitudinal component of the primary digital mode, and further details pertaining to the flight control system are given in reference 50.

Propulsion System

The X-29A was powered by a single General Electric F404-GE-400 turbofan engine (General Electric, Lynn, Massachusetts) rated at 16,000 lb of thrust for sea-level static conditions for full afterburner. The nozzle region was relatively clean, as were the various vents and scoops that accompany turbofan installations. Additional details about this engine are found in reference 51.

Engine air was supplied through two side fuselage-mounted inlets that merged 18 in. in front of the engine face. The inlets were of simple fixed geometry, designed for optimum performance near M = 0.9 (one of the primary design goals). Reference 48 showed details of the lip geometry and dimensions.

DATA ACQUISITION SYSTEM

Instrumentation

A total of 691 parameters were measured. Because the wing was quite thin and fuselage space was limited, there was no onboard recording system. Consequently, the data were transmitted to the ground for recording, real-time analysis, and control-room monitoring. The five-module 10-bit pulse code modulation system, combined with a single frequency modulation system, were presented in block format in reference 48. All data were transmitted in encrypted form and then decrypted and decommutated on the ground for recording and display.

Figure 5 shows the distribution of research data parameters among several disciplines. The majority of the measurements used for this paper are listed under the “basic parameters” heading. An external array of sensors was contained on the noseboom, which was a derivative of a standard NACA–NASA airdata head (ref. 52). Details on the instrumentation system are reported in references 41, 42, and 43; and background information pertaining to the engine sensors and their location are found in references 51, 53, 54, and 55.

Data Uncertainty

Reference 56 discussed the permissible uncertainty for several of the most important parameters with respect to the definition of drag coefficient C_D. The measurement uncertainties considered there were based on specifications for the various sensors that were anticipated, or assumed limitations in the state of the art. Based upon these individual measurement uncertainties and on a projected drag coefficient value from a simulation model, the percentage of drag-coefficient error was calculated for several flight conditions. Reference 56 concluded that “to achieve reasonable net uncertainty levels in C_D, the maximum limit error in thrust should be near 3 percent.” By assuming a limit thrust error of ±3 percent, reference 56 determined that the several other most important error sources combined to produce a net uncertainty in drag coefficient of 2.6 and 2.4 percent for level flight and maximum lift-drag ratio, respectively, at M = 0.9 and 30,000 ft altitude.

The authors now have the advantage of experience with the instrumentation system and can apply this experience to defining new values to the data uncertainties for the important parameters. This has been done, and the resulting uncertainties in the important parameters are shown in table 2.

Table 3 shows, for M = 0.9 and an altitude of 30,000 ft, the net uncertainty as calculated by the procedures used in reference 56. The percentage of uncertainty is larger for level flight because the denominator, C_D, is significantly lower than it is for maximum lift-to-drag ratio.

Table 2. Major data uncertainties.

Parameter	Individual limit error
Longitudinal acceleration	±0.001 *g*
Normal acceleration	±0.003 *g*
Static pressure	±0.01 percent
Mach number	±0.004
Angle of attack	±0.25°
Net thrust	±2.5 percent
Weight	±1.0 percent

Table 3. Uncertainties at $M = 0.9$ and 30,000 ft.

	Level flight	Maximum *L/D*
ΔC_D	±0.00162	±0.00196
C_D	0.0380	0.0580
$\frac{\Delta C_D}{C_D}$, percent	±4.3	±3.4

METHOD AND PROCEDURES

The forces that combine to provide lift and drag coefficients were obtained from the accelerometer method, which has been used in flight since the 1940s (ref. 57). Reference 58 adapted the equations for use with turbojet powered aircraft, and reference 48 detailed how the accelerometer data were resolved for the present X-29A investigation.

Data Reduction and Correction Procedures

The data were reduced through the Uniform Flight Test Analysis System (UFTAS), a documented but unpublished procedure developed by the Air Force-Flight Test Center, Edwards, California. Reference 48 described the data correction procedures and the calculation of in-flight thrust. Other significant propulsion-related information is contained in references 51 and 53 through 55.

Test Maneuvers and Flight Conditions

Pushover-pullup and constant Mach number windup turns were used to obtain lift and drag throughout the range of angle of attack covered for this investigation. The pushover (from level flight) covered the lower lift region; the pullup then reached the medium lift range; and the windup turn covered the medium to high-angle-of-attack range.*

A nominal maneuver began at level flight with velocity stabilized. A gradual pushover was then initiated followed by a pullup to about a 2-*g* load factor and a recovery back to level flight. The rate of change in load factor during the maneuver was about 0.2 *g*/sec; and the entire maneuver was achieved in about 20 sec. Maneuvers also were performed at higher and lower onset rates to assess the effects of maneuver rates on drag. It was determined from these data (not included here) that the 0.2 *g*/sec rate used for these maneuvers provided lift-drag relationships that were not adversely influenced by the onset rates. To achieve higher load factors windup turns were used. To keep Mach number nearly constant, altitude would sometimes be sacrificed as load factor was increased. Level flight acceleration runs also were flown. Reference 59 gave details of these and other flight test techniques.

RESULTS AND DISCUSSION

This section will first present the basic X-29A flight lift curves and drag polars. These data will be followed by zero-lift drag data, lift-related drag data and lift curve slope results that are derived from the basic flight data. The last part of this section will compare the X-29A flight data with corresponding results for three other aircraft.

X-29A

Basic Drag Polar and Lift Curve Data

The basic flight data plotted in figure 6 present lift coefficient as a function of both drag coefficient and angle of attack. The data are presented over the

* For the present investigation angles of attack approaching the 15° to 20° range are considered high. It is acknowledged that at low speeds the angle-of-attack range has been extended to 67° (refs. 44–46).

Mach-number range from 0.4 to 1.3 in figure parts 6(a) through 6(j), respectively. Each part of figure 6 contains trimmed ACC flight data and ACC schedule predictions for trimmed, stable flight. The following analysis will concern primarily the ACC schedule flight data and comparisons with simple theory and some contemporary aircraft. The ACC schedule prediction curves will not be a part of the present analysis. The only reason that the predicted ACC schedule curves are included in figure 6 is that they add evidence that the maneuver rates used in the turns and pushovers did not adversely affect the lift-drag characteristics of the airplane. The data and comparisons for the MCC mode will be limited to one Mach number, $M = 0.6$.

Figure 7 shows drag coefficient plotted as a function of Mach number for a family of constant lift-coefficients (trimmed flight, ACC mode). The solid curves are separated by lift-coefficient increments of 0.3. The dashed curve at $C_L = 0.5$ is included because *maximum lift-to-drag ratio* occurs close to this condition throughout the subsonic portion of the Mach-number range. At supersonic speeds maximum *L/D* is obtained closer to a C_L value of 0.6. Excepting the dashed curve, notice the increasing increment in drag coefficient as each 0.3 increment in C_L is considered, from $C_L = 0$ to 1.2. In spite of the noted increasing *lift-related drag*, the *drag-rise Mach number* (indicated by tick marks) remains relatively unchanged, except the curve for $C_L = 1.2$. The transonic increment of *wave drag* also is evident in this figure. Each of the expressions of drag that have been typeset italic in this paragraph will be shown and discussed in greater detail in subsection portions of this paper to follow.

Lift-to-Drag Ratio

Figure 8 shows the variation of *L/D* with Mach number as obtained in flight. The circular symbols represent the maximum *L/D* value and the squares show *L/D* at the transonic ($M = 0.9$) design C_L value of 0.92. The relative significance of the X-29A lift-to-drag ratios will become more apparent later in the paper when they are compared with values from some contemporary, high-performance, fighter-type aircraft.

Figure 9 shows the envelope of lift coefficient and angle of attack that will provide 95 to 100 percent of maximum lift-drag ratio over the Mach-number range of these tests. The breadth of the angle-of-attack envelope varies from about 2.5° at low subsonic speeds to 1.5° near the drag-rise Mach number; then the envelope broadens to nearly 3° above the drag-rise Mach number. The zero-lift angle of attack, α_0, also is included in the figure.

Lift-Related Drag

Figure 10 shows the drag-due-to-lift factor $\frac{\Delta C_D}{\Delta C_L^2}$ as a function of Mach number for the ACC mode. Two forms of the factor are plotted because the polar shapes for this airplane, in most instances, do not result in a linear relationship when C_D is plotted against C_L^2. Figure 11 is a schematic representation of a plot of C_L^2 as a function of C_D that explains the origin of the open and solid symbol values in figure 10. The open symbols of figure 10 correspond to the slope of the straight-line fairing, in figure 11, from the upper solid symbol to the intersection at $C_L^2 = 0$. The solid symbols of figure 10 result from inserting the two C_D values represented by the solid symbols of figure 11 into the expression:

$$\frac{\Delta C_D}{C_L^2} = \frac{C_D - C_{D_0}}{C_L^2} \qquad (1)$$

for the range of C_L from 0 to 0.6. This range of C_L is considered because it extends near or somewhat beyond the lift coefficient required to achieve maximum lift-to-drag ratio.

Figure 10 also shows relationships for the expressions $\frac{1}{\pi A}$ and $\frac{\Delta \alpha}{\Delta C_L}$, which are theoretical values for the drag-due-to-lift factor for 100 percent and zero leading-edge suction, respectively. As can be seen, the X-29A drag-due-to-lift factor is qualitatively between the two criteria at subsonic speeds, and exceeds the zero-suction criterion at transonic and low supersonic speeds. This is not unusual for aircraft that reach these Mach numbers.

Figure 12 shows another way of evaluating lift-related drag to these criteria. The ordinate *e* is the ratio

of $\frac{1}{\pi A}$ to $\frac{\Delta C_D}{\Delta C_L{}^2}$ for Mach numbers below 1. Above Mach 1 the ordinate factor K' is used. The factor K' is the ratio of $\frac{\Delta\alpha}{\Delta C_L}$ to $\frac{\Delta C_D}{\Delta C_L{}^2}$. The open and solid symbols are derived from the corresponding symbols of figure 10. The range of the factor *e*, which is Oswald's airplane lifting efficiency factor from reference 60, is mostly within the range of values (i.e., from 0.85 to 1.0) one would expect for a cantilever monoplane at the lower Mach numbers. At transonic Mach numbers (0.9 to 1.1), the *e* and K' factors are each significantly below unity. This trend is somewhat representative of compressibility effects that occur on all high-performance aircraft. The continuation of K' values below 1 at the highest Mach number may represent shock-induced flow separation that increases with lift along with less-than-optimum trim conditions (excess trim drag). Lift-related drag will also be discussed later in this paper relative to the X-29A and some contemporary aircraft.

Drag-Rise Mach Number

Figure 7 displays tick marks on each member of the family of curves showing the variation of drag coefficient with Mach number. Each tick represents the Mach number at which the slope of the respective curve, $\frac{\Delta C_D}{\Delta M}$, is equal to 0.1. This is the definition used for identifying the drag-rise Mach number. The M_{DR} values from figure 7 have been combined with other X-29A data for C_L values of 0.8, 1.0, and 1.1 and plotted in figure 13 as a function of lift coefficient. The approximate angles of attack that correspond to the nearest data symbol are shown.

It is not surprising that the drag-rise Mach number decreases significantly for lift coefficients above the design value of 0.92. The legends or captions that accompany the solid symbols indicate that the respective M_{DR}–C_L or M_{DR}–α combinations occur under conditions involving lifting surface buffet as defined in reference 61. Thus it is reasonable to expect diminishing values of drag-rise Mach number in this region, particularly near buffet intensity rise (BIR) for the wing.

Note that from 95 to 100 percent of maximum lift-drag ratio can be obtained at lift coefficients for which the drag-rise Mach number is between 0.895 and 0.91. The zero-lift drag-rise Mach number is 0.925.

Transonic Wave Drag Increment

Figure 14 shows the variation of zero-lift drag coefficient with Mach number. The increment of zero-lift drag coefficient between the highest Mach number and the Mach-number region in which significant compressibility effects are about to begin (assumed to be $M = 0.8$) is identified in figure 14 as transonic wave drag. Based on the wing reference area, the wave drag coefficient increment is 0.0365.

Because wave drag is more a function of cross-sectional area than wing reference area, it is appropriate to consider the wave drag coefficient as based on the X-29A maximum cross-sectional area. The maximum cross-sectional area was derived from the cross-sectional area development plot shown in figure 15. The value derived used the peak area shown in figure 15 with nine-tenths of the inlet capture area subtracted, which assumes an inlet mass-flow ratio of 0.9. Based on the resulting cross-sectional area of 21.09 ft^2, the wave drag coefficient is 0.320. Wave drag for the X-29A will be more meaningful when compared with other supersonic aircraft in a later section of this paper.

Lift-Curve Slope

Figure 16 shows the variation of the lift-curve slope with Mach number for the X-29A in the ACC mode. These data are derived from the trimmed flight data of figure 6, augmented by corresponding data from reference 47. The level of the lift-curve slope shown in figure 16 is high by usual standards (by a factor of 2 to 3). This matter will be discussed in following paragraphs.

An example of how high the values of figure 16 are compared with other sources can be seen by relating the subsonic values shown and the slope for $\Lambda \approx -30°$ in figure 17. Figure 17, adapted from reference 27, shows an expected C_{L_α} value between 0.05 and 0.06 for the sweep and aspect-ratio range of the X-29A. This supports the previous comment, in parentheses, about the X-29A slopes appearing to be high by a factor of from 2 to 3.

A primary reason for these inordinately high slopes relates to the variable-wing camber feature, which is used in the ACC mode. This is evident in figure 18(a) in which the variable-camber slope of the lift curve for the ACC mode can be compared with the slopes for three different fixed flaperon settings (or fixed camber) for the MCC mode at $M = 0.6$.

The slopes for the three fixed flaperon (camber) settings are nearly the same, and they are significantly lower than the slope of the trimmed ACC data. In spite of the significantly lower slopes for the X-29A with fixed flaps, they are still greater than would be predicted by the method of Diederich, which accounts for the sweep and aspect ratio of the X-29A wing (solid line curve from ref. 62).

The three nearly parallel lift curves shown in figure 18 for constant flaperon deflections of –5°, 0°, and 5° are characteristic of the data pattern for even higher flaperon deflections. That is, higher fixed flaperon deflections would result in ever lower, to negative, values of angle of attack for zero lift. This is, of course, also characteristic of conventional trailing-edge high-lift devices that have been used over the last five decades for takeoff and landing. Figure 19 (adapted from ref. 63) shows an example of such a conventional data set. Notice the high apparent slope of the section lift curve (added dashed line) when the trailing-edge flap deflection was varied accordingly as angle of attack was increased. Thus it would be expected that the X-29A in the ACC mode would have a correspondingly high effective lift curve slope when flaperon deflection varies from near zero at low lift to nearly 15° at the higher angles of attack. That is, the variable camber aspects of the X-29A would be expected to provide an effectively higher lift-curve slope in the same way as was demonstrated by the high-lift, double-slotted flap data shown in figure 19.

Another factor, however, inflates the lift curve slopes (and other force coefficient parameters), which include the wing reference area in their definition. As mentioned earlier, the three MCC curves in figure 18, for fixed flaperon deflections, had lift-curve slopes higher than would be predicted by the method shown in reference 62. Evidence shows that these flight-measured slopes are high because the force coefficients are based on an unreasonably small reference area. Figure 20 shows this reference area, $S = 185$ ft^2, as the lightly shaded area in the schematic planform. The resulting relationship of the flight-measured and predicted lift-curves is shown in the upper portion of figure 21 for $M = 0.6$ and $\delta_f = 0°$. The same relationship is evident in figure 18(a).

The darkly shaded portions of the planform in figure 20 show reasonable added increments of reference area that can significantly influence the relationship of predicted and measured lift curves. Table 4 shows the effect of the added increments of reference area on total reference area and aspect ratio.*

Table 4. Actual and hypothetical alternative reference areas and aspect ratios.

Description	ΔS, ft^2	S, ft^2	S', ft^2	A	A'
Basic swept-forward wing	–	185	–	4.00	–
Stationary lift surfaces, exposed	27	–	212	–	3.49
Stationary lift surfaces, projected to centerline	79	–	264	–	2.80

When these increments of reference area are considered and the resulting values of S' and aspect-ratio are applied, the relationships of flight-determined and predicted lift curves are as shown in the two lower portions of figure 21. As can be seen, Diederich's theory from reference 62 (which accounts for sweep, aspect-ratio, and compressibility effects) does not approach the flight-derived lift-curve slope until the largest reference area is used. The authors do not pretend to define the most appropriate reference area; however, the relationships shown in figure 21 are believed to provide evidence that the reference area originally used ($S = 185$ ft^2) is not the appropriate value if meaningful comparisons are to be made with force coefficients from other aircraft. Thus, it is believed that the inordinately high lift-curve slopes of the X-29A, as shown in figure 16, have two explainable sources—variable wing camber, in ACC mode, and unrealistic (too small) reference area.

Furthermore, these two factors would also be expected to influence other lift-related parameters, especially lift-induced drag, and the unrealistic reference area alone will bias any aerodynamic

* The exposed “lifting canard” area could also be rationalized to be a portion of the reference area, but it is not necessary to do this to demonstrate that the reference area actually used for the X-29A is unreasonably small.

parameters containing uncancelled reference areas. For example, reference area obviously cannot bias a ratio such as *L/D* (from $\frac{C_L}{C_D}$) in which the reference area effects cancel. However, all of the solitary force coefficients are biased; an example of this will be included in the following section.

Comparisons With Other Aircraft

Zero Lift-Drag Coefficients

The first comparisons of the X-29A data with flight data from other contemporary aircraft involve the configurations shown in planform in figure 22. Figure 23 shows zero-lift drag coefficients and maximum lift-drag ratios for these four configurations as a function of Mach number. The zero-lift-drag coefficient comparisons, upper part of the figure, demonstrate the influence of a reference area that is too small in that the C_{D_0} values for the X-29A are inordinately high. Notice that if the drag coefficient is based on a reference area of 264 ft^2 as discussed relative to figures 20 and 21 (solid circular symbol at M = 0.7 and 1.2), the resulting values of C_{D_0} are within the range of values for the three other aircraft. As stated before, the 264 ft^2 value for reference area is not proposed as the proper value, but it illustrates the inadequacy of the value of 185 ft^2. Serious comparisons of X-29A drag characteristics with other aircraft results in this paper will use parameters that avoid dependency on the choice of wing reference area. An appendix is included that discusses the subject of uncertain or debatable reference area in greater detail. The data for the F-15C and F-16C are based on unpublished flight tests, and the F/A-18 data are from reference 64.

Lift-to-Drag Ratio

The lower part of figure 23 compares maximum lift-drag ratios for the four aircraft. As was the case for the zero-lift drag comparisons, only a selected few Mach numbers are included for the three contemporaries of the X-29A. Below the speed of sound the F-16C and F/A-18 have higher maximum lift-drag ratios than the X-29A or F-15C has. At M = 1.3 the value of maximum lift-drag ratio for the X-29A is near the average of the values for the other three aircraft. The reader should recall that comparisons on the basis of *L/D* avoid dependence upon the choice of reference area.

Lift-Related Drag

Figure 24 presents lift-related drag characteristics for the same four configurations. The drag-due-to-lift factor, $\frac{\Delta C_D}{\Delta C_L{}^2}$, shown in the upper portion of the figure is subject to the aforementioned reference area bias; however, it is shown for two reasons. The first reason is to demonstrate that X-29A drag characteristics can appear to be too high or low when compared with those from other aircraft, depending on whether the uncancelled reference area is in the numerator or denominator of the lift or drag parameter. A comparison of the upper portion of figures 23 and 24 provides evidence of this fact. The second reason for including the upper portion of figure 24 is because the parameters in the lower part of figure 24 are derived from the respective $\frac{\Delta C_D}{\Delta C_L{}^2}$ data.

The lower portion of figure 24 compares the various configurations on the basis of two lifting efficiency factors, e and K', which are not affected by reference area. The factor e is to be considered for Mach numbers below 1, and K' is applicable at supersonic speeds. With the exception of the X-29A datum at M = 0.4, the subsonic values of e for the various airplanes are close to the norm for a cantilever monoplane as defined by Oswald in reference 60, that is, from 0.85 to 1.0. This statement would not be expected to apply above $M \approx 0.8$ where compressibility effects probably determine that the e values will be lower than were considered by Oswald. Based on e values as defined when $\frac{\Delta C_D}{\Delta C_L{}^2}$ is calculated from equation (1) or defining e as

$$e = \frac{C_L{}^2}{\pi \cdot A(C_D - C_{D_0})} \qquad (2)$$

the lift-related drag of the other aircraft would appear to be higher than for the X-29A, below M = 1.

At Mach numbers above 1 the X-29A lifting efficiency as defined by factor K' is low. A value for K' of 1 would represent the theoretical drag-due-to-lift for zero leading-edge suction, untrimmed. This suggests,

as was mentioned previously, that the X-29A is experiencing either significant trim drag for the ACC mode or increasing shock losses with lift at Mach numbers above the speed of sound. The higher K' values for the other three aircraft suggest that their trim drag was lower. Because these other aircraft are operational in significant numbers, it would be expected that more effort to reduce trim drag would be expended for them than for the two X-29A aircraft.

The Effect of Load Factor on Efficiency

Having established that the parameters *e* and *L/D* should be reliable means of avoiding bias of performance definition caused by an unrealistic reference area, it is also reasonable to examine these parameters for several maneuvering load factors. Figure 25 shows lift-drag polars and load factor–C_L relationships for the four aircraft previously considered at $M = 0.9$. Load factors from 1 to 3 are indicated on these polars for each 0.5 increment of load factor. The significant variation in C_L, for a given load factor, among the four aircraft indicates why comparisons will be made at comparable load factors rather than for a range of constant lift coefficients.

Figure 26(a) shows the variation of *e* for the four aircraft over the same range of load factors at $M = 0.9$. Note that *e* is defined according to the equation shown on the figure, which inflates the resulting *e* where C_{D_0}, that is, the drag at zero lift, is not the minimum drag coefficient. This is why the apparent values of *e* for the lower load factors for three of the aircraft are artificially high and do not, without qualification, represent the real lifting efficiency of the respective configurations. At higher load factors this problem is diminished somewhat, especially for load factors of 2 and above. However, even at elevated load factors these values of *e* are not reliable indicators of lifting efficiency because of polar asymmetry displayed by three of these configurations. By polar asymmetry it is meant that the minimum drag coefficient, or the vertex of the parabola, does not occur at $C_L = 0$.

Arguably a better way of defining the lift-induced drag characteristics (or the lifting efficiency factor *e*) for various configurations in spite of varying amounts of polar asymmetry was proposed by Wendt (ref. 65). Wendt defined *e* by plotting the drag coefficient as a function of $(C_L - C_{L_{min}})^2$ where $C_{L_{min}}$ is the lift coefficient that provides minimum drag coefficient. Thus, the equation used in figure 26(a) is transformed to $e = \dfrac{(C_L - C_{L_{min}})^2}{\pi A(C_D - C_{D_{min}})}$.

This expression has been applied to the polars shown in figure 25 using the $C_{D_{min}}$ and $C_{L_{min}}$ relationships resulting from the $C_{L_{min}}$ values tabulated in the same figure. The resulting lifting efficiency factors (now adjusted for asymmetry) are plotted in figure 26(b) as a function of load factor.

According to Oswald's criteria (ref. 60), the highest of these values of *e* represent somewhat low lifting efficiency for a cantilevered monoplane. However, his criteria was established without consideration of local shock losses, which these configurations experience at $M = 0.9$. Effective maneuvering flight at $M \approx 0.9$ was an important consideration for these four airplanes. This, apparently, is why the variation of *e* with load factor is relatively small for all four configurations at this Mach number. This range of *e* values for the three production airplanes, over the range of load factors (symbols) is probably representative of this class of fighter-interceptor aircraft at $M \approx 0.9$.

The X-29A aircraft was excluded from the preceding statement because of the complicating influence of its greater polar asymmetry and the causal automatic camber. The polar adjustment proposed by Wendt results in lower values of *e* for the X-29A. However, because $C_{D_{min}}$ occurs at a substantial positive lift condition, $C_L = 0.08$, lifting efficiency derived in this manner will result in an inordinately harsh definition of *e* for the X-29A lifting system,* because the airplane has not been credited for the lift increment below the C_L for $C_{D_{min}}$.

Because polar asymmetry complicates the interpretation of the lifting efficiency factor *e* and three of the four subject aircraft display some degree of polar

* The expression *lifting system* has been chosen deliberately. It is intended to emphasize that the five values of *e* for the X-29A (for various load factors) represent as many wing profile shapes because the ACC schedule represents preprogrammed variable geometry. In other words, each value of *e* represents the lifting efficiency for a specific wing profile and load factor.

asymmetry for $M = 0.9$, lift-to-drag ratio is probably a more definitive way of comparing these aircraft at these flight conditions. Consequently figure 26(c) shows the variation of *L/D* with load factor for the same four airplanes. The F-16C and the F/A-18 have lift-drag ratios that are significantly higher than the X-29A and F-15C results for load factors up to 2.5. At a load factor of 2 the F-16C and the F/A-18 lift-drag ratios are on the order of 1 unit higher than the X-29A value. The X-29A lift-drag ratio for this condition is about 0.3 units greater than the F-15C. At a load factor of 3 the X-29A lift-drag ratio is about the average value for the various airplanes.

Figure 27 presents similar comparisons of *e* and *L/D* for three of the airplanes (F-15C data were not available) for $M = 0.6$ where compressibility effects should be negligible. Note that for a load factor of 1, all *e* values are below unity, in contrast to the data for $M = 0.9$, figure 26(a). This indicates that all three polars for $M = 0.6$ are essentially symmetrical about zero lift.

Considering both lifting efficiency parameter *e* and *L/D* in figure 27, somewhere throughout the load-factor range shown each configuration experiences small advantages or disadvantages in relation to at least one of the other airplanes. Note that the rate of loss with load factor, for each lifting efficiency parameter, is nearly the same for the three configurations. For the load-factor range considered and for subcritical speeds, both of these parameters tend to rank these three airplanes as nearly equal. In retrospect, the inequalities seen in figure 26, for $M = 0.9$, would seem primarily to represent losses caused by compressibility effects at lifting conditions. Thus, the lifting efficiency of the X-29A was probably penalized significantly by the actuator fairings and hinges on the wing lower surface (which would cause greater shock losses than would otherwise occur). These protuberances would likely be refined or even eliminated for a production version of such an airplane.

Wave Drag, Transonic

The zero-lift transonic wave drag coefficient of the X-29A and the results from the same three contemporary aircraft will be compared with numerous other airplanes on the basis of fineness ratio. The denominator for the fineness ratio is the equivalent diameter of a body of revolution having the same maximum cross-sectional area as the respective fuselage plus wings, canopy, and empennage. For the X-29A the maximum cross-sectional area was derived from the area development curve shown in figure 15. Nine-tenths of the inlet capture area was subtracted, for all four contemporary aircraft, in an attempt to approximate mass-flow ratio effects.

The results for the X-29A, F-15C, F-16C, and the F/A-18 are included on a plot adapted from reference 66 (fig. 28). The ordinate is referenced to the maximum cross-sectional area from which the equivalent diameter was derived (rather than wing reference area). The author of reference 66 included more than 20 other configurations in his correlation; and he concluded that there were three identifiable generations of supersonic aircraft, with each subsequent generation tending to have lower wave drag coefficients. It was recognized in reference 66 that a few of the latest aircraft displayed a regressive trend toward higher transonic wave drag. This observation is consistent with the wave drag characteristics currently shown for the X-29A, F-15C, F-16C, and F/A-18 airplanes. The author of reference 66 states that most of the data in his original correlation are derived from flight.

Another format for correlating wave drag was suggested by Bellman in reference 67. This format retains the wave drag coefficient based on the wing reference area as the ordinate, while the maximum cross-sectional area is used in the abscissa as $(\frac{A_c}{S})$ to the 5/3 power (an exponent associated with the transonic similarity rules) (fig. 29). In this figure all data were derived from flight. The four contemporary aircraft compared in previous figures are represented by the solid symbols. Again, as for the format of figure 28, these four aircraft are revealed as having relatively high wave drag as compared with some significantly older configurations. This is especially evident for the F-15C. The data which supplement Bellman's original plot were derived from references 68 through 84.

Subsonic, Nonlifting, Aerodynamic Efficiency (Parasite Drag)

An interesting format for comparing the nonlifting drag of aircraft at subsonic speeds is to multiply the conventional drag coefficient, based on wing reference

area *S*, by *S*, so that the possibility of having used an arbitrary or debatable reference area is avoided. Then the resulting parasite area, *f*, is either plotted against the aircraft wetted area* or divided by the wetted area to provide an equivalent friction coefficient, C_{F_e}. This format has been used by aircraft designers, references 85 and 86, who apparently borrowed it from Perkins and Hage, reference 87. The subsonic zero-lift drag of the X-29A and the three other contemporary aircraft have been transformed to the equivalent parasite area format in figure 30. Data from other aircraft, some not previously published in this format (refs. 69, 70, 74, 75, 77, 78, 81, 82, 88, 89, and data from the authors' files) are included. All data are derived from flight and none were from propeller-driven aircraft.

The data shown in figure 30 represent a variety of planforms—unswept, aft swept, delta, and, of course, the forward-swept X-29A. A wide range of wetted areas is represented; the largest is more than 25 times greater than the smallest. There are two symbols for the X-29A: a solid circle with and without a flag. The flagged symbol represents the equivalent parasite area after the drag attributable to the several wing lower surface fairings and hinge protuberances was estimated and subtracted.

Notice that more than half of the aircraft have parasite-area values that are close to or lower than the line for $C_{F_e} = 0.003$. This accumulation of data near the line for 0.003 would seem to confirm the notion expressed in reference 10 that 0.003 was a reasonable practical goal or reference standard for defining subsonic, nonlifting aerodynamic efficiency or cleanness. Consequently, the previously compared four contemporary aircraft will be evaluated by this criterion, as follows:

$$\eta_a = \frac{0.003}{C_{F_e}} \quad \text{for subject aircraft,}$$

$$C_{F_e} = C_{D_0} \times \frac{S}{A_w} \tag{3}$$

where η_a = aerodynamic efficiency for subsonic, nonlifting flight, trimmed. Table 5 shows the resulting η_a values.

Table 5. Zero-lift aero-efficiency: X-29A and contemporary aircraft.

Aircraft	C_{D_0}	C_{F_e}	η_a
X-29A baseline	0.0310	0.00492	0.61
X-29A clean wing	0.0276	0.00438	0.68
F-15C	0.0218	0.00505	0.59
F-16C	0.0199	0.00399	0.75
F/A-18	0.0239	0.00471	0.64

There are other criteria for evaluating η_a besides the experimentally evolved reference value of 0.003 as the effective friction coefficient. One logical reference value (for the numerator in the ratio defining η_a) would be the theoretical flat-plate turbulent friction coefficient for subsonic flight at 30,000 ft altitude based on an area-weighted mean flow length. Another reference coefficient could be this same flat-plate value after adjustment for a component-area-weighted form factor to account for the three-dimensionality of the airplane. These calculations have been performed for the X-29A; and for the three-dimensional case a form factor of 1.06 was used after proper area weighting. Table 6 shows the results.

Table 6. X-29A zero-lift aero-efficiency.

Condition	C_{D_0}	C_{F_e}	η_a	$\eta_{\bar{a}}$	$\eta_{\hat{a}}$
Baseline	0.0310	0.00492	0.61	0.44	0.47
Clean wing	0.0276	0.00438	0.68	0.50	0.53

These values of aerodynamic efficiency or cleanness, though seemingly low, should not be regarded as evidence that is damaging to the concept of forward-swept wings. For cases in which theoretical turbulent flow friction coefficients were used as the reference numerator (for $\eta_{\bar{a}}$ and $\eta_{\hat{a}}$), it should be realized that these are rigid standards that would challenge all production aircraft designed to be highly maneuverable at

* For the aircraft configurations considered here, wetted area can be defined conclusively for nonlifting conditions.

transonic speeds. The design priority for the X-29A was to get the forward-sweep concept (along with close-coupled canard and variable camber) into flight quickly. Some external lines of the X-29A were defined by components borrowed from other aircraft (the forward fuselage, including the canopy, was obtained from an F-5A), and the fixed inlet was not optimized, which probably caused spillage drag for some flight conditions. In addition, it could be argued, the increment in drag or η_a between the baseline and clean-wing values (or at least a significant portion of the increment) is a penalty that should be charged to the variable camber feature of the wing. Thus the drag caused by the external hinges and fairings on the lower surfaces of the wing can be thought of as a constant increment to be added to the lift-related drag.*

Referring back to the three contemporary aircraft (F-15C, F-16C, and F/A-18) it is obvious that they have relatively high zero-lift drag compared with the empirically established equivalent friction reference value of 0.003. The X-29A aerodynamic efficiency for zero-lift was also challenged by this criterion. All four of these aircraft were designed to have high maneuverability at $M \approx 0.9$. It is suggested that this common feature may be an important factor regarding their somewhat low values of η_a. This commonality of function is also believed to have influenced the cross-sectional area distribution in a manner that caused these configurations to have relatively high wave drag coefficients (figs. 28 and 29).

CONCLUDING REMARKS

The lift and drag characteristics of the X-29A airplane have been obtained in flight for a Mach-number range from 0.4 to about 1.3. The data were obtained for altitudes from 5,000 to 42,000 ft; though most of the data and the analysis involve altitudes near 30,000 ft. The angle of attack for these tests was limited to values below about 16° and the Reynolds number, based on the mean aerodynamic chord, ranged from 11 million to 34 million. More than 90 percent of the data were obtained in the automatic camber control mode.

The X-29A lift and drag characteristics are compared with corresponding flight data from contemporary high-performance operational aircraft. Serious comparisons are made only for those aerodynamic parameters that avoid uncertainties associated with the choice or definition of force coefficient reference area. A few comparisons are made for cases in which uncancelled wing reference areas remain so that the risk of this practice can be demonstrated.

The subsonic range of the Oswald lifting efficiency factor, *e*, for the X-29A is about average for a monoplane of cantilever construction. When *e* for the X-29A is compared with the contemporary aircraft at elevated load factors (up to 3) for $M = 0.6$, all three aircraft experience a similar decrease in *e* as load factor is increased. Somewhere throughout this load-factor range each airplane experiences a small advantage or disadvantage relative to at least one of the other aircraft.

A comparison of the X-29A with these same airplanes on the basis of *L/D* for $M = 0.6$ provides similar results. That is, all of these aircraft experience similar decreases in lift-to-drag ratio as load factor increases. Likewise, each airplane has a small advantage (or disadvantage) relative to another aircraft somewhere over the load-factor range.

At $M = 0.9$ the X-29A lift-to-drag ratio is compared with those of three contemporary high-performance aircraft over the same, 1 to 3, load-factor range. Although these kinds of comparisons at $M = 0.6$ showed results that were similar, at $M = 0.9$ where compressibility becomes important, there are significant differences. At a load factor of 2 the lift-to-drag ratios of the F-16C and F/A-18 are on the order of 1 unit higher than the X-29A value whereas the F-15C value is about 0.3 units lower than the X-29A. At a load factor of 3 the X-29A lift-to-drag ratio is about the average of the values for the other three aircraft. Considering that the various aircraft had nearly equal lift-to-drag ratio at subcritical speed ($M = 0.6$) and that significant differences occur at $M = 0.9$, it seems apparent that the X-29A and F-15C suffered greater shock losses than the other two aircraft. The X-29A was probably penalized significantly by the underwing actuator

* On the other hand, if the X-29A were to be produced in large quantities, the hinge and actuator design for the flaperons would likely be refined so that this source of drag would be significantly reduced or even eliminated.

fairings and hinges. These protuberances would likely be refined for a production version of such an airplane.

All four airplanes were compared with aircraft of the previous three to four decades on the basis of wave drag and subsonic aerodynamic cleanness. As a group these four aircraft are characterized by high wave drag and high equivalent parasite area (poor aerodynamic cleanness) when compared with the older airplanes. It is suggested that the design missions of the X-29A and the three contemporary aircraft (that is, high maneuverability for $M \approx 0.90$ and altitude in the 30,000-to 40,000-ft range) were important factors in causing the relatively high wave drag and equivalent parasite area.

At supersonic speeds the lift-related drag of the X-29A is high compared with that for the three contemporary aircraft (based on the ratio of the lift angle to the drag-due-to-lift factor). This is believed to be caused by high trim drag, perhaps inherent in the particular blending of the three longitudinal control surfaces of the X-29A in the automatic camber control mode. Because the other three aircraft are operational and produced in large quantities, it would be expected that greater effort would be devoted to reducing trim drag for them than for the X-29A, which was an experimental technology demonstrator.

Dryden Flight Research Center
National Aeronautics and Space Administration
Edwards, California, September 14, 1993

REFERENCES

1. Munk, Max M., *Note on the Relative Effect of the Dihedral and the Sweep Back of Airplane Wings*, NACA TN-177, Jan. 1924.
2. Lademann, Robert W.E., *Development of Tailless and All-Wing Gliders and Airplanes*, NACA TM-666, Apr. 1932.
3. Heinze, Edwin P.A., *The Dreieck I Tailless Airplane (German), A Low-Wing Cantilever Monoplane*, NACA AC-159, Mar. 1932.
4. Knight, Montgomery and Richard W. Noyes, *Span-Load Distribution as a Factor in Stability in Roll*, NACA Report No. 393, 1931.
5. Busemann, A., "Aerodynamischer Auftrieb bei Ü berschallgeschwindigkeit," [Aerodynamic Lift at Supersonic Speeds], *Luftfahrtforschung*, vol. 12, no. 6, Oct. 3, 1935, pp. 210–220.
6. Jones, Robert T., *Properties of Low-Aspect-Ratio Pointed Wings at Speeds Below and Above the Speed of Sound*, NACA Report No. 835, 1946.
7. Jones, Robert T., *Wing Plan Forms for High-Speed Flight*, NACA Report No. 863, 1947.
8. Bowers, Peter M., *Unconventional Aircraft*, 2nd ed., Tab Books, Blue Ridge Summit, PA, 1990.
9. Walker, Bryce, *Fighting Jets*, Time-Life Books Inc., Alexandria, VA, 1983.
10. Hoerner, Sighard F., *Fluid-Dynamic Drag*, Dr.-Ing. S.F. Hoerner, Midland Park, NJ 07432, 1965.
11. Stone, Ralph W., Jr. and Lee T. Daughtridge, Jr., *Free-Spinning, Longitudinal-Trim, and Tumbling Tests of 1/17.8-Scale Models of the Cornelius XFG-1 Glider*, NACA MR-L5K21, Jan. 1946.
12. Alexander, Sidney R., *Drag Measurements of a 34° Swept-Forward and Swept-Back NACA 65-009 Airfoil of Aspect-Ratio 2.7 as Determined by Flight Tests at Supersonic Speeds*, NACA RM No. L6I11, Feb. 1947.
13. Whitcomb, Richard T., *An Investigation of the Effects of Sweep on the Characteristics of a High-Aspect-Ratio Wing in the Langley 8-Foot High-Speed Tunnel*, NACA RM No. L6J01a, 1947.
14. McCormack, Gerald M. and Victor I. Stevens, Jr., *An Investigation of the Low-Speed Stability and Control Characteristics of Swept-Forward and Swept-Back Wings in the Ames 40-By-80 Foot Wind Tunnel*, NACA RM No. A6K15, 1947.
15. Conner, D. William and Patrick A. Cancro, *Low-Speed Characteristics in Pitch of a 34° Swept-forward Wing With Circular-Arc Airfoil Sections*, NACA RM No. L7F04a, Jan. 1948.
16. Diederich, Franklin W. and Bernard Budiansky, *Divergence of Swept Wings*, NACA TN-1680, 1948.
17. Spearman, M. Leroy and Paul Comisarow, *An Investigation of the Low-Speed Static Stability Characteristics of Complete Models Having Sweptback and Sweptforward Wings*, NACA RM No. L8H31, 1948.
18. McCormack, Gerald M. and Woodrow L. Cook, *A Study of Stall Phenomena on a 45° Swept-Forward Wing*, NACA TN-1797, 1949.
19. McCormack, Gerald M. and Woodrow L. Cook, *Effects of Several Leading-Edge Modifications on the Stalling Characteristics of a 45° Swep-Forward Wing*, NACA RM No. A9D29, 1949.
20. McCormack, Gerald M. and Woodrow L. Cook, *Effects of Boundary-Layer Control on the Longitudinal Characteristics of a 45° Swept-Forward Wing-Fuselage Combination*, NACA RM No. A9K02a, 1950.
21. Graham, Robert R., *Lateral-Control Investigation at a Reynolds Number of 5,300,000 of a Wing of Aspect Ratio 5.8 Sweptforward 32° at the Leading Edge*, NACA RM No. L9H18, Feb. 1950.
22. Martina, Albert P. and Owen J. Deters, *Maximum Lift and Longitudinal Stability Characteristics at Reynolds Numbers up to 7.8 × 10^6 of a 35° Sweptforward Wing Equipped With High-Lift and Stall-Control Devices, Fuselage, and Horizontal Tail*, NACA RM No. L9H18a, Feb. 1950.
23. Hopkins, Edward J., *Lift, Pitching Moment, and Span Load Characteristics of Wings at Low Speed as Affected by Variations of Sweep and Aspect Ratio*, NACA TN-2284, Jan. 1951.
24. Whitcomb, Richard T., *An Experimental Study at Moderate and High Subsonic Speeds of the Flow Over Wings With 30° and 45° of Sweepforward in Conjunction With a Fuselage*, NACA RM No. L50K28, June 1951.
25. Purser, Paul E. and M. Leroy Spearman, *Wind-Tunnel Tests at Low Speed of Swept and Yawed Wings Having Various Plan Forms*, NACA TN-2445, Dec. 1951. Supersedes NACA RM No. L7D23.

26. Furlong, G. Chester and James G. McHugh, *A Summary and Analysis of the Low-Speed Longitudinal Characteristics of Swept Wings at High Reynolds Number*, NACA Report 1339, 1957.
27. Hoerner, Sighard F. and Henry V. Borst, *Fluid-Dynamic Lift*, Mrs. Liselotte A. Hoerner, Hoerner Fluid Dynamics, Brick Town, NJ 08723, 1975.
28. Taylor, John W.R., ed., J*ane's All the Worlds Aircraft 1970–71*, Jane's Yearbooks, London W1A 2LG, England, 1971.
29. Krone, Norris J., Jr., Lt. Col., "Divergence Elimination with Advanced Composites," AIAA Paper No. 75-1009, AIAA 1975 Aircraft Systems and Technology Meeting, Los Angeles, CA, Aug. 4–7, 1975.
30. Huffman, Jarrett K. and Charles H. Fox, Jr., *Subsonic Longitudinal and Lateral-Directional Static Aerodynamic Characteristics for a Close-Coupled Wing-Canard Model in Both Swept Back and Swept Forward Configurations*, NASA TM-74092, 1978.
31. Huffman, Jarrett K. and Charles H. Fox Jr., *Subsonic Longitudinal and Lateral-Directional Static Aerodynamic Characteristics for a Model with Swept Back and Swept Forward Wings*, NASA TM-74093, 1978.
32. Huffman, Jarrett K. and Charles H. Fox, Jr., *The Effect of Canard Relative Size and Vertical Location on the Subsonic Longitudinal and Lateral-Directional Static Aerodynamic Characteristics for a Model with a Swept Forward Wing*, NASA TM-78739, 1979.
33. Ricketts, Rodney H. and Robert V. Dogget Jr., *Wind-Tunnel Experiments on Divergence of Forward-Swept Wings*, NASA TP-1685, 1980.
34. "Forward-Swept Wing Potential Studied," *Aviation Week and Space Technology*, Jan. 29, 1979.
35. Krone, N.J., Jr., "Forward Swept Wing Flight Demonstrator," AIAA-80-1882, AIAA Aircraft Systems and Technology Meeting, Anaheim, CA, Aug. 4–6, 1980.
36. Löbert, G., "Spanwise Lift Distribution of Forward-and Aft-Swept Wings in Comparison to the Optimum Distribution Form," AIAA 81-4187, *J. Aircraft*, vol. 18, no. 6, June 1981.
37. Uhuad, G.C., T.M. Weeks, and R. Large, "Wind Tunnel Investigation of the Transonic Aerodynamic Characteristics of Forward Swept Wings," *J. Aircraft*, vol. 20, no. 3, Mar. 1983.
38. Spacht, G., "The Forward Swept Wing: A Unique Design Challenge," AIAA-80-1885, AIAA Aircraft Systems Meeting, Anaheim, CA, Aug. 4–6,1980.
39. Moore, M. and D. Frei, "X-29 Forward Swept Wing Aerodynamic Overview," AIAA-83-1834, AIAA Applied Aerodynamics Conference, Danvers, MA, July 13–15, 1983.
40. Nangia, R.K., ed., *Proceedings International Conference, Forward Swept Wing Aircraft*, University of Bristol, Bristol, U.K. March 24–26, 1982.
41. Putnam, Terrill W., *X-29 Flight-Research Program*, NASA TM-86025, 1984.
42. Sefic, Walter J. and Cleo M. Maxwell, *X-29A Technology Demonstrator Flight Test Program Overview*, NASA TM-86809, 1986.
43. Sefic, Walter, J. and William Cutler, "X-29A Advanced Technology Demonstrator Program Overview," AIAA-86-9727, AIAA/AHS/CASI/DGLR/IES/ISA/ITEA/SEP/FTE 3rd Flight Testing Conference, Las Vegas, NV, Apr. 2–4 1986.
44. Fisher, David F., David M. Richwine, and Stephen Landers, *Correlation of Forebody Pressures and Aircraft Yawing Moments on the X-29A Aircraft at High Angles of Attack*, NASA TM-4417, 1992.
45. Del Frate, John H. and John A. Saltzman, *In-Flight Flow Visualization Results from the X-29A Aircraft at High Angles of Attack*, NASA TM-4430, 1992.
46. Webster, Fredrick R. and Dana Purifoy, "X-29 High Angle-of-Attack Flying Qualities," AFFTC-TR-91-15, July 1991. (Available to U.S. government agencies and contractors; others should contact WL/FIMT, Wright-Patterson AFB, OH 45433-6523.)
47. Huckabone, Thomas C., and Harry C. Walker III, "Performance Evaluation of the X-29A Research Aircraft," AFFTC-TR-87-51, Mar. 1988.
48. Hicks, John W. and Thomas Huckabone, *Preliminary Flight-Determined Subsonic Lift and Drag Characteristics of the X-29A Forward-Swept-Wing Airplane*, NASA TM-100409, 1989.

49. Hicks, John W. and Bryan J. Moulton, *Effects of Maneuver Dynamics on Drag Polars of the X-29 Forward-Swept-Wing Aircraft With Automatic Wing Camber Control*, NASA TM-100422, 1988.
50. Gera, J., J.T. Bosworth, and T.H. Cox, *X-29A Flight Test Techniques and Results: Flight Controls*, NASA TP-3121, 1991.
51. Alexander, R.I. and R.J. Ray, *Development and Flight Test of a Real-Time Thrust Measurement Technique on the X-29A/F404 Advanced Technology Demonstrator*, NASA TM-101707, 1989. (Available to U.S. government agencies and contractors; others should contact WL/FIMT, Wright-Patterson AFB, OH 45433-6523.)
52. Richardson, Norman R. and Albin O. Pearson, *Wind-Tunnel Calibrations of a Combined Pitot-Static Tube, Vane-Type Flow-Direction Transmitter, and Stagnation-Temperature Element at Mach Numbers from 0.60 to 2.87*, NASA TN-D-122, 1959.
53. Ray, Ronald J., *Evaluation of Various Thrust Calculation Techniques on an F404 Engine*, NASA TP-3001, 1990.
54. Burns, Maureen E. and Thomas A. Kirchgessner, *Airflow Calibration and Exhaust Pressure/Temperature Survey of an F404, S/N 215-109, Turbofan Engine*, NASA TM-100159, 1987.
55. Conners, Timothy R., *Measurement Effects on the Calculation of In-Flight Thrust for an F404 Turbofan Engine*, NASA TM-4140, 1989.
56. Powers, Sheryll Goecke, *Predicted X-29A Lift and Drag Coefficient Uncertainties Caused by Errors in Selected Parameters*, NASA TM-86747, 1985.
57. Keller, Thomas L. and Robert F. Keuper, *Comparison of the Energy Method With the Accelerometer Method of Computing Drag Coefficients From Flight Data*, NACA CB No. 5H31, Oct. 1945.
58. Beeler, De E., Donald R. Bellman, and Edwin J. Saltzman, *Flight Techniques for Determining Airplane Drag at High Mach Numbers*, NACA TN-3821, Aug. 1956.
59. Hicks, John W., James M. Cooper, Jr., and Walter J. Sefic, *Flight Test Techniques for the X-29A Aircraft*, NASA TM-88289, 1987.
60. Oswald, W. Bailey, *General Formulas and Charts for the Calculation of Airplane Performance*, NACA Report No. 408, 1932.
61. Friend, Edward L., *Initial Flight Buffet Characteristics of the X-29A Airplane Including Comparisons With Other Contemporary Designs*, NASA TM-4159, 1990. (ITAR restricted; available from AFWAL/FIF, Wright-Patterson AFB, OH 45433.)
62. Diederich, Franklin W., *A Plan-Form Parameter for Correlating Certain Aerodynamic Characteristics of Swept Wings*, NACA TN-2335, Apr. 1951.
63. Abbott, Ira H., and Albert E. Von Doenhoff, *Theory of Wing Sections*, Dover Publications, Inc., New York, NY, 1959.
64. Peters, G.E., S.L. Parker, C.M. Pulley, and B.R. Williams, "F/A-18 Basic Aerodynamic Data (U)," Report No. MDC A8575, McDonnell Aircraft Company, St. Louis, MO 63166, Mar. 1984.
65. Wendt, R.E., "A Method of Airplane Performance Calculation Applicable to Any Polar," *J. Aeronaut. Sci.*, vol. 14, no. 4, Apr. 1947, pp. 243–250.
66. Jobe, Charles E., "Prediction of Aerodynamic Drag," AFWAL-TM-84-203, Flight Dynamics Laboratory, Air Force Wright Aeronautical Laboratories, Wright-Patterson Air Force Base, OH 45433, July 1984.
67. Bellman, Donald R., *A Summary of Flight Determined Transonic Lift and Drag Characteristics of Several Research Airplane Configurations*, NASA MEMO 3-3-59H, Apr. 1959.
68. Nugent Jack, *Lift and Drag of the Bell X-5 Research Airplane in the 45° Sweptback Configuration at Transonic Speeds*, NACA RM No. H56E02, July 1956.
69. Saltzman, Edwin J. and William P. Asher, *Transonic Flight Evaluation of the Effects of Fuselage Extension and Indentation on the Drag of a 60° Delta-Wing Interceptor Airplane*, NACA RM No. H57E29, Sept. 1957.
70. Carman, L. Robert and John R. Carden, *Lift and Drag Coefficients for the Bell X-1 Airplane (8-Percent-Thick Wing) in Power-Off Transonic Flight*, NACA RM No. L51E08, June 1951.
71. Saltzman, Edwin J., *Flight Measurements of Lift and Drag for the Bell X-1 Research Airplane Having a 10-Percent-Thick Wing*, NACA RM No. L53F08, Sept. 1953.

72. Rolls, L. Stewart and Rodney C. Wingrove, *An Investigation of the Drag Characteristics of a Tailless Delta-Wing Airplane in Flight, Including Comparison with Wind-Tunnel Data*, NASA MEMO 10-8-58A, Nov. 1958.
73. Purser, Paul E., *Comparison of Wind-Tunnel, Rocket, and Flight Drag Measurements for Eight Airplane Configurations at Mach Numbers Between 0.7 and 1.6*, NACA RM No. L54F18, Sept. 1954.
74. Nugent, Jack, *Lift and Drag of a Swept-Wing Fighter Airplane at Transonic and Supersonic Speeds*, NASA MEMO 10-1-58H, Jan. 1959.
75. Arnaiz, Henry H., *Flight-Measured Lift and Drag Characteristics of a Large, Flexible, High Supersonic Cruise Airplane*, NASA TM X-3532, May 1977.
76. Pyle, Jon S. and Louis L. Steers, *Flight-Determined Lift and Drag Characteristics of an F-8 Airplane Modified With a Supercritical Wing With Comparisons to Wind-Tunnel Results*, NASA TM X-3250, June 1975.
77. Cooper, James M., Jr., Donald L. Hughes, and Kenneth Rawlings III, "Transonic Aircraft Technology—Flight-Derived Lift and Drag Character-istics, Volume I of II," AFFTC-TR-77-12, July 1977.
78. Finley, D.B., "Final F-16XL Aerodynamic Status Report and Flight Test Results," CDRL Sequence Number 3008, DI-E-3135/M) Contract F33657-78G-0004-0009, Sept. 1985.
79. Saltzman, Edwin J. and Darwin J. Garringer, *Summary of Full-Scale Lift and Drag Characteristics of the X-15 Airplane*, NASA TN D-3343, 1966.
80. Bellman, Donald R., *Lift and Drag Characteristics of the Bell X-5 Research Airplane at 59° Sweepback for Mach Numbers From 0.60 to 1.03*, NACA RM No. L53A09c, Feb. 1953.
81. Bellman, Donald R. and Thomas R. Sisk, *Preliminary Drag Measurements of the Consolidated Vultee XF-92A Delta-Wing Airplane in Flight Tests to a Mach Number of 1.01*, NACA RM No. L53J23, Jan. 1954.
82. Nugent, Jack, *Lift and Drag Characteristics of the Douglas D-558-II Research Airplane Obtained in Exploratory Flights to a Mach Number of 2.0*, NACA RM No. L54F03, Aug. 1954.
83. Bellman, Donald R. and Edward D. Murphy, *Lift and Drag Characteristics of the Douglas X-3 Research Airplane Obtained During Demonstration Flights to a Mach Number of 1.20*, NACA RM No. H54I17, Dec. 1954.
84. Saltzman, Edwin J., Donald R. Bellman, and Norman T. Musialowski, *Flight-Determined Transonic Lift and Drag Characteristics of the YF-102 Airplane With Two Wing Configurations*, NACA RM No. H56E08, July 1956.
85. Corning, Gerald, *Supersonic and Subsonic Airplane Design*, 3rd edition, College Park, MD, 1970.
86. Stinton, Darrol, *The Design of the Aeroplane*, Van Nostrand Reinhold Co., New York, 1983.
87. Perkins, Courtland D. and Robert E. Hage, *Airplane Performance Stability and Control*, John Wiley & Sons, New York, NY, 1949.
88. Wong, Kent J., "AFTI/F-111 Mission Adaptive Wing Lift and Drag Flight Test Results, Volume I," AFFTC-TR-87-02, Apr. 1987. (Distribution restricted to U.S. government agencies only. Other requestors should contact AFTI/F-111 (MAW) Program Office (AFWAL/FIMF), Wright-Patterson AFB, OH 45433-6503.)
89. Fox, M.K. and E.A. Wadsworth, "Correlation of the Supersonic Thrust and Drag of the B-58A Airplane," General Dynamics Report FZA-4-415, Dec. 1963.
90. Ames Research Center, *Collected Works of Robert T. Jones*, NASA TM X-3334, Feb. 1976.
91. Munk, Max M., *The Minimum Induced Drag of Aerofoils*, NACA Report No. 121, 1921.
92. Prandtl, L., *Applications of Modern Hydrodynamics to Aeronautics*, NACA Report No. 116, 1921.
93. Prandtl, L. and O. G. Tietjens, *Applied Hydro- and Aeromechanics*, Dover Publications, Inc., New York, 1957.
94. Walker, Harold J., *Performance Evaluation Method for Dissimilar Aircraft Designs*, NASA RP-1042, 1979.

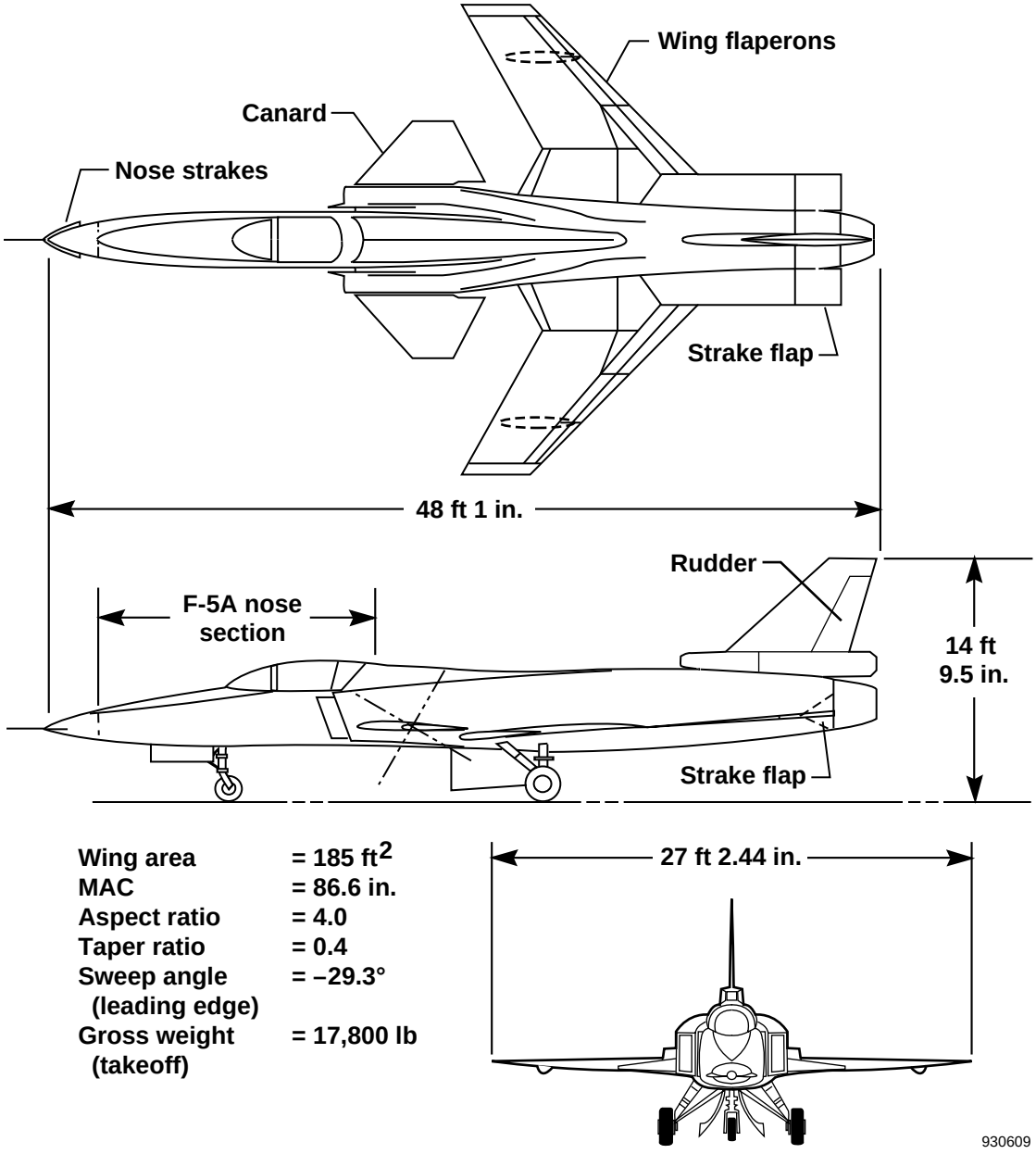

(a) Three view.

Figure 1. X-29A airplane.

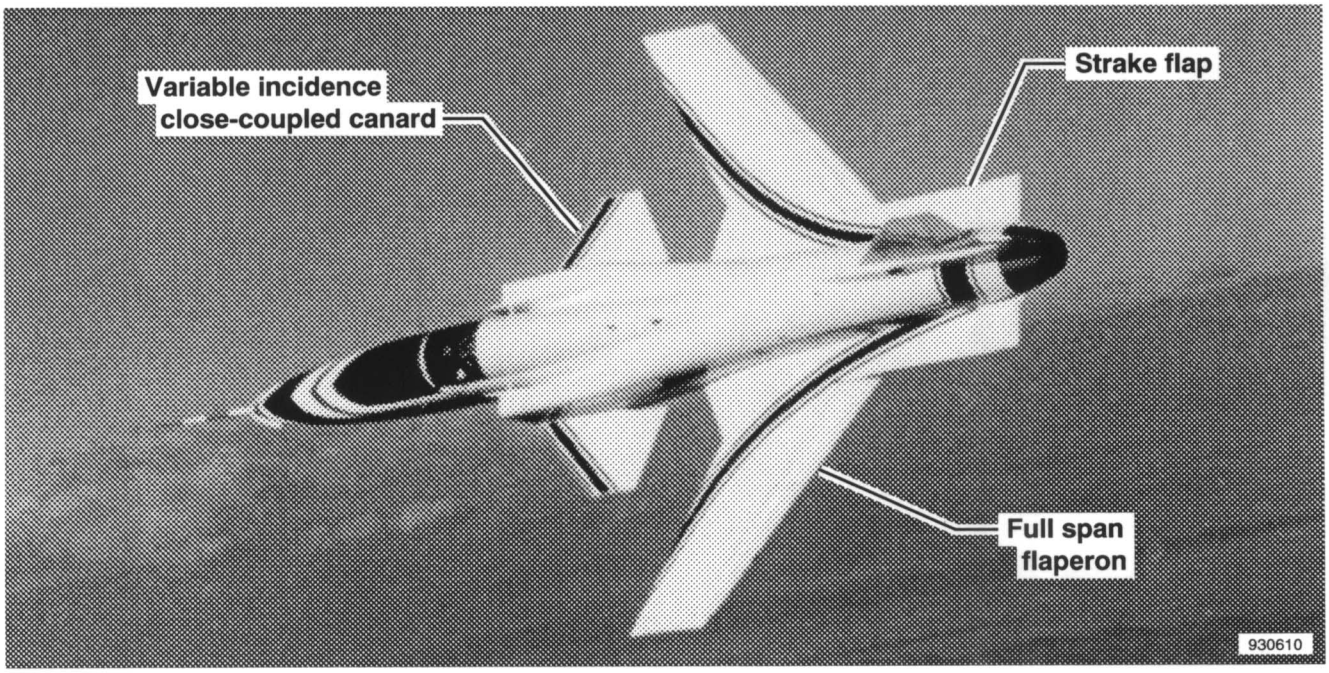

(b) In-flight view.

Figure 1. Concluded.

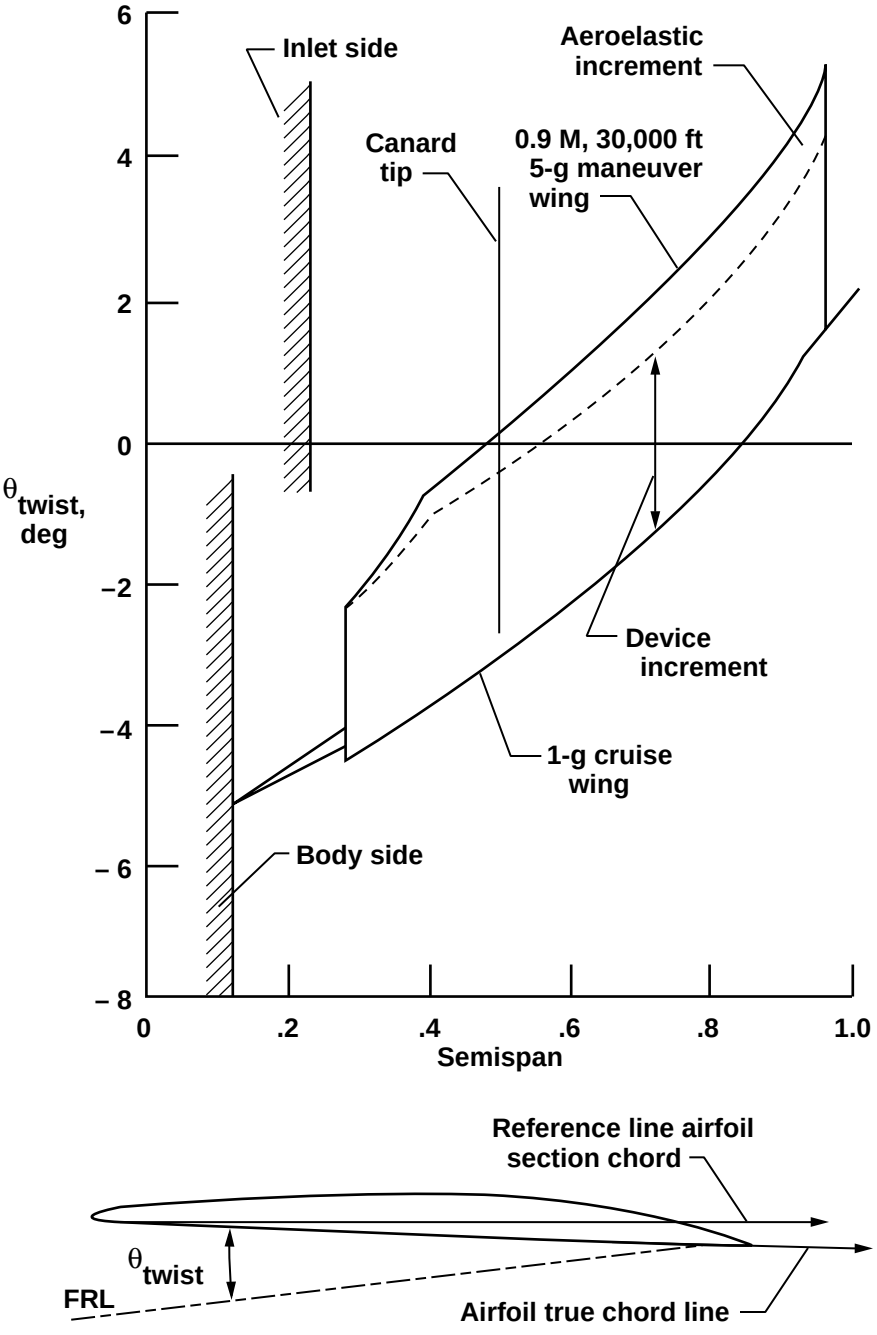

Figure 2. Wing twist distribution, adapted from reference 48.

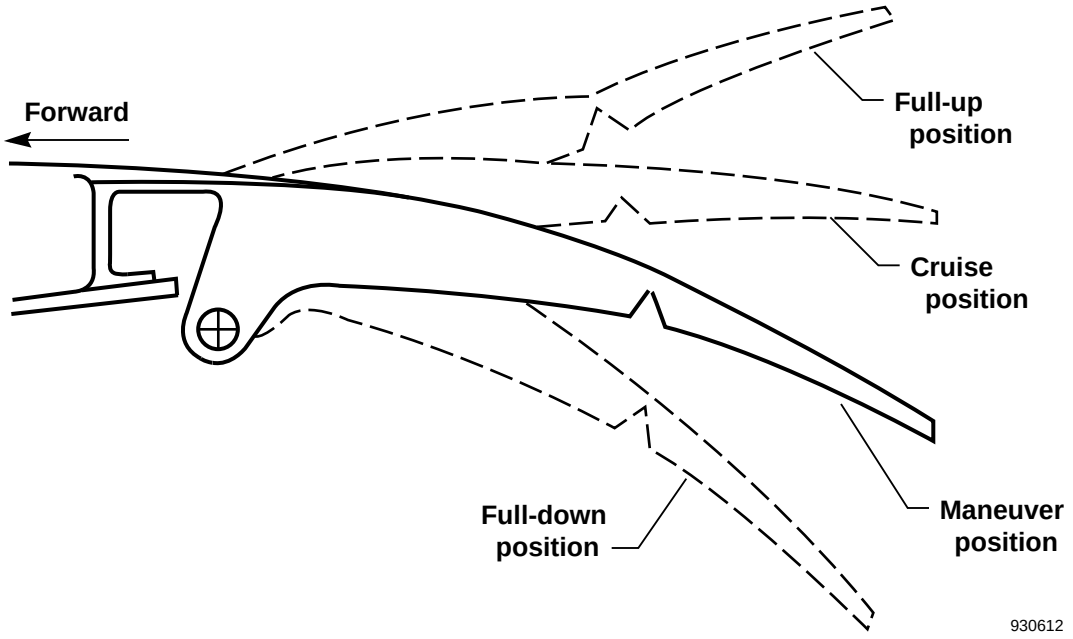

Figure 3. X-29A full-span flaperon profile.

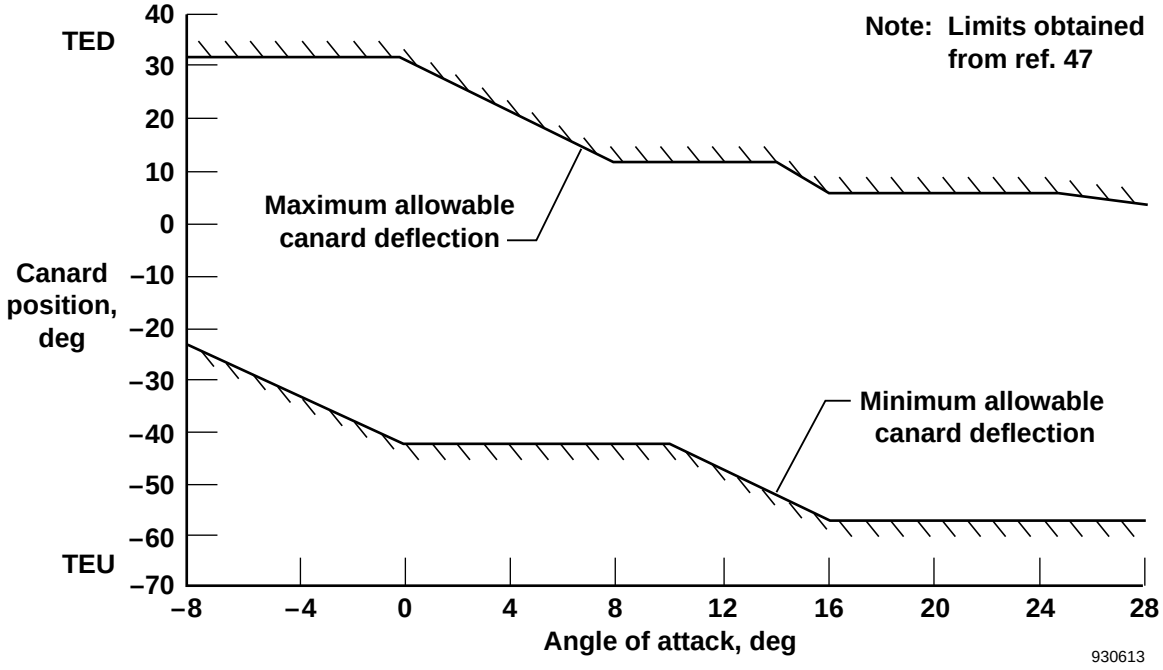

(a) Canard.

Figure 4. Permissible longitudinal control surface deflections.

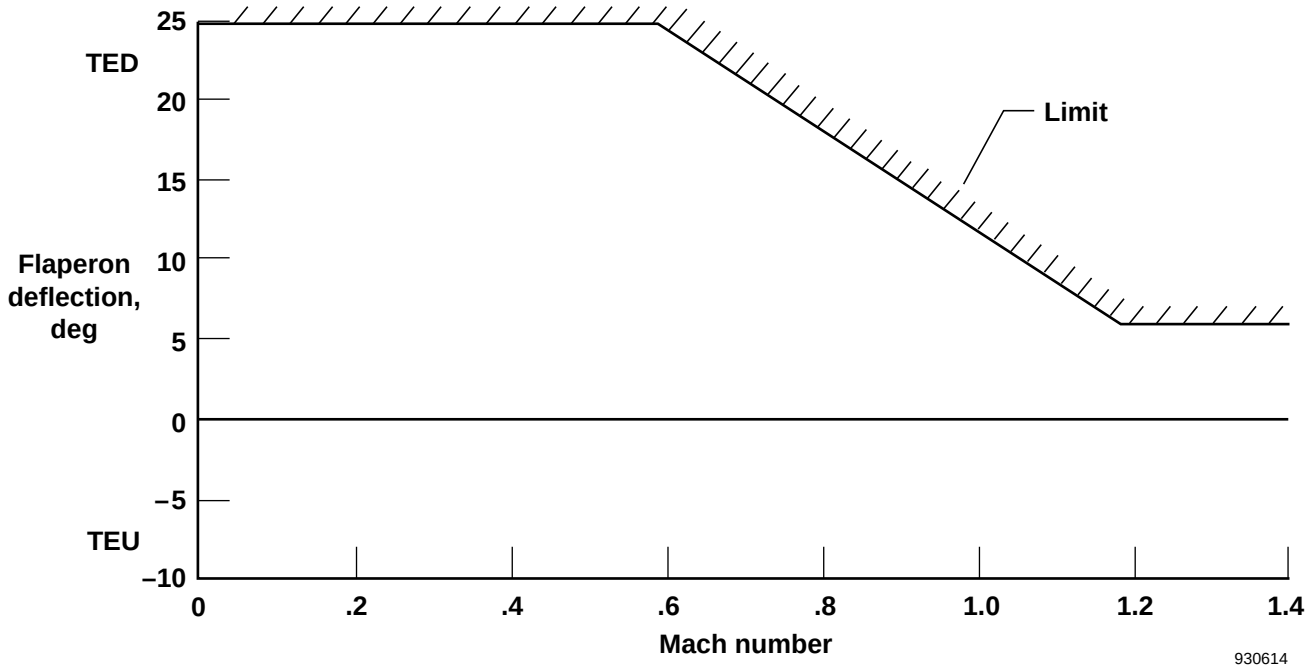

(b) Flaperon.

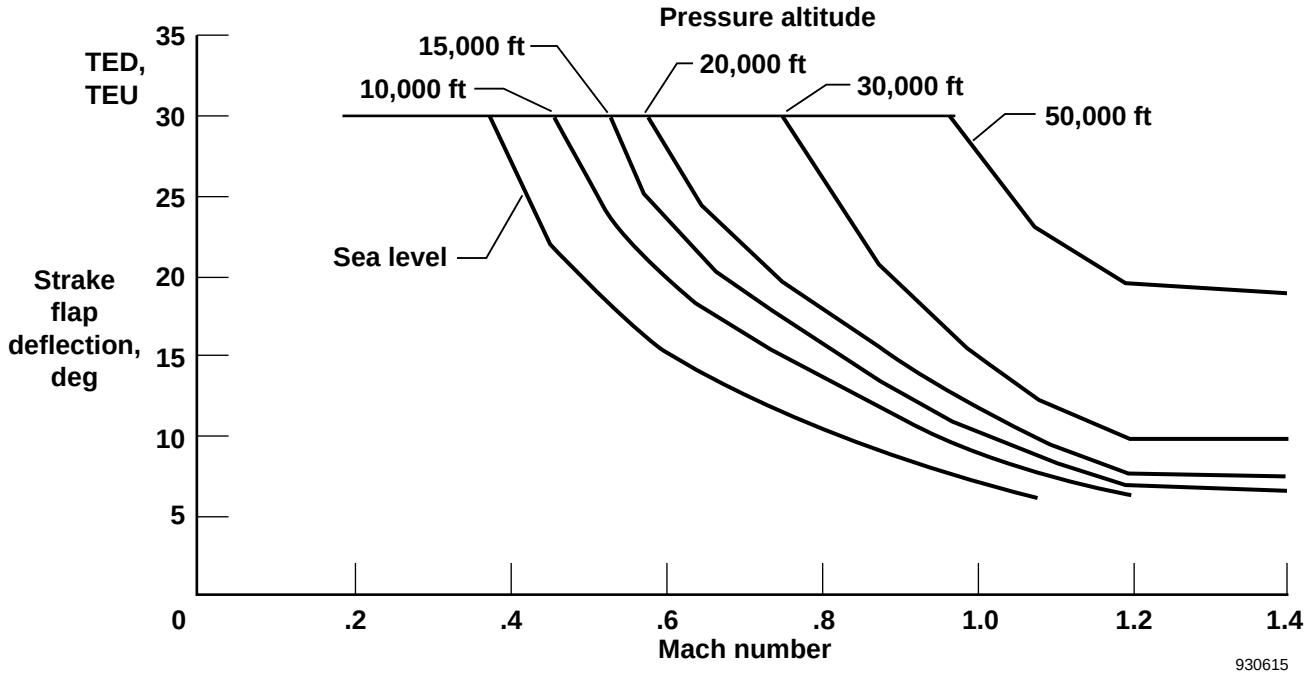

(c) Strake flap (includes TED and TEU).

Figure 4. Concluded.

Basic parameters
- **Airdata (9)**
- **Angles of attack and sideslip (4)**
- **Pitch, roll, and yaw attitudes, rates, and accelerations (10)**
- **Center-of-gravity accelerations (6)**
- **Engine speed, temperature, pressure, and nozzle positions (21)**
- **Surface positions (9)**

Flight-control system
- **Computer parameters (429 bus) (64)**
- **Stick, rudder pedal position, and forces (6)**
- **Cockpit accelerations (2)**

Flutter and buffet
- **Accelerometers (23)**
- **Velocities (4)**
- **Flap tab shaker (3)**

Structures
- **Strain gauges (112)**
- **Optical deflection measurement system (12)**

Aerodynamic
- **Wing/strake static pressure (152)**
- **Canard static pressures (29)**

Miscellaneous
- **Hydraulic (9)**
- **Electrical (10)**
- **Temperature (46)**
- **Vibration (8)**
- **Other (22)**

930616

Figure 5. X-29A measurands (ref. 41).

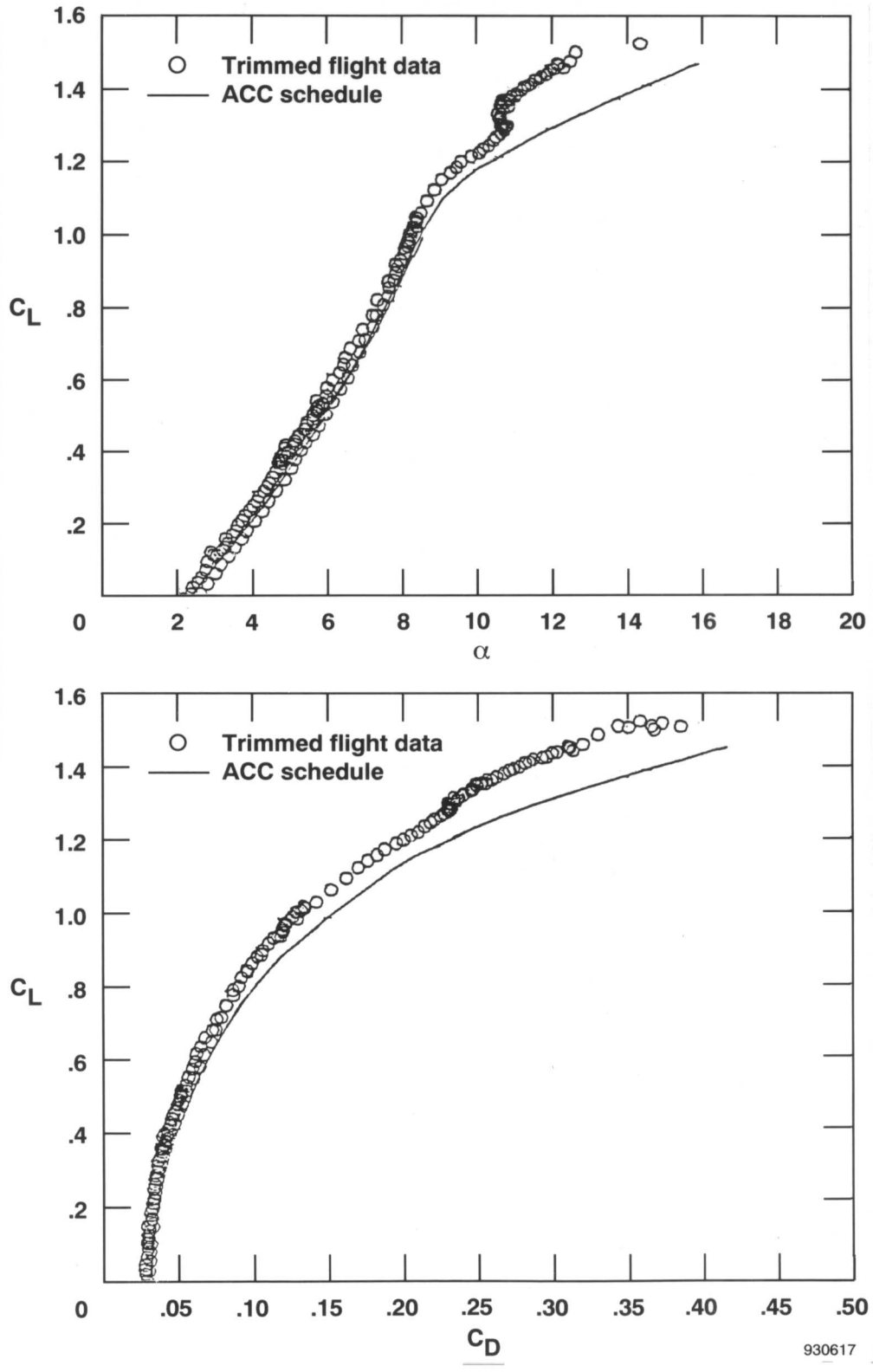

(a) $M = 0.40$. (Note: Units for α, above, are degrees.)

Figure 6. Lift curves and drag polars for Mach numbers from 0.4 to 1.3; ACC schedule.

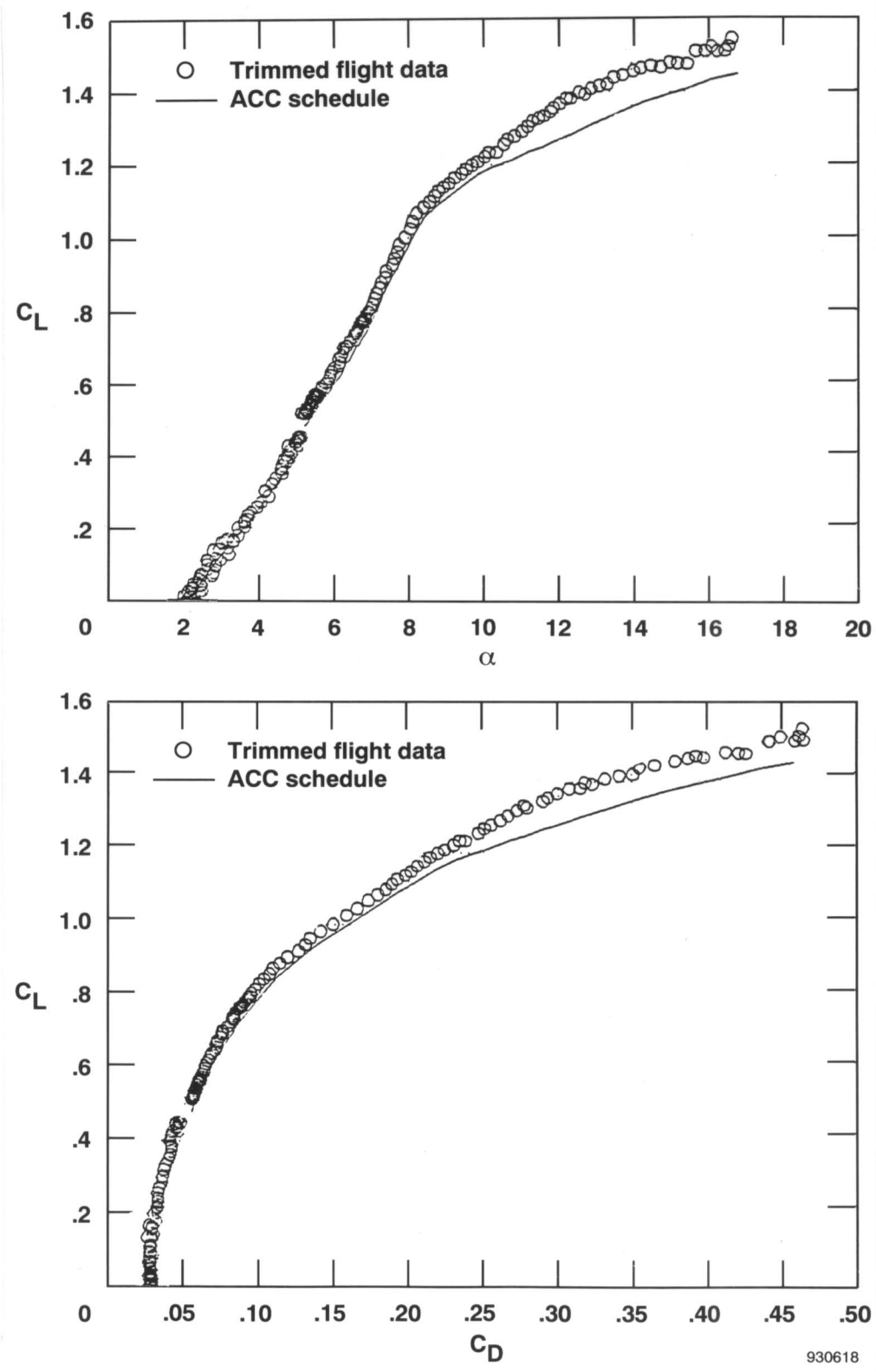

(b) $M = 0.60$. (Note: Units for α, above, are degrees.)

Figure 6. Continued.

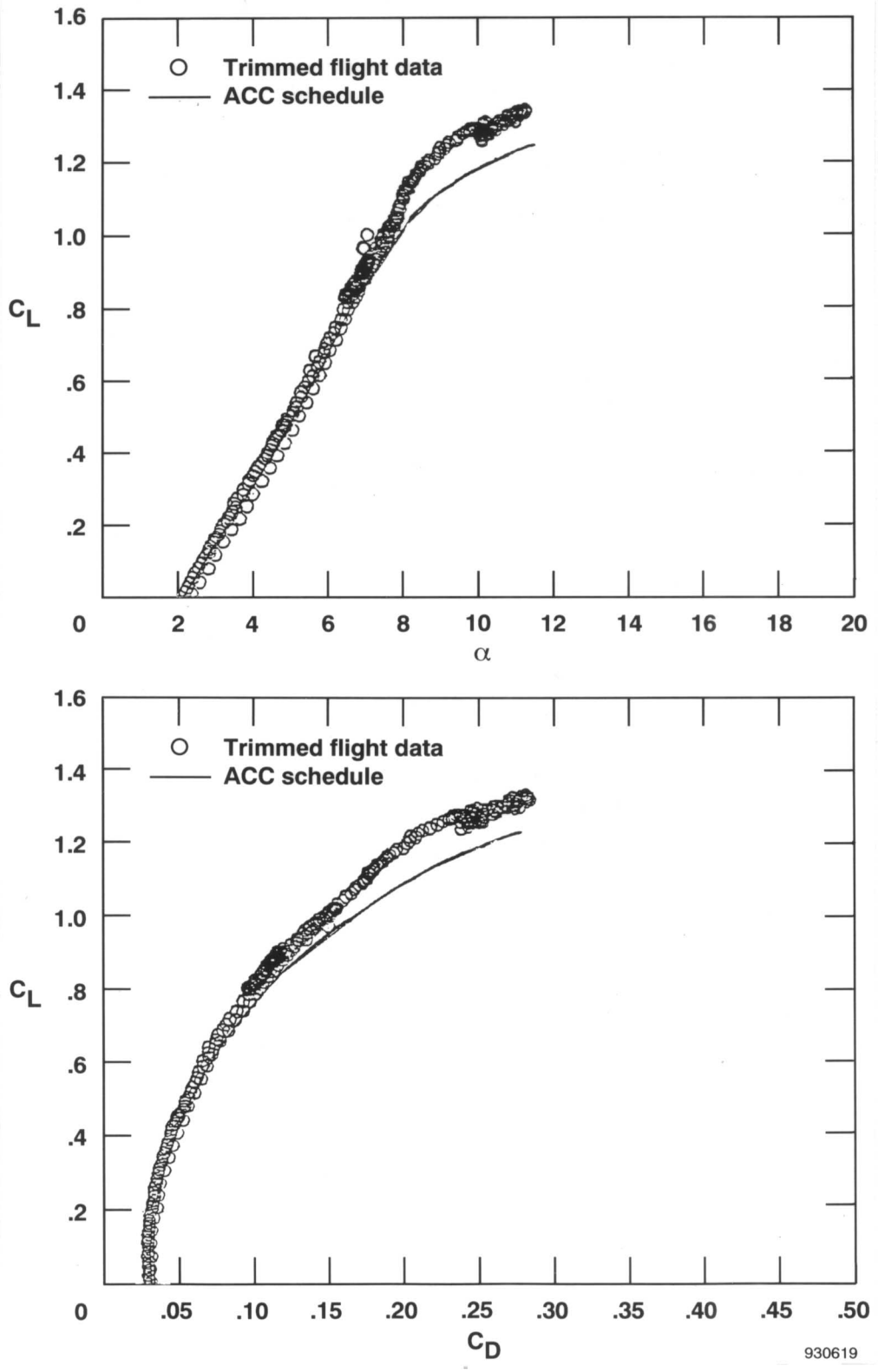

(c) $M = 0.70$. (Note: Units for α, above, are degrees.)

Figure 6. Continued.

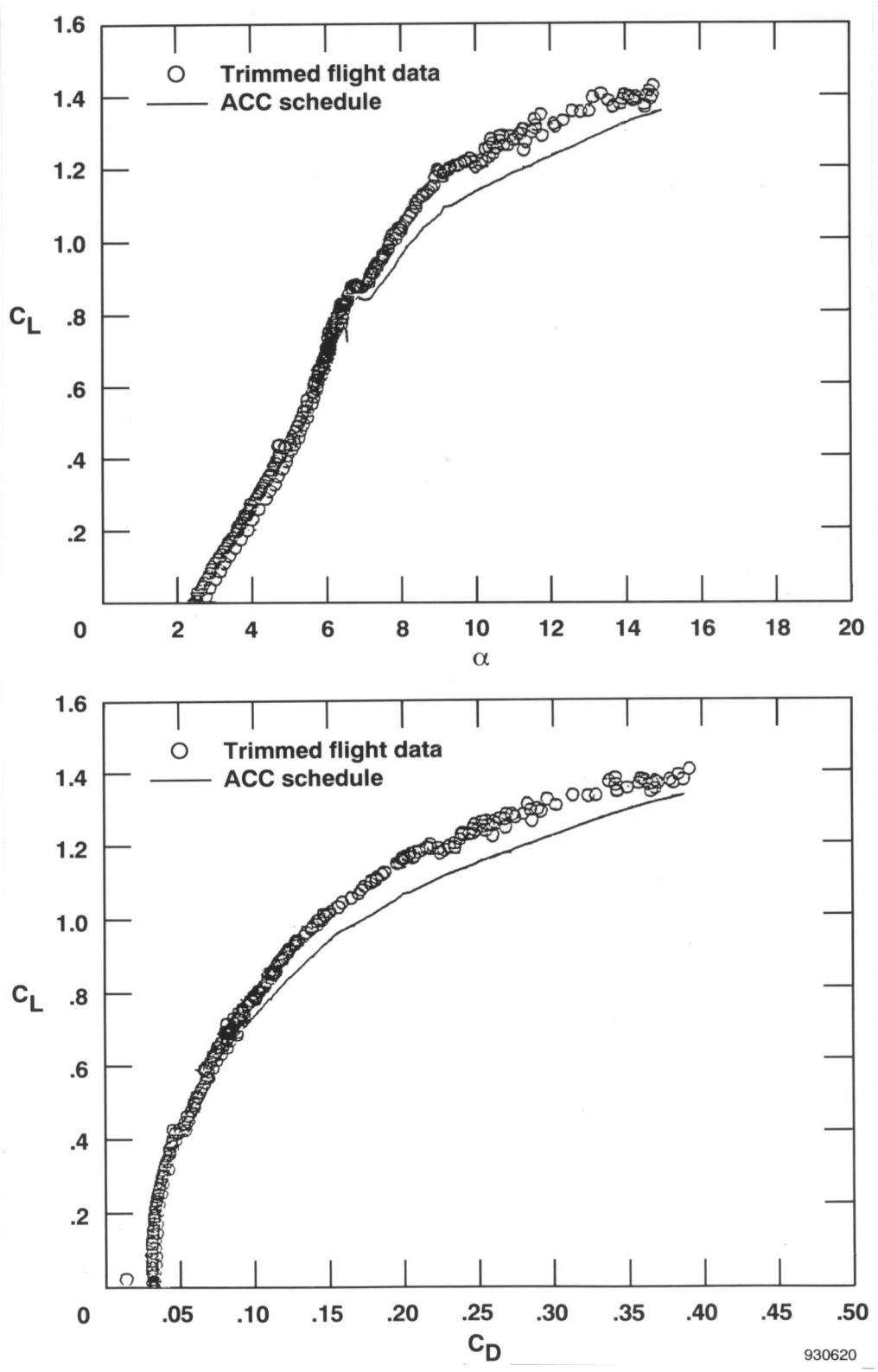

(d) $M = 0.80$. (Note: Units for α, above, are degrees.)

Figure 6. Continued.

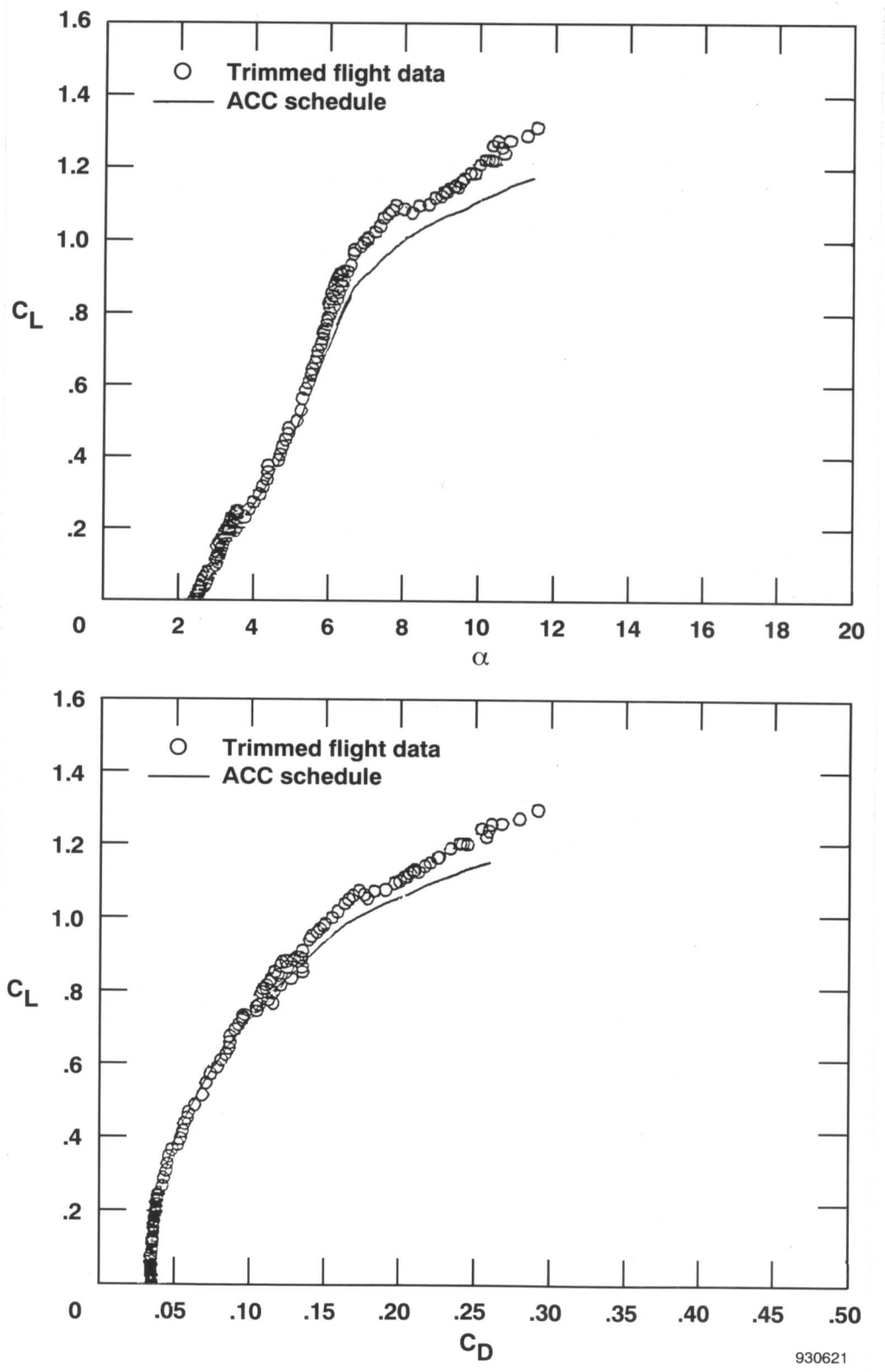

(e) $M = 0.90$. (Note: Units for α, above, are degrees.)

Figure 6. Continued.

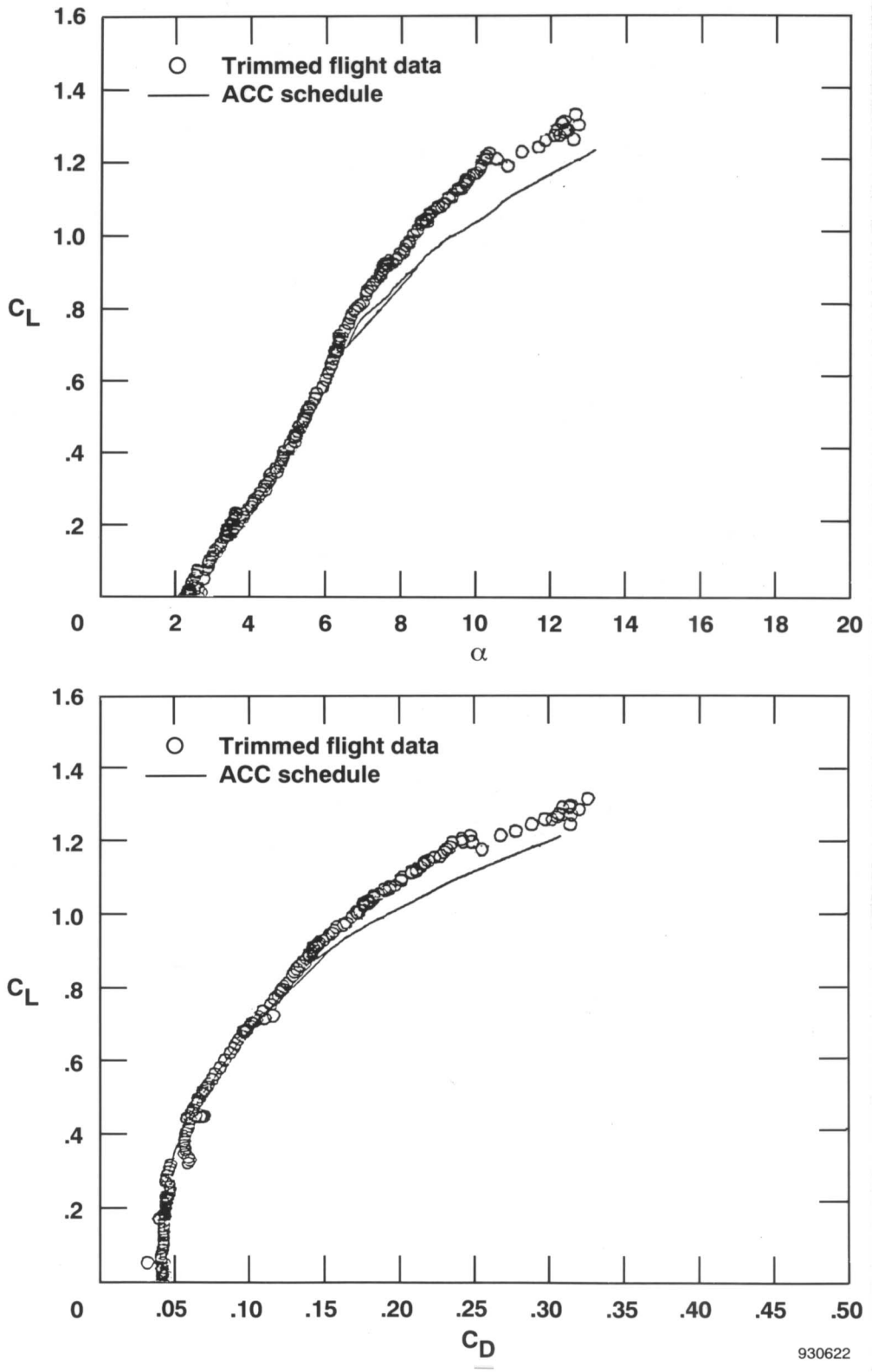

(f) $M = 0.95$. (Note: Units for α, above, are degrees.)

Figure 6. Continued.

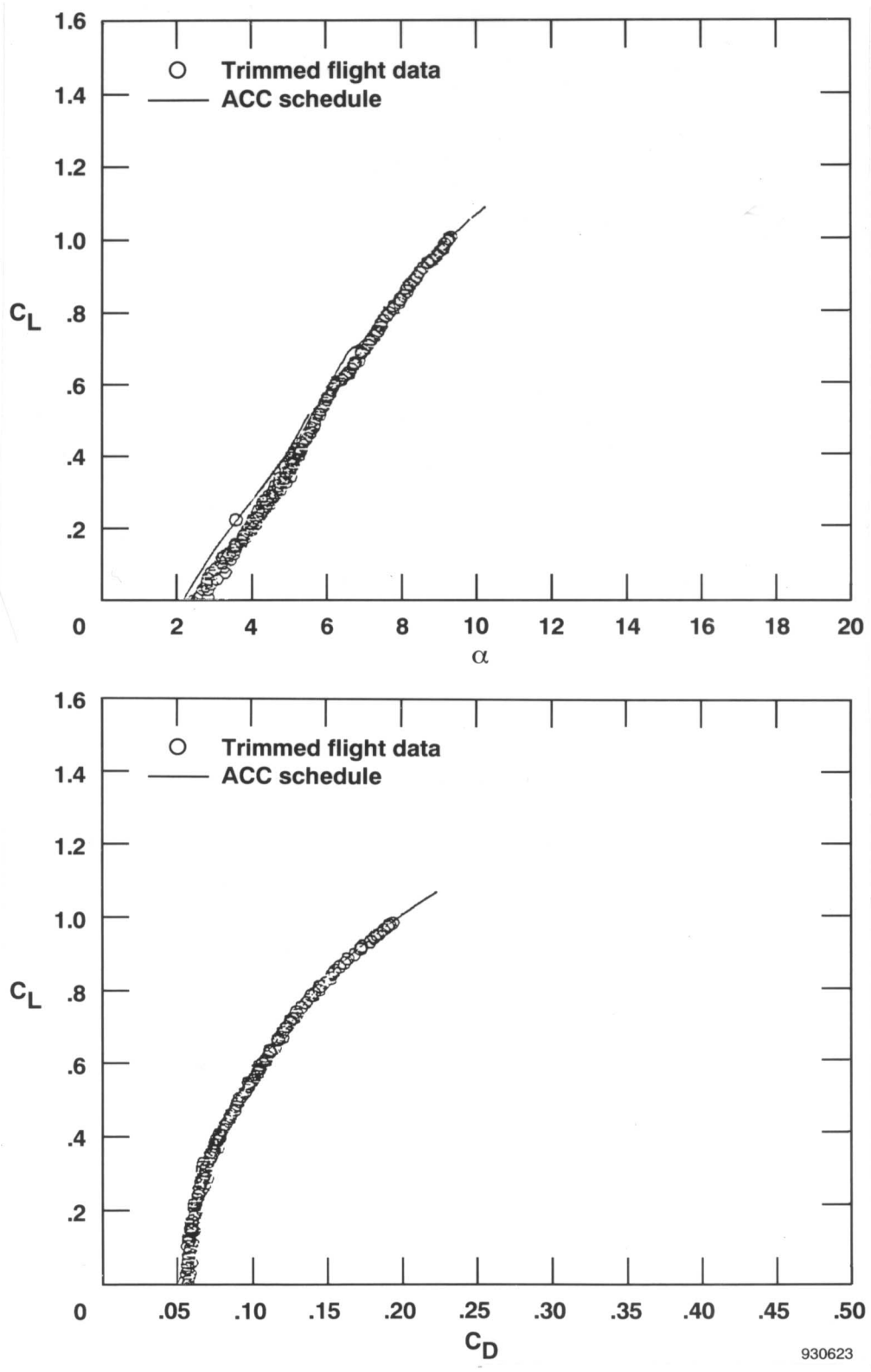

(g) $M = 1.05$. (Note: Units for α, above, are degrees.)

Figure 6. Continued.

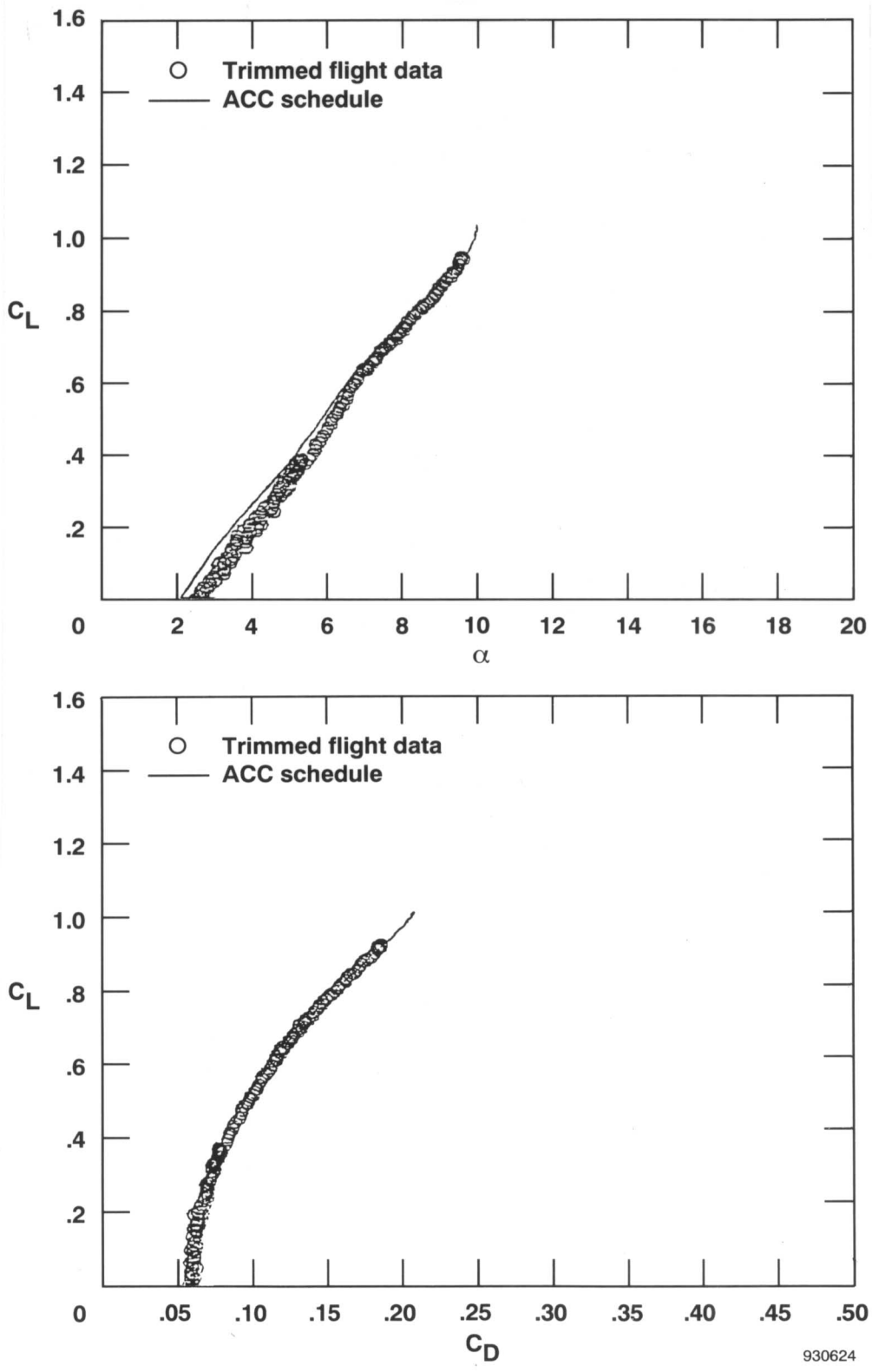

(h) $M = 1.10$. (Note: Units for α, above, are degrees.)

Figure 6. Continued.

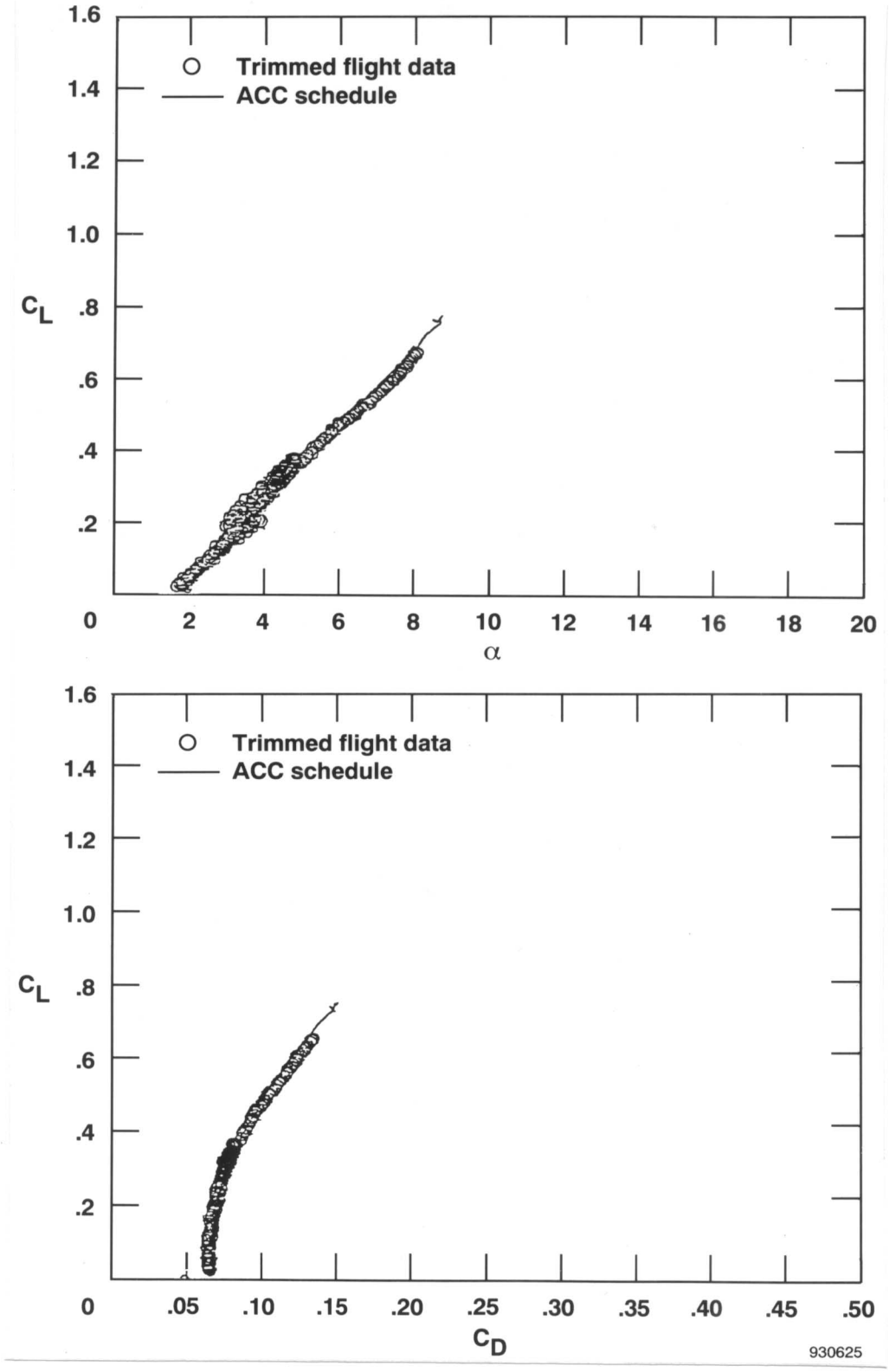

(i) $M = 1.20$. (Note: Units for α, above, are degrees.)

Figure 6. Continued.

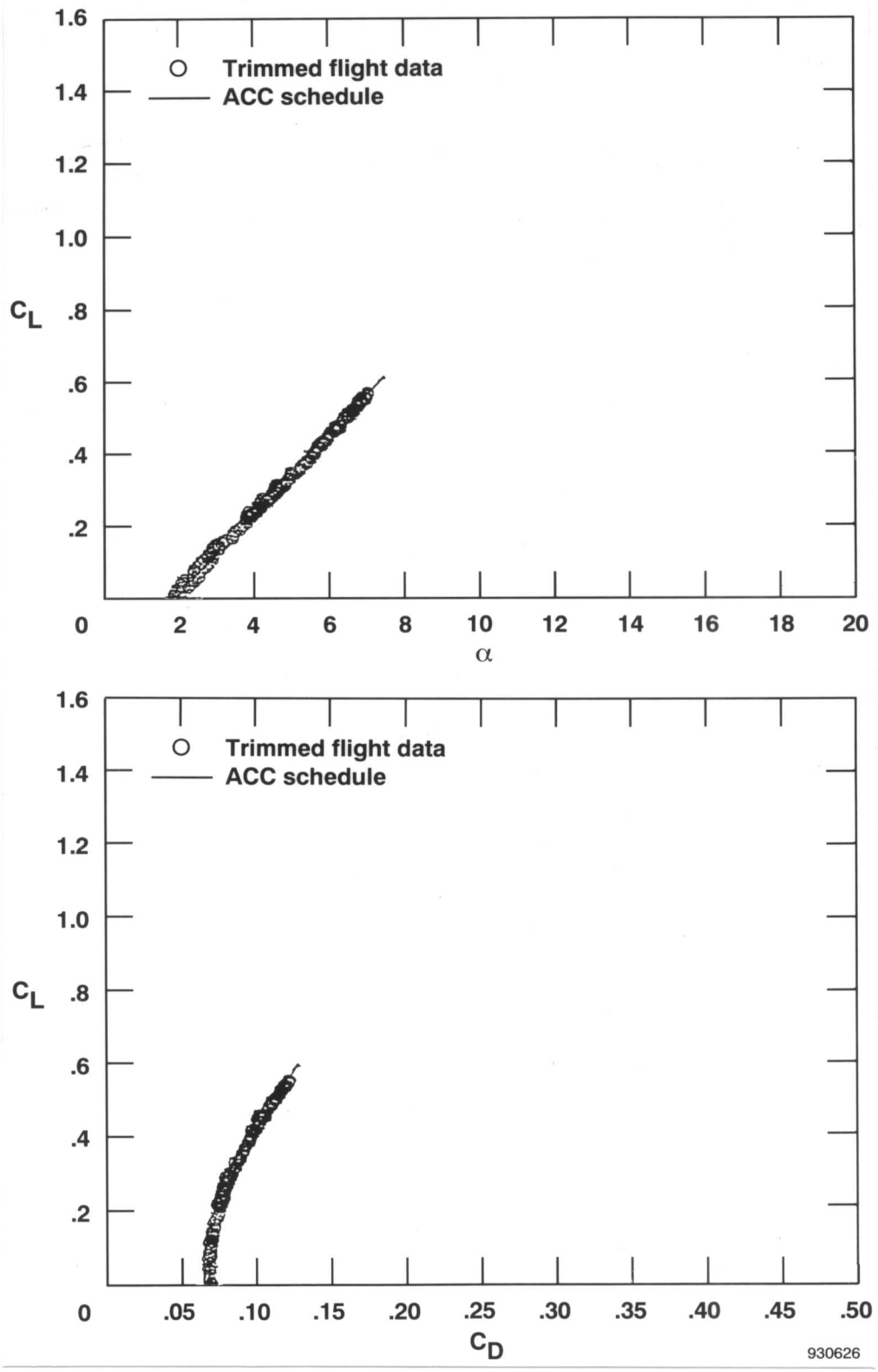

(j) $M = 1.30$. (Note: Units for α, above, are degrees.)

Figure 6. Concluded.

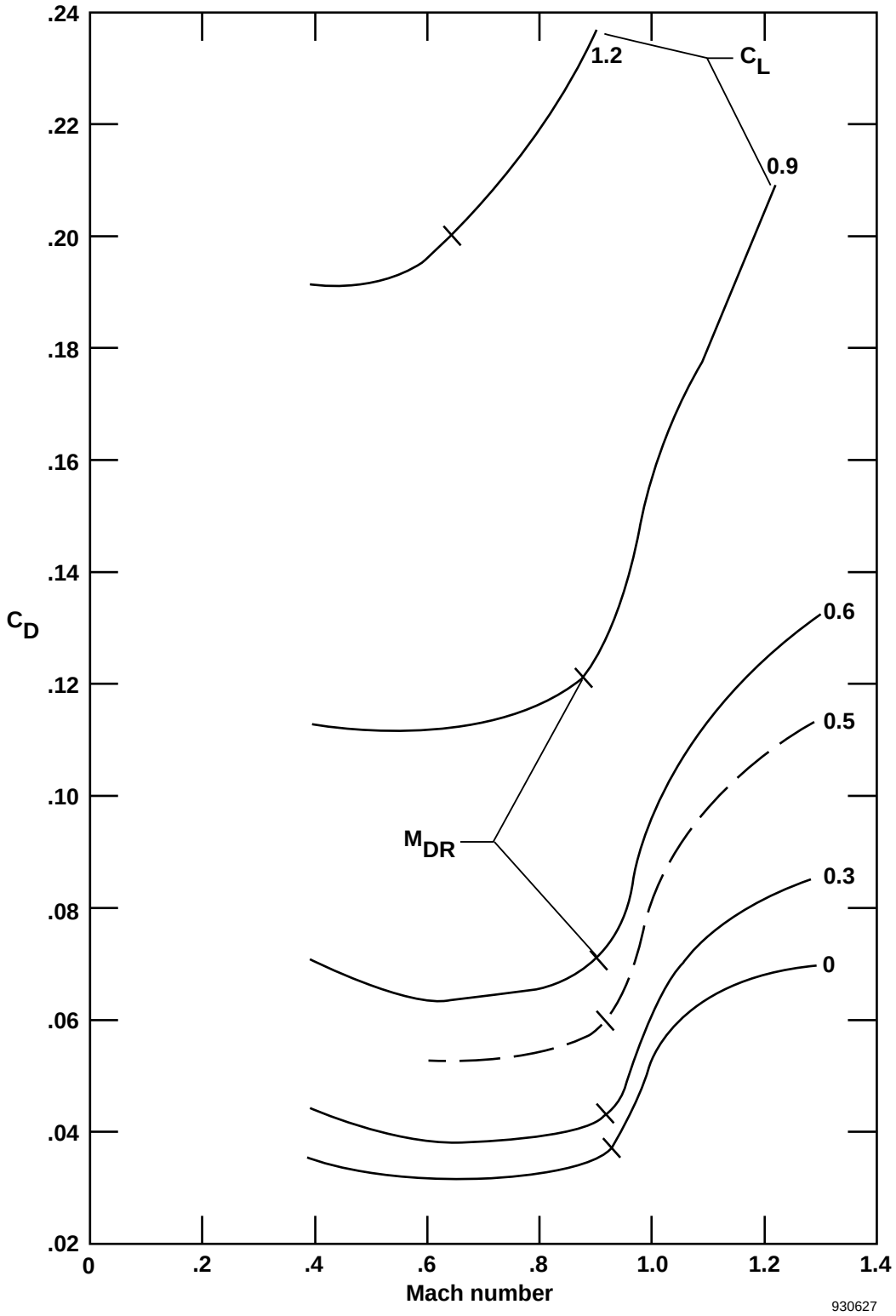

Figure 7. Variation of drag coefficient with Mach number for constant lift coefficient; trimmed flight, ACC mode.

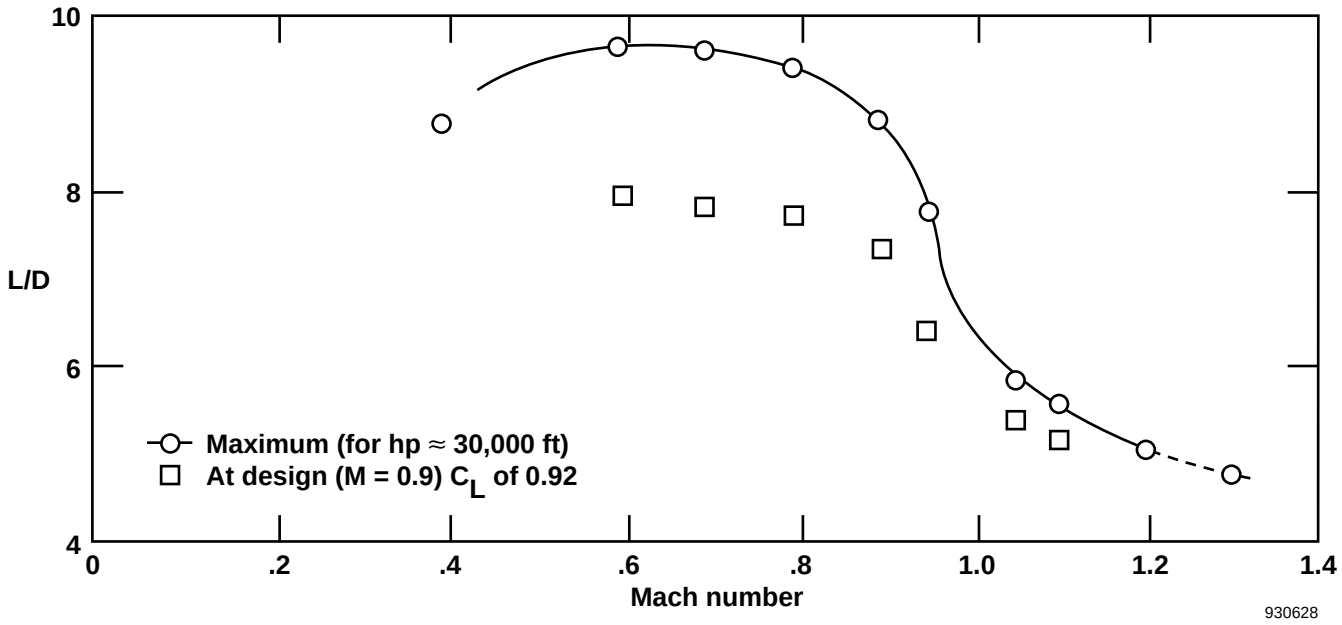

Figure 8. Variation of lift-drag ratio with Mach number; trimmed flight, ACC control mode.

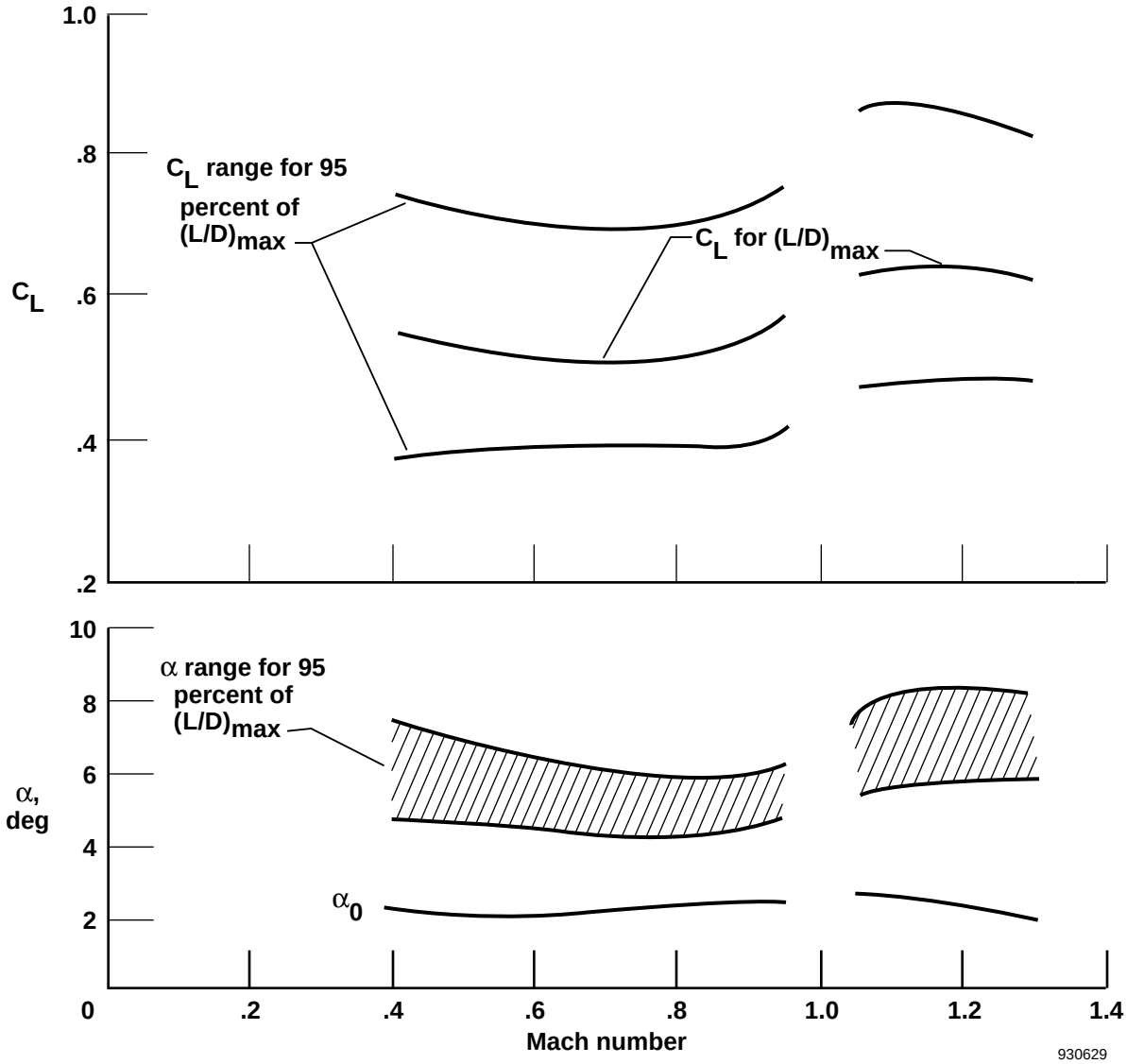

Figure 9. Lift coefficients and angles of attack that provide 95 to 100 percent of maximum lift-drag ratio; and angle of attack for zero-lift; trimmed flight in ACC mode.

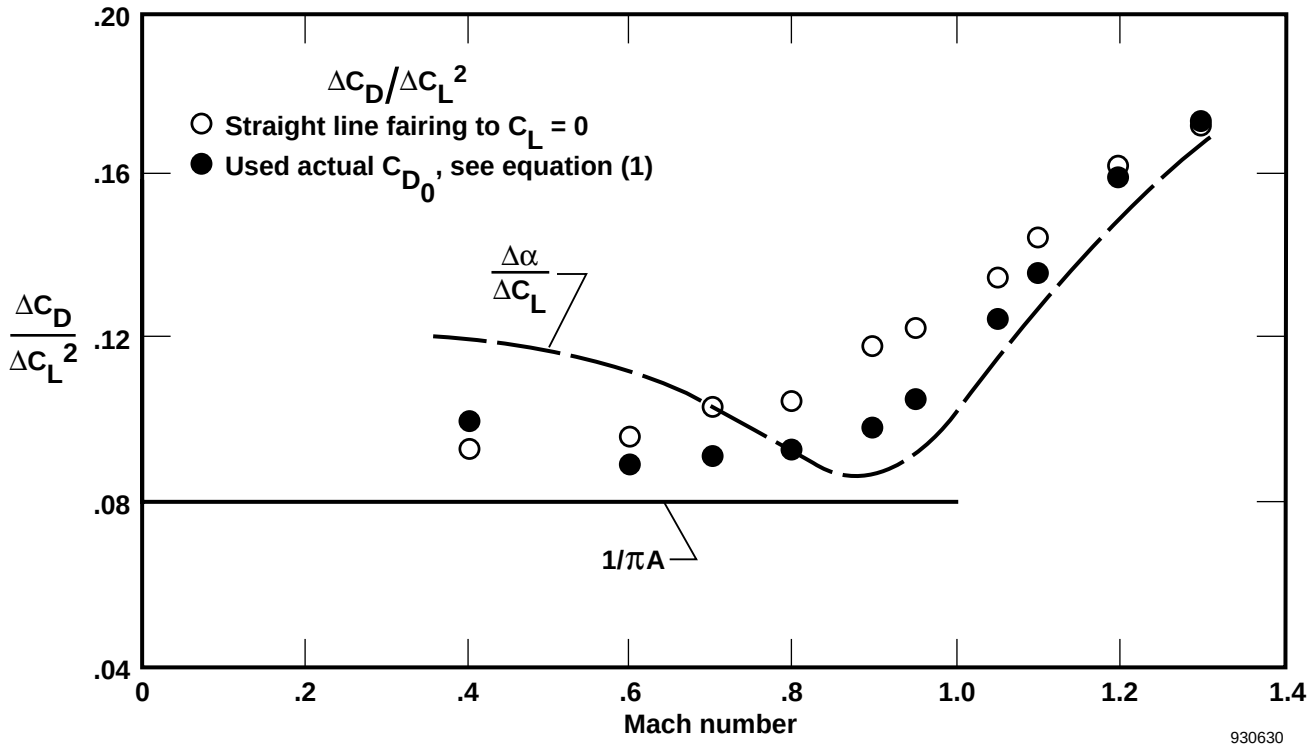

Figure 10. Variation of drag-due-to-lift factor with Mach number; trimmed flight, ACC mode.

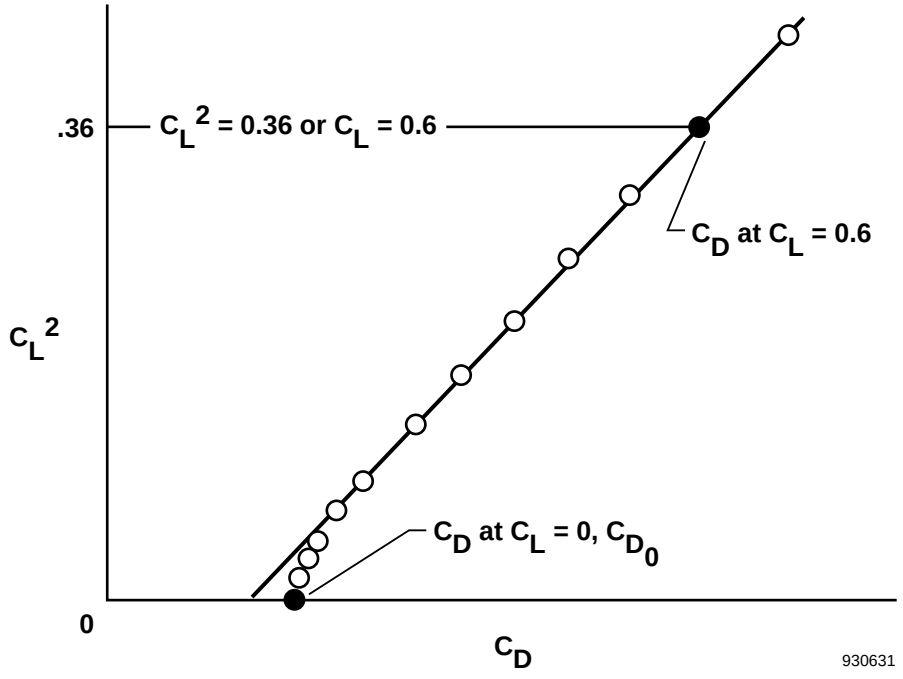

Figure 11. The $C_L{}^2$–C_D relationship for illustrating the origin of two definitions of drag-due-to-lift factor for a constant Mach number.

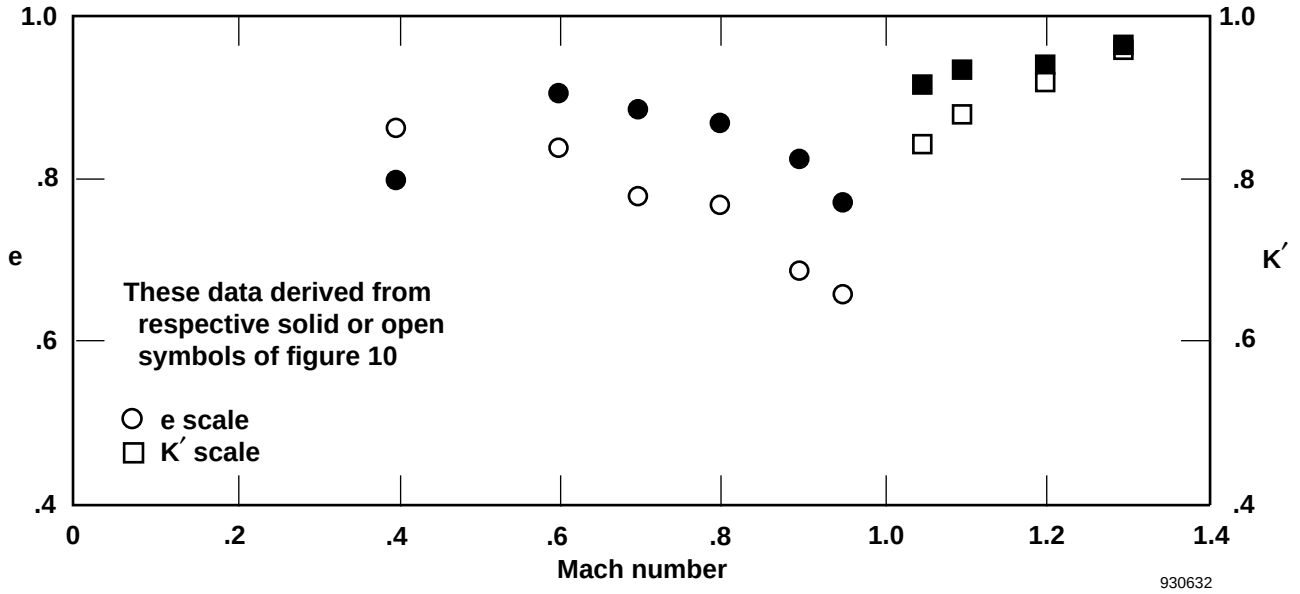

Figure 12. Variation of airplane lifting efficiency factors, e and K', with Mach number; trimmed flight, ACC mode.

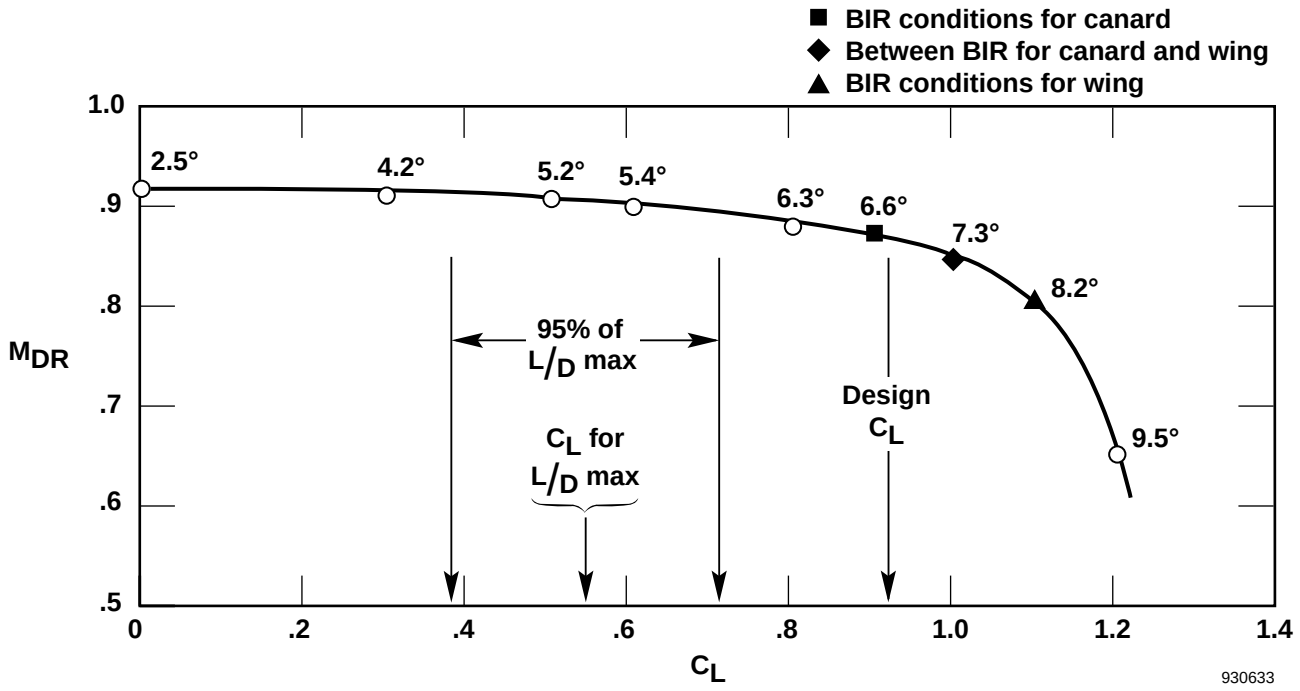

Figure 13. Relationship of drag-rise Mach number with C_L, angle of attack, and some secondary flight conditions; ACC mode.

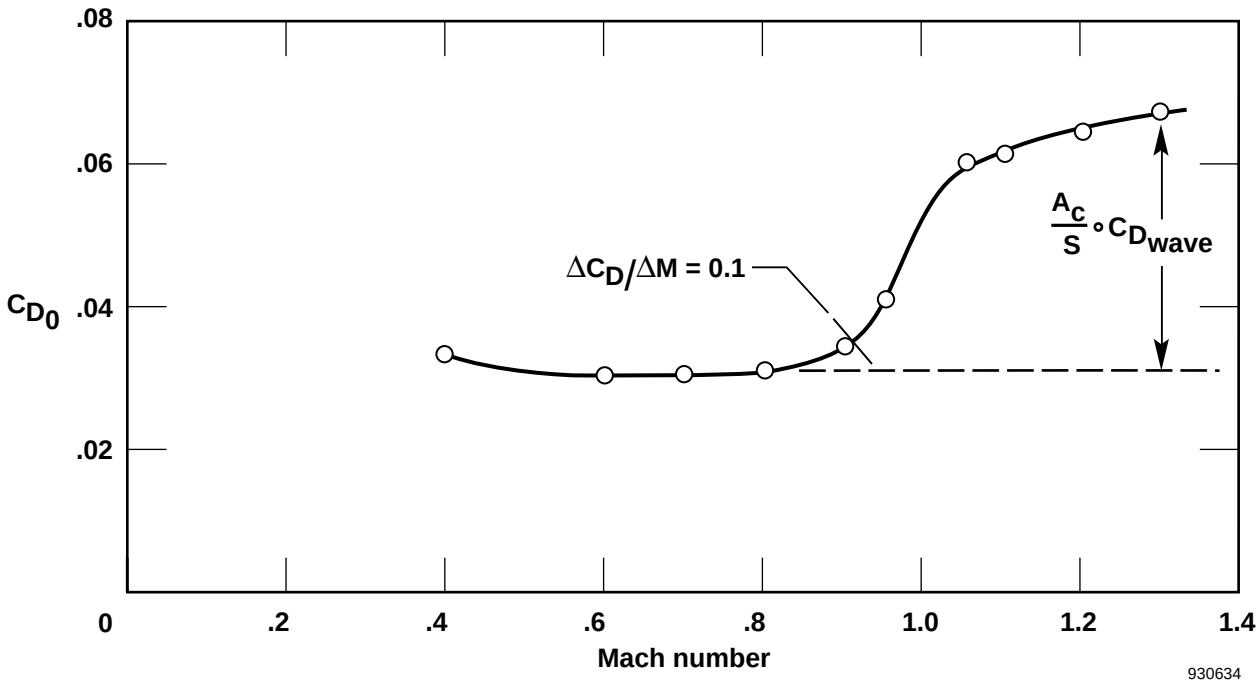

Figure 14. Variation of zero-lift-drag coefficient with Mach number and illustration of transonic wave drag increment; trimmed flight, ACC mode.

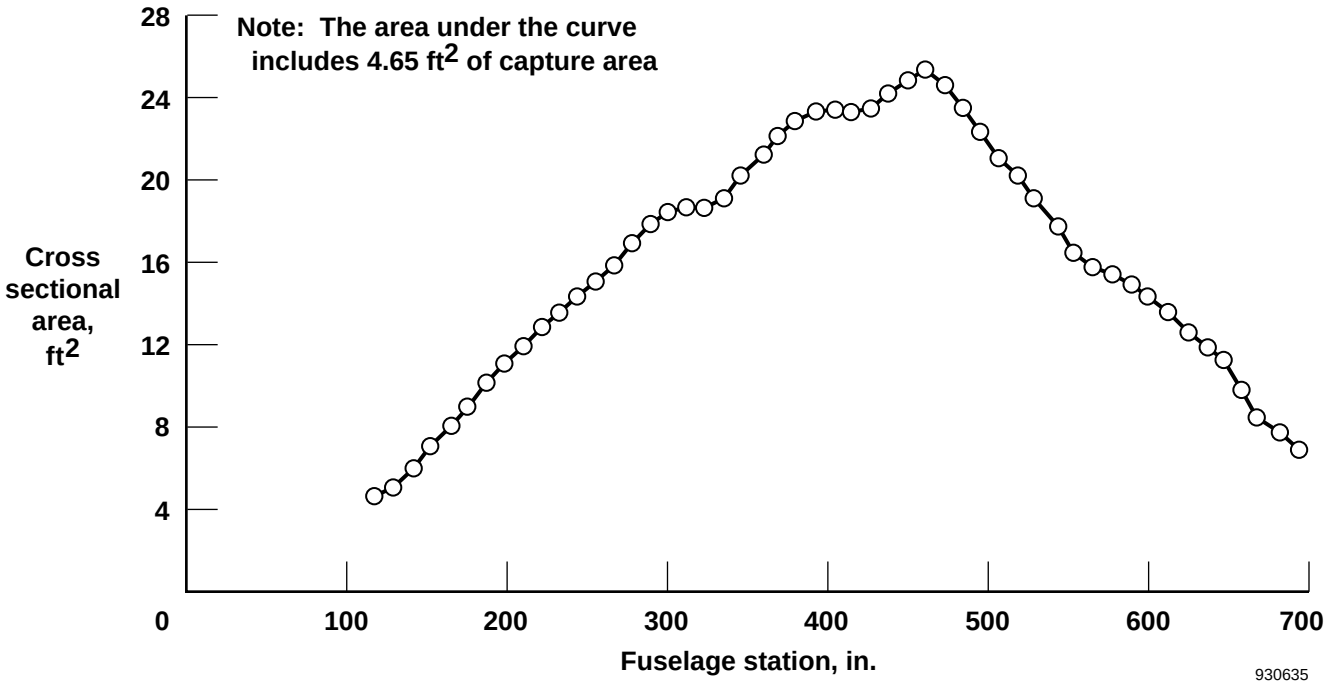

Figure 15. X-29A cross-sectional area distribution.

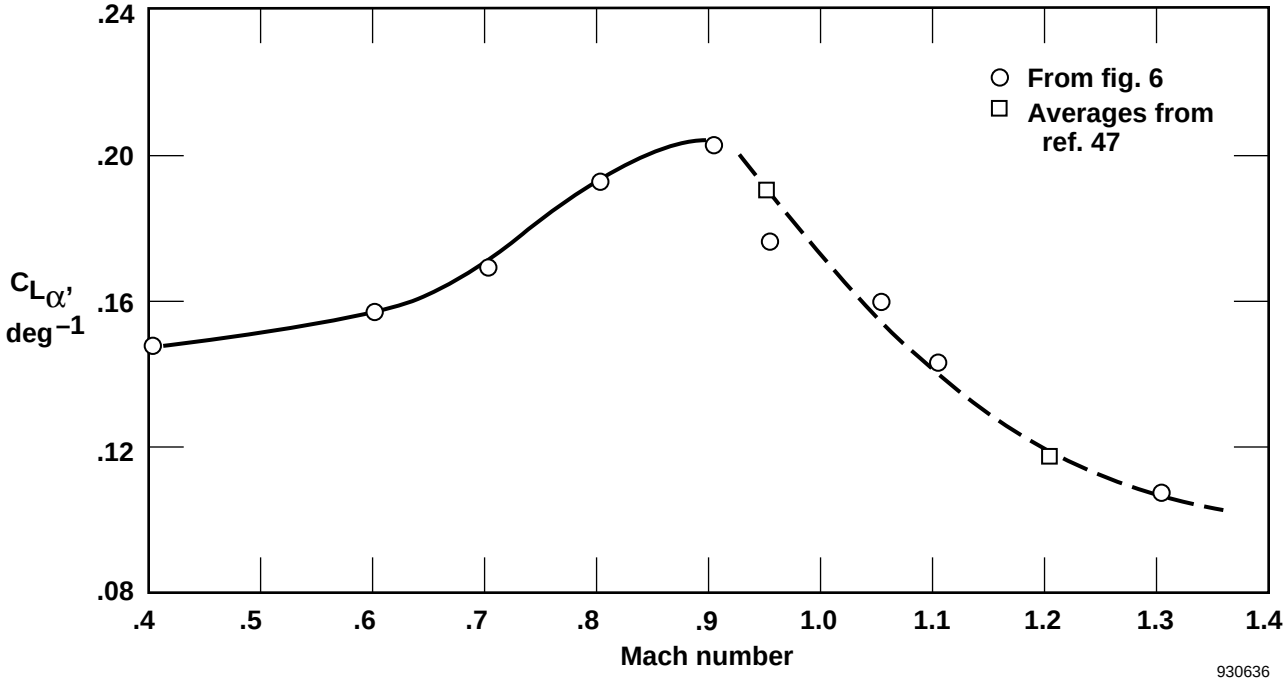

Figure 16. Variation of lift-curve slope with Mach number; trimmed flight, ACC mode

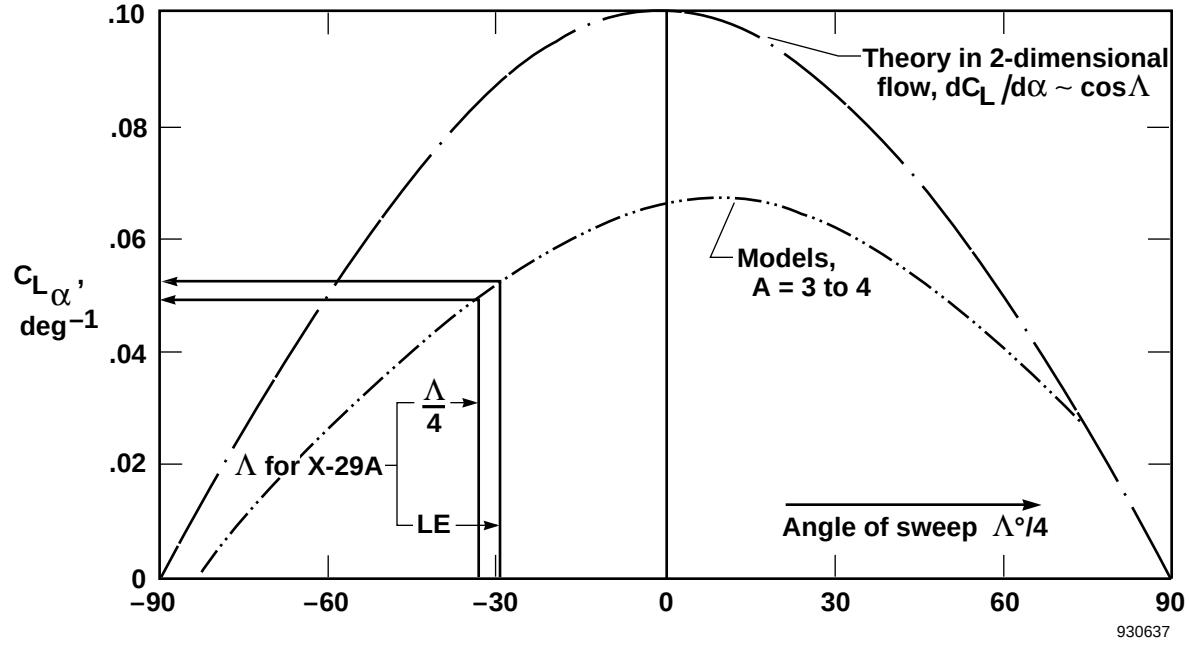

Figure 17. Lift-curve slopes of wings having aspect ratios between 3 and 4 (ref. 27).

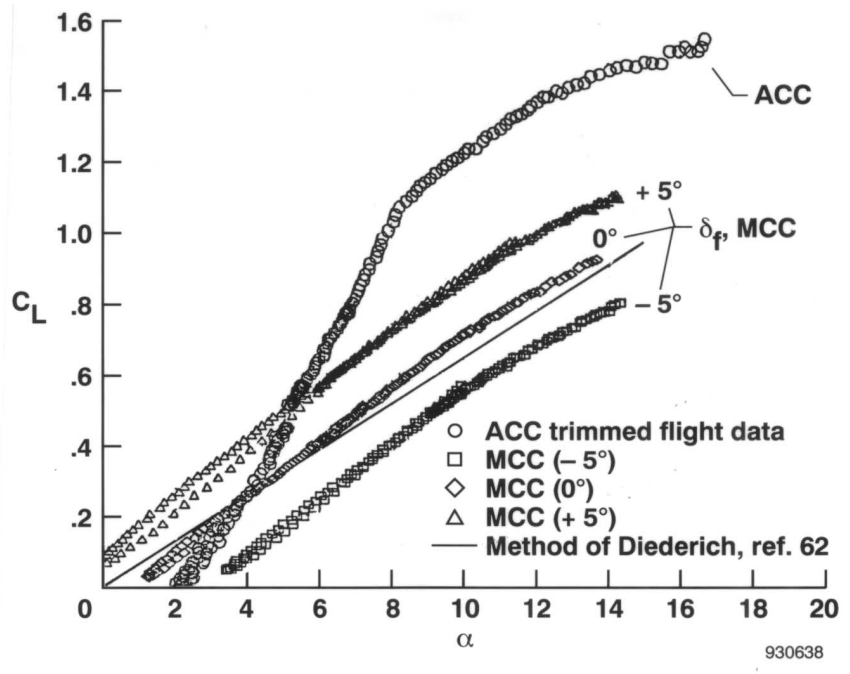

(a) Lift-curve.

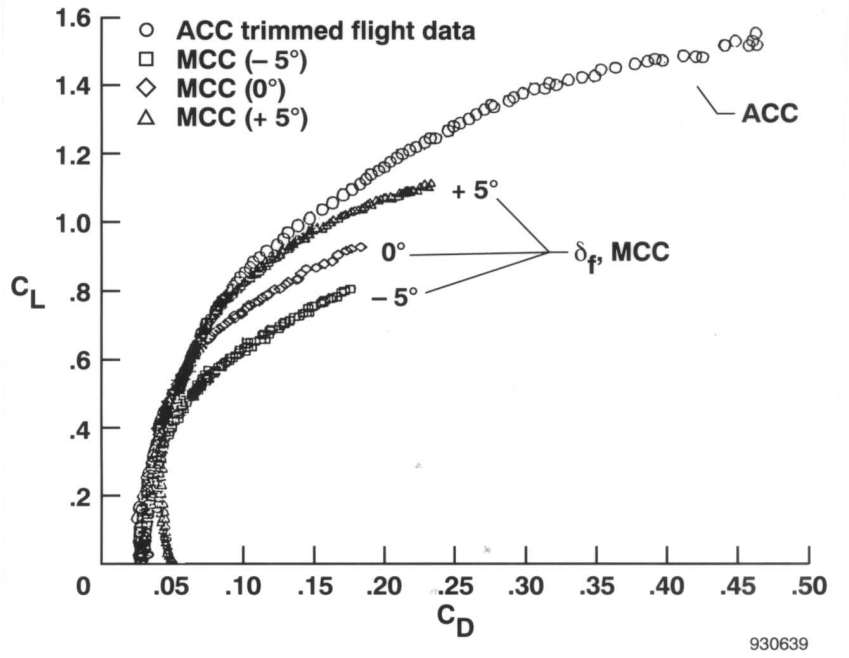

(b) Drag polar.

Figure 18. Comparison of results from ACC and MCC modes for X-29A at $M = 0.6$ and $h = 30{,}000$ ft (MCC also trimmed flight data).

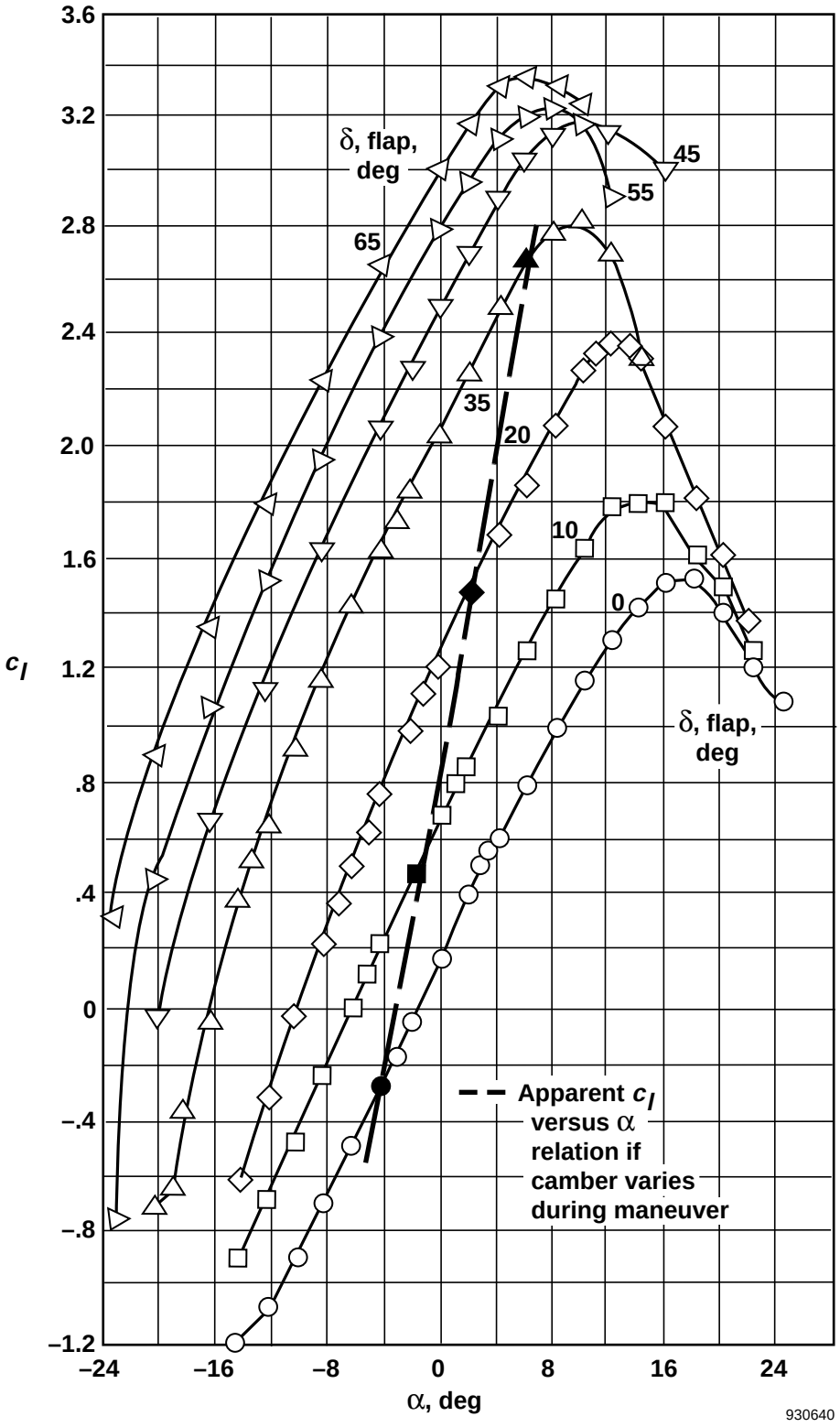

Figure 19. NACA airfoil section with 0.309c double-slotted flap (low speed) (ref. 63).

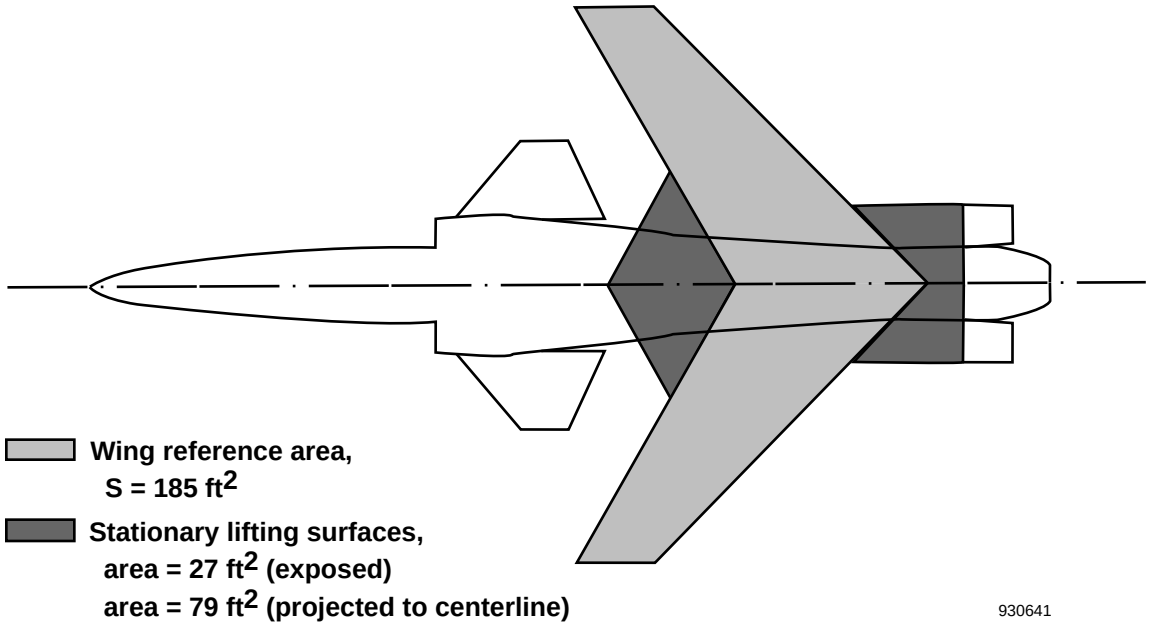

Figure 20. Planform view of X-29A airplane.

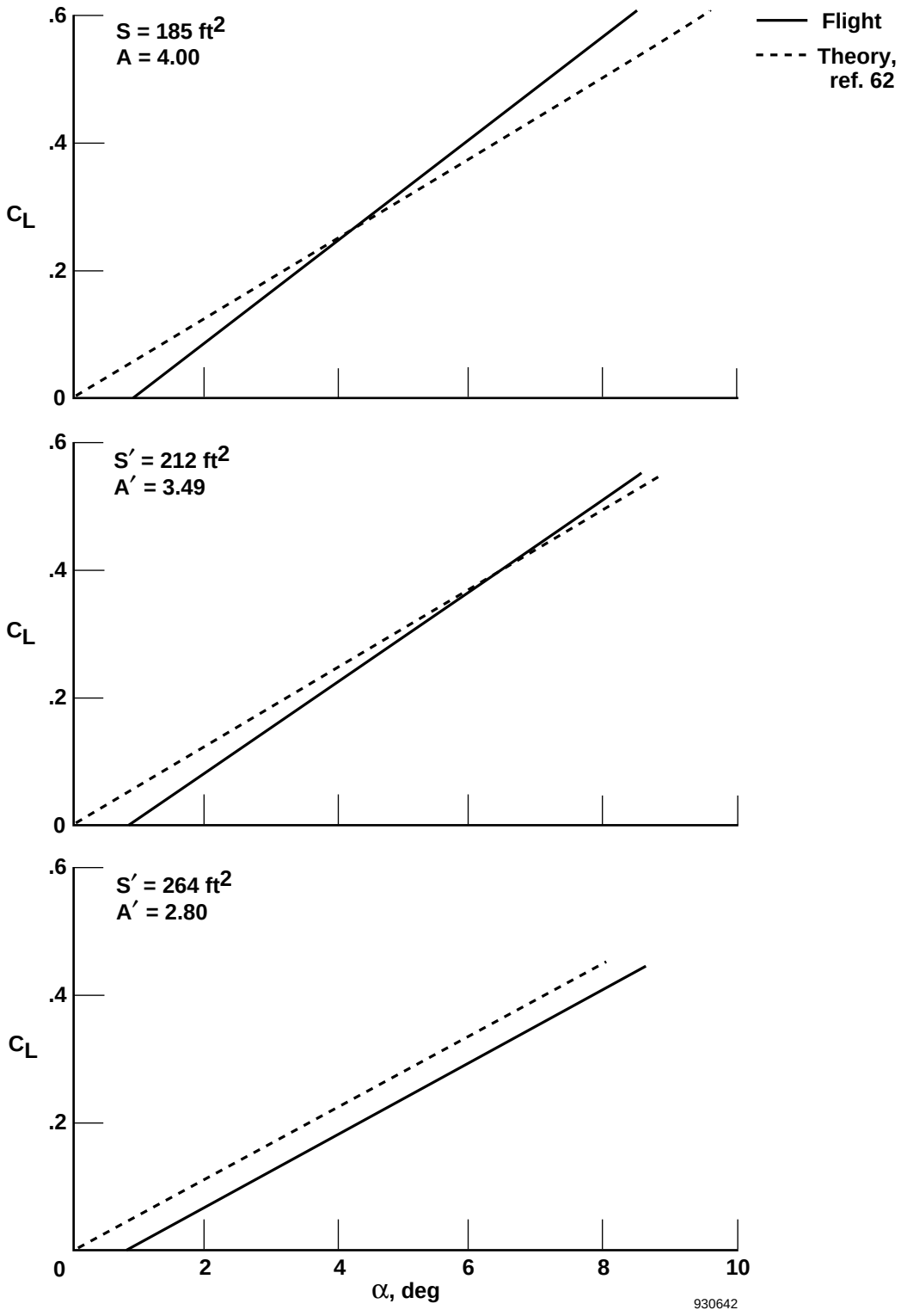

Figure 21. Comparison of flight-measured lift-curve with theory for three reference areas; M = 0.6, δ_f = 0°; X-29A in MCC mode.

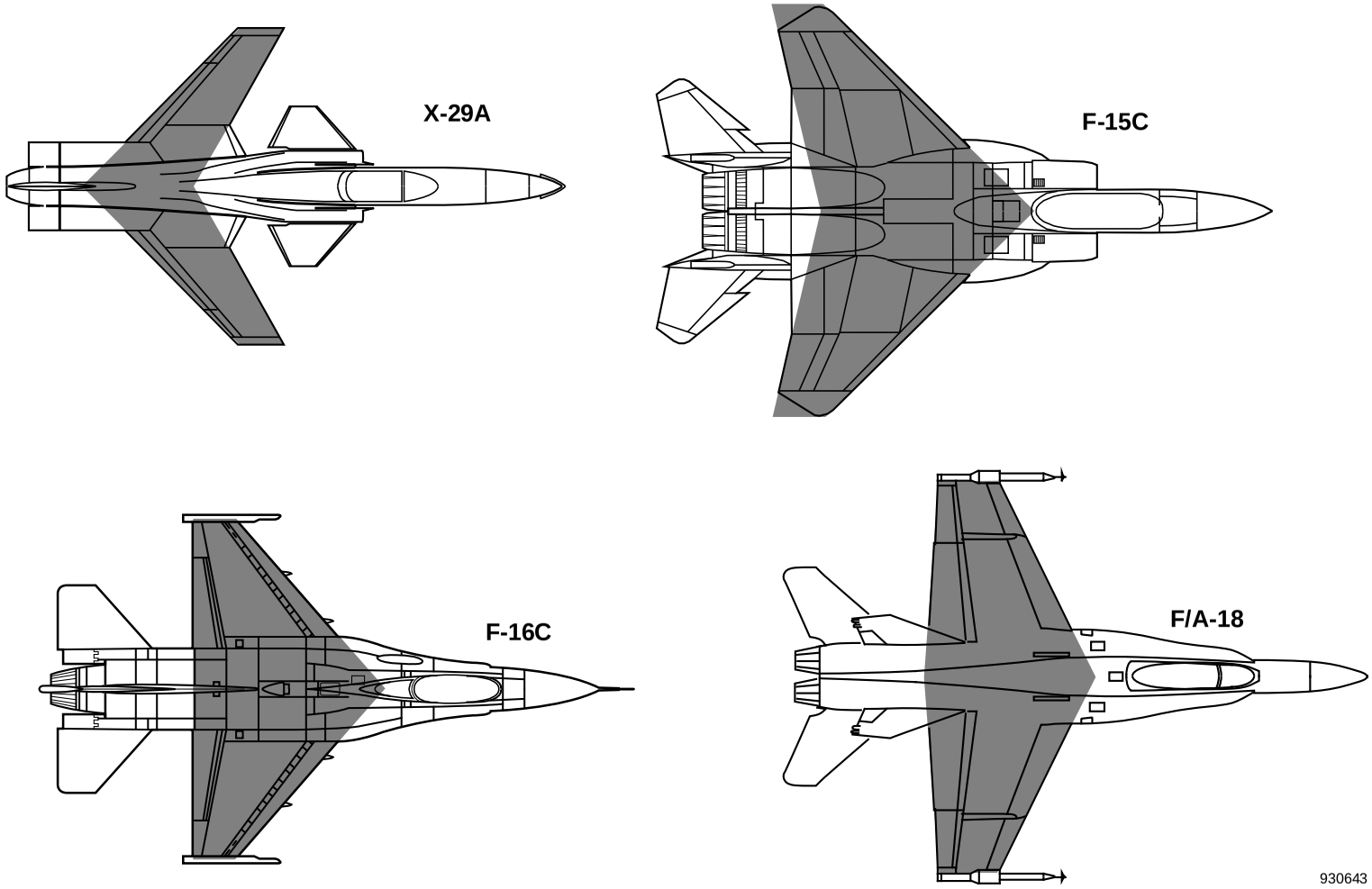

Figure 22. Planforms of X-29A and three contemporary aircraft; scale of each configuration is approximately correct; reference area, *S*, defined by shaded region.

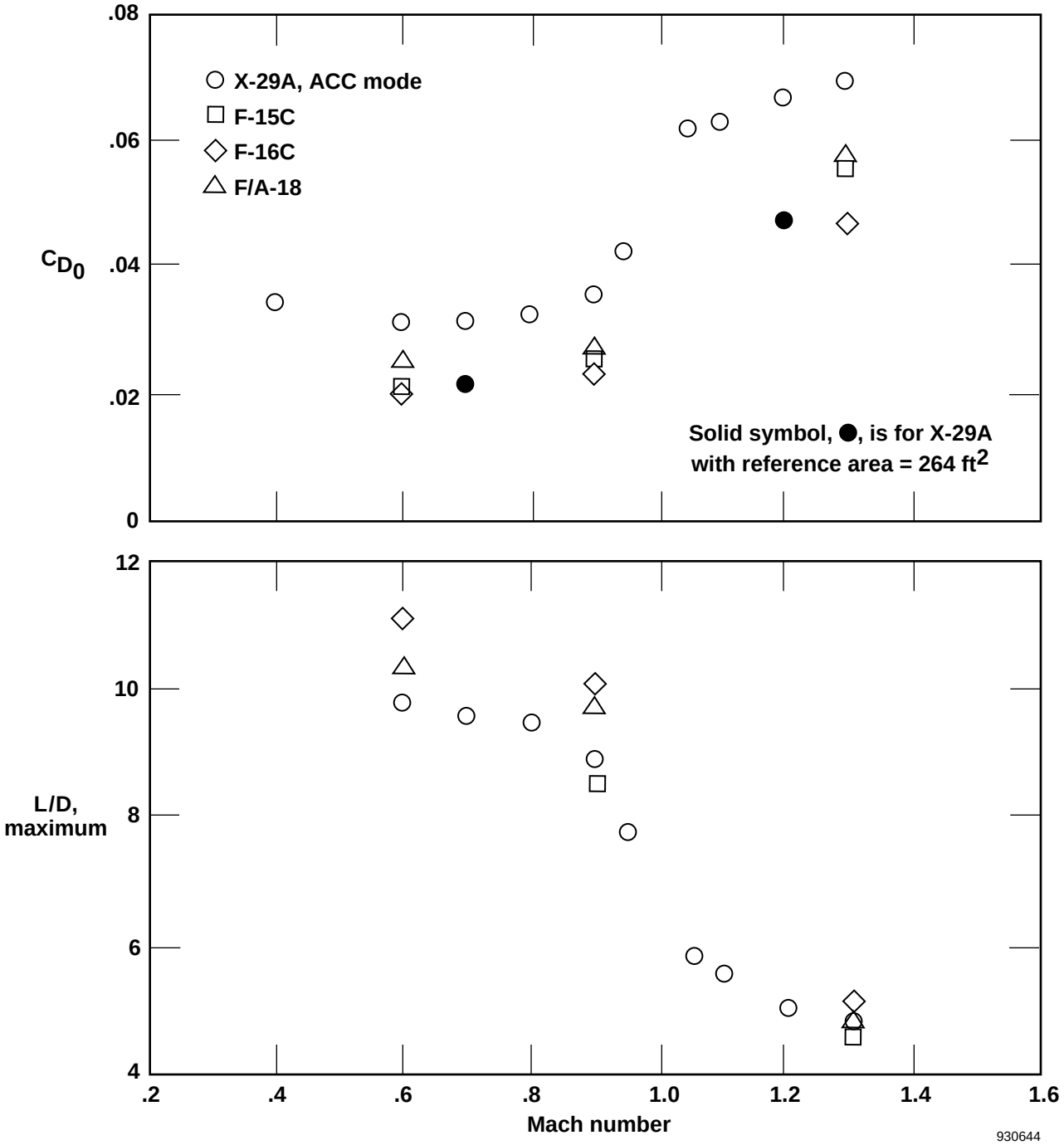

Figure 23. Variation of zero-lift-drag coefficient and maximum *L/D* with Mach number for X-29A and three contemporary aircraft.

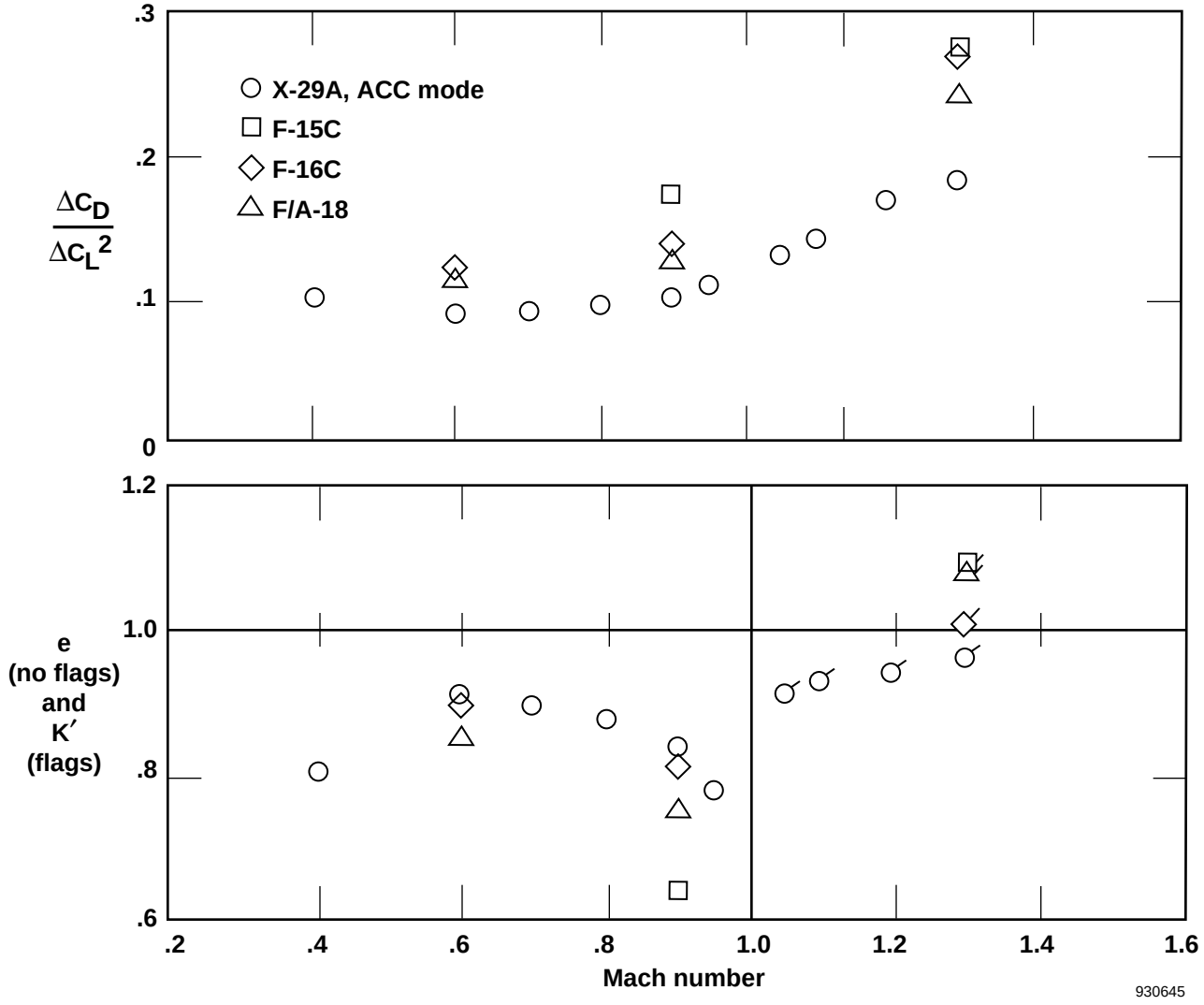

Figure 24. Variation of drag-due-to-lift factor and lifting efficiency factors (e and K') with Mach number for X-29A and three contemporary aircraft.

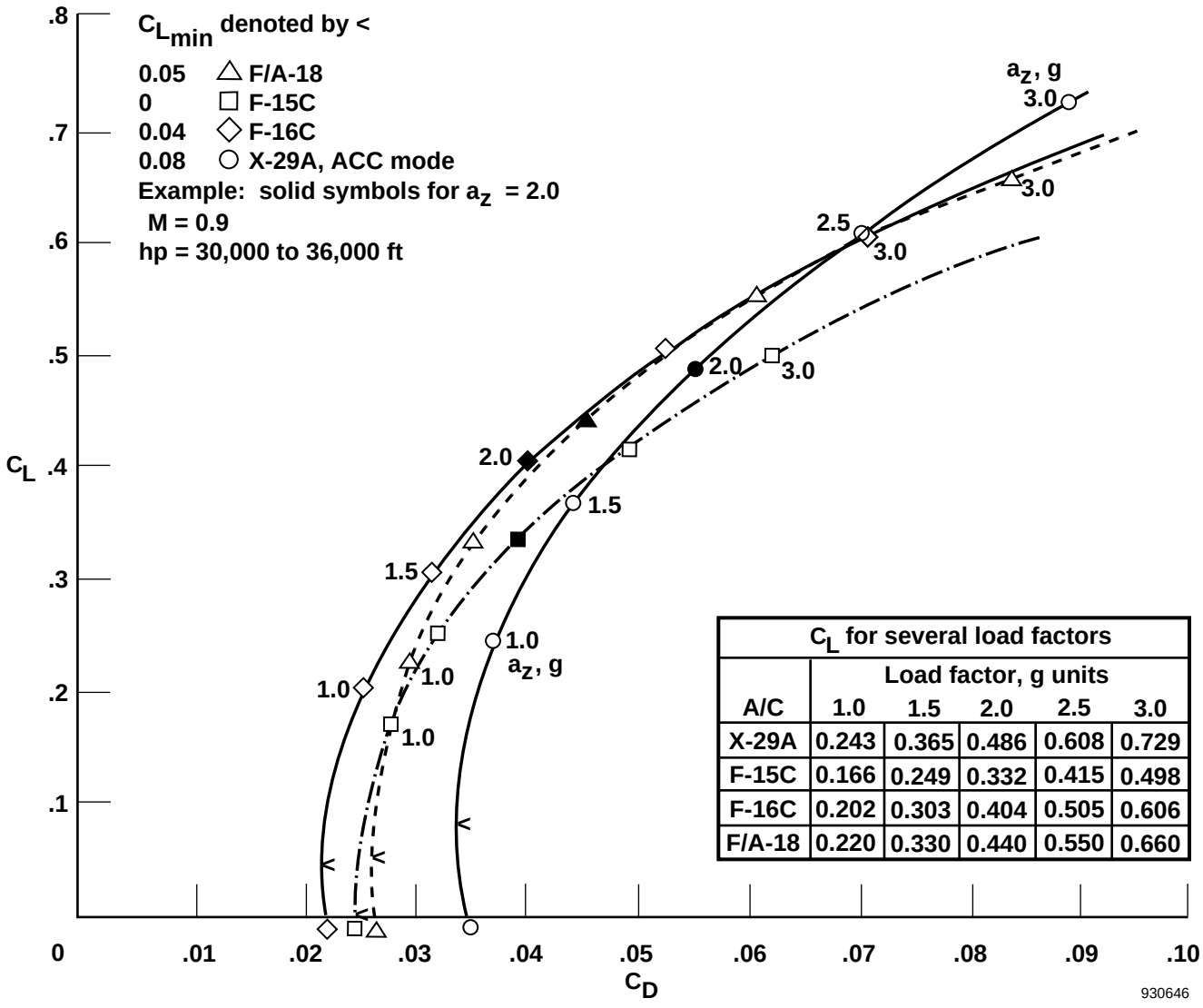

C_L for several load factors					
	Load factor, g units				
A/C	1.0	1.5	2.0	2.5	3.0
X-29A	0.243	0.365	0.486	0.608	0.729
F-15C	0.166	0.249	0.332	0.415	0.498
F-16C	0.202	0.303	0.404	0.505	0.606
F/A-18	0.220	0.330	0.440	0.550	0.660

Figure 25. Relationship of lift and drag coefficients for contemporary aircraft at several constant load factors.

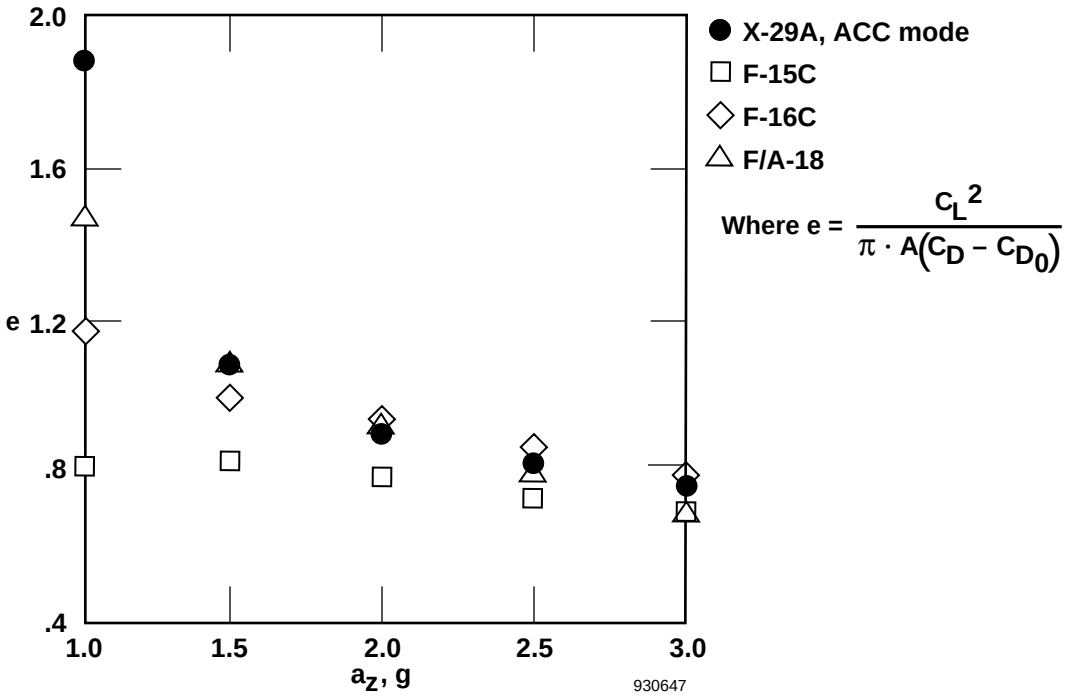

(a) Asymmetric polars for X-29A, F/A-18, and F-16C.

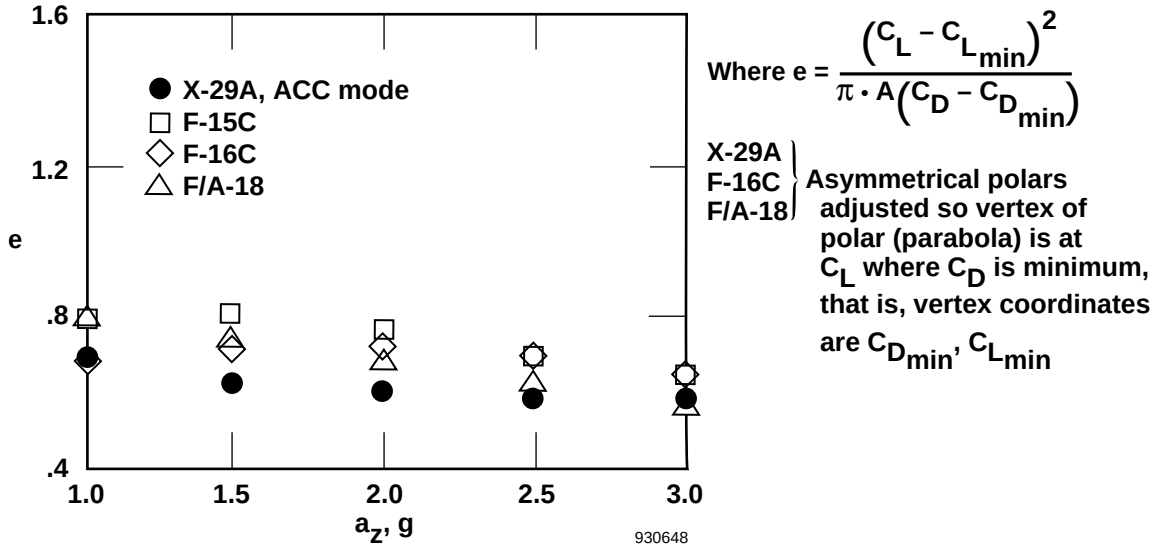

(b) Values of *e* when all polars symmetrical.

Figure 26. Variation of efficiency parameters *e* and *L/D* with load factor for four contemporary aircraft; $M = 0.90$.

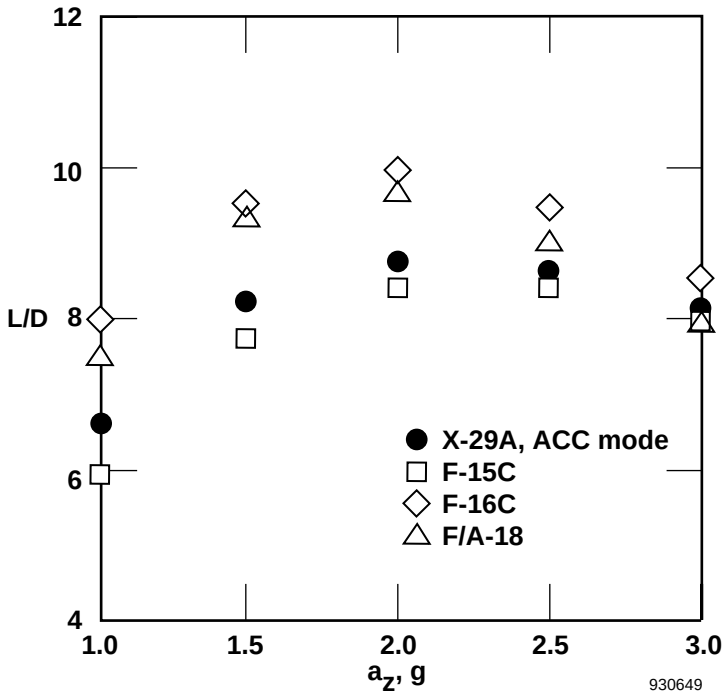

(c) Variation of *L/D* with load factor.

Figure 26. Concluded.

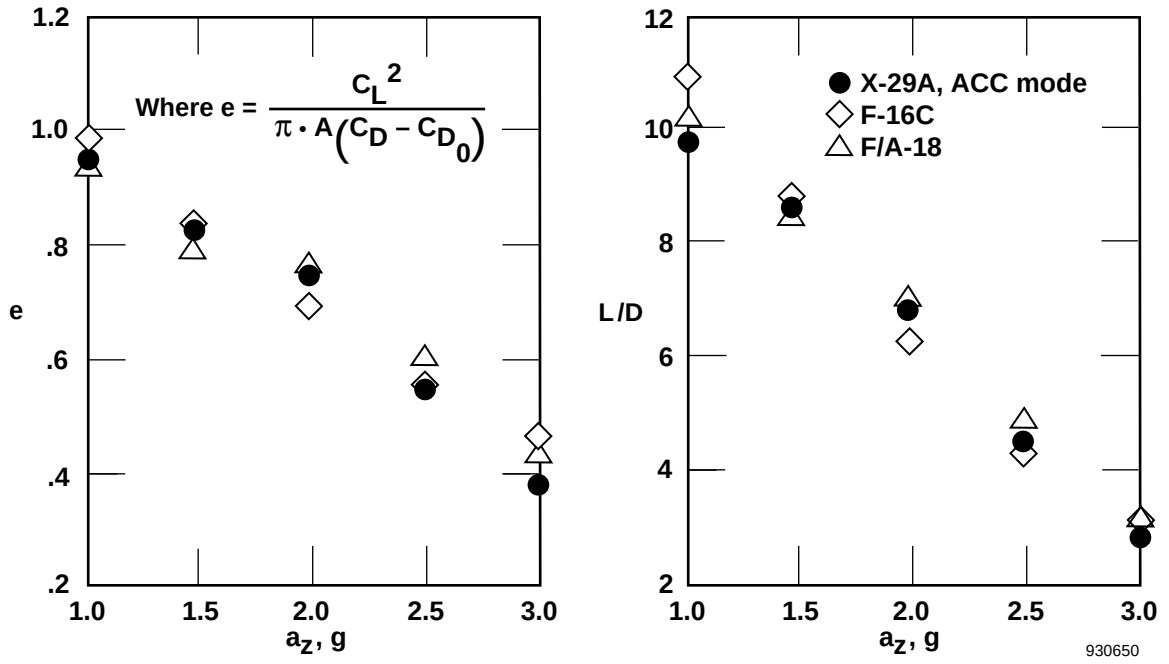

Figure 27. Variation of efficiency parameters *e* and *L/D* with load factor for three contemporary aircraft; *M = 0.60*.

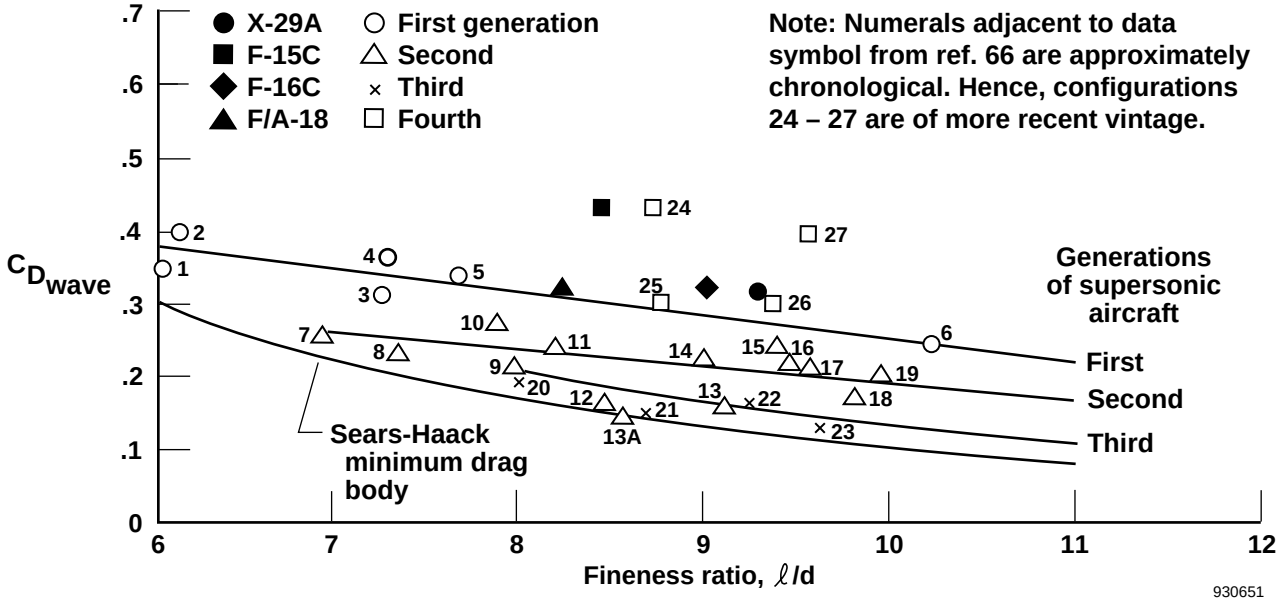

Figure 28. Comparision of transonic wave drag as determined for X-29A and three contemporary aircraft, with correlation of reference 66.

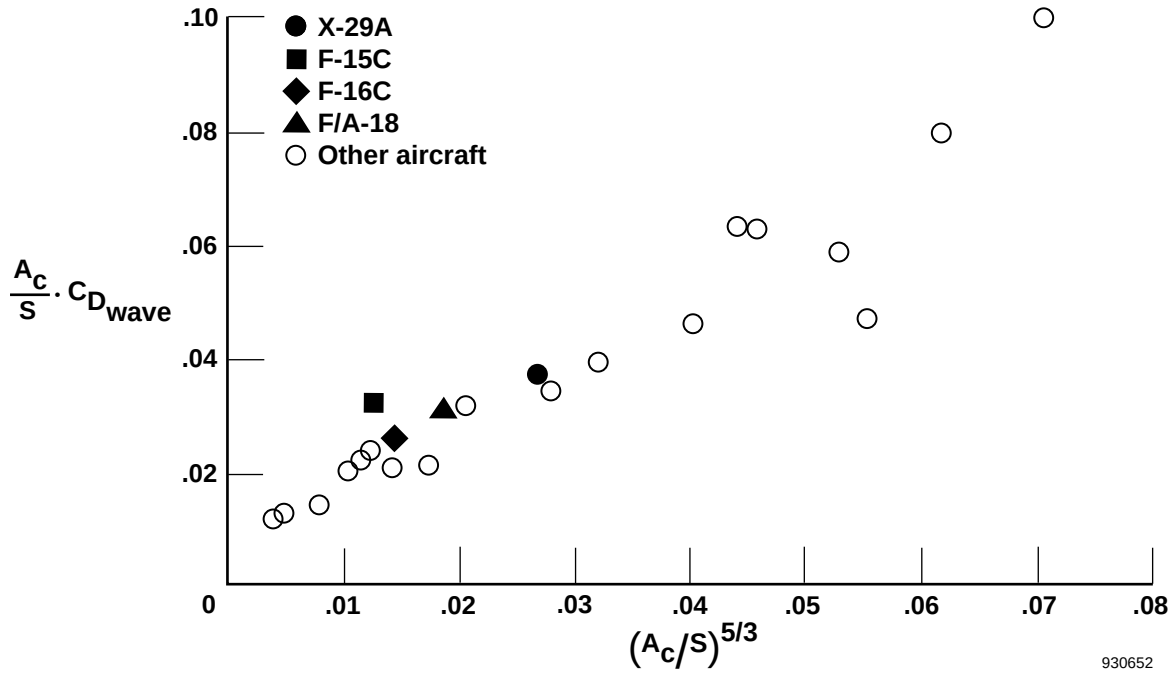

Figure 29. Relationship of wave drag increment to reference-area ratio factor for X-29A, three contemporary aircraft, and several other airplanes.

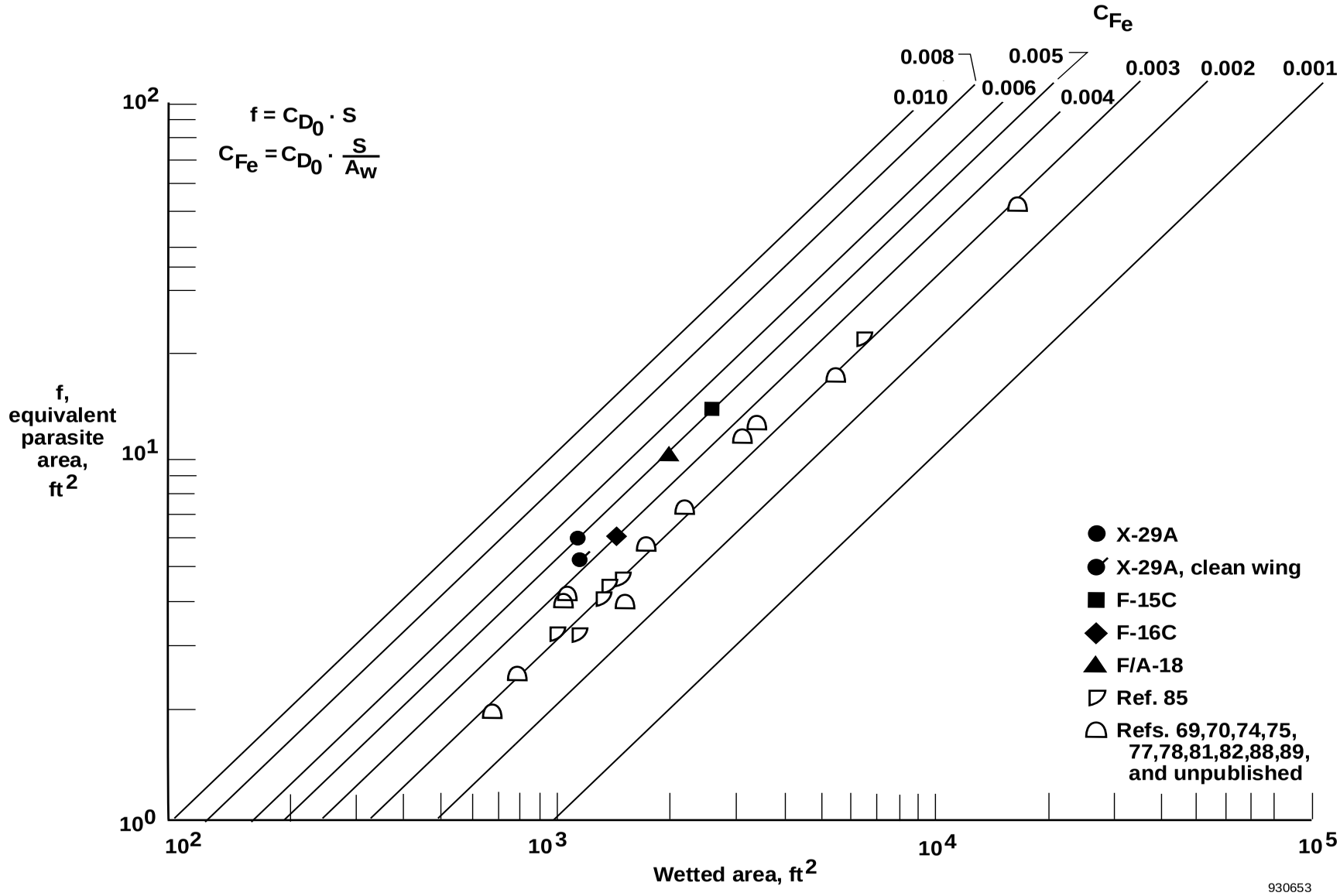

Figure 30. Relationship of equivalent parasite area and C_{f_e} to total wetted area for several aircraft at subsonic Mach numbers; flight data.

APPENDIX

COMMENTS ON PROCEDURES FOR DEFINING AIRCRAFT DRAG

Lift-Related Drag

The use of an inappropriate reference area has been shown to result in unreliable lift and drag coefficients, i.e., unreliable for comparison with force coefficients of other aircraft. Consequently, to make reliable comparisons of lifting efficiency between various aircraft, it is advisable to use the Oswald efficiency factor, *e*, or the lift-to-drag ratio to cancel the effects of a questionable reference area.

However, as has been noted, when the lift-drag polar is asymmetric another problem occurs. In the case of three of the aircraft considered here, the value of *e* became inflated if the polar asymmetry were ignored. On the other hand, when the asymmetry was accounted for, there was a residual increment of lift below $C_{L_{min}}$ that was not accredited to the airplane through the parameter *e*. It seems apparent, then, that when both polar asymmetry and an uncertain reference area are present, the lift-to-drag ratio, *L/D*, is the most definitive parameter for comparing the lift-related drag of various airplanes for a given flight condition. For a specific Mach number–altitude condition the lift-to-drag ratio of the aircraft to be compared should be plotted as a function of load factor rather than C_L or angle of attack. This is because making comparisons between contending aircraft at a common C_L or α does not ensure that all vehicles are performing the same task.

It is appropriate to consider figure 22 again, in which the assigned reference areas of the four aircraft can be compared with other probable lifting surfaces of each configuration, mostly upstream from the wing. For the X-29A the canard provides lift for some important flight conditions, and the other three airplanes each have the potential for generating lift from their chine or strake-like surfaces ahead of the wing. It is probable that future competing configurations will use refined versions of these upstream devices and other means (perhaps primarily at the wingtips) to enhance lifting efficiency. Therefore, uncertainties and disagreements on the *correct* way to define reference area will become even more commonplace. This discussion has been allotted appendix space to make clear the impact of the problem and to accredit a means of circumvention. Having emphasized the problem and offered a solution, mention of this will be added to the concluding remarks.

Another Approach to the Reference Area Problem for Lift-Related Drag

In the late 1970's Harold Walker began a comparative analysis of the performance of about 20 widely diverse aircraft configurations. Because the planforms were so varied, he too was confronted with the problem of defining an unambiguous basis (reference area) for his comparative analysis. Consequently, he studied theoretical works by R. T. Jones, M. Munk, and L. Prandtl (refs. 90–93) in search of a valid solution to his problem.

He concluded that theory, as developed in these and other works, supported wingspan squared as a logical reference area that would avoid ambiguity when comparing the aerodynamic performance of different aircraft. Reference 94 presents the careful development of his rationale in support of the span-squared method. References 6 and 60 also support the rationale for this method of comparative evaluation.

Subsonic and Transonic Drag at Zero Lift

The problem of inappropriate, or hard-to-define, reference areas also affects drag coefficients for nonlifting conditions. As is evident from the body of the text, other investigators, as well as the authors of this paper, recommend circumvention of the reference area problem for definition of drag coefficient at zero lift by using the less arbitrary areas for reference purposes as follows:

Subsonic C_{D_0}: use A_w as reference area and base comparisons on C_{F_e}; example,

$$C_{F_e} = C_{D_0} \cdot \frac{S}{A_w}$$

Transonic $C_{D_{wave}}$: base $C_{D_{wave}}$ on A_c; example,

$$C_{D_{wave}} = C_{D_0} \cdot \frac{S}{A_c}$$

REPORT DOCUMENTATION PAGE

Form Approved
OMB No. 0704-0188

1. AGENCY USE ONLY (Leave blank)	2. REPORT DATE	3. REPORT TYPE AND DATES COVERED
	December 1994	Technical Paper

4. TITLE AND SUBTITLE

In-Flight Lift-Drag Characteristics for a Forward-Swept-Wing Aircraft (and Comparisions With Contemporary Aircraft)

5. FUNDING NUMBERS

WU 505-68-50

6. AUTHOR(S)

Edwin J. Saltzman and John W. Hicks

7. PERFORMING ORGANIZATION NAME(S) AND ADDRESS(ES)

NASA Dryden Flight Research Center
P.O. Box 273
Edwards, California 93523-0273

8. PERFORMING ORGANIZATION REPORT NUMBER

H-1913

9. SPONSORING/MONOTORING AGENCY NAME(S) AND ADDRESS(ES)

National Aeronautics and Space Administration
Washington, DC 20546-0001

10. SPONSORING/MONITORING AGENCY REPORT NUMBER

NASA TP-3414

11. SUPPLEMENTARY NOTES

Sue Luke, editor

12a. DISTRIBUTION/AVAILABILITY STATEMENT

Unclassified—Unlimited
Subject Category 05, 02

12b. DISTRIBUTION CODE

13. ABSTRACT (Maximum 200 words)

Lift (L) and drag (D) characteristics have been obtained in flight for the X-29A airplane (a forward-swept-wing demonstrator) for Mach numbers (M) from 0.4 to 1.3. Most of the data were obtained near an altitude of 30,000 ft. A representative Reynolds number, for M = 0.9 and a pressure altitude of 30,000 ft, is 18.6×10^6 based on the mean aerodynamic chord. The X-29A data (forward-swept wing) are compared with three high-performance fighter aircraft—the F-15C, F-16C, and F/A18. The lifting efficiency of the X-29A, as defined by the Oswald lifting efficiency factor, e, is about average for a cantilevered monoplane for M = 0.6 and angles of attack up to those required for maximum L/D. At M = 0.6 the level of L/D and e, as a function of load factor, for the X-29A was about the same as for the contemporary aircraft. The X-29A and its contemporaries have high transonic wave drag and equivalent parasite area compared with aircraft of the 1940s through 1960s.

14. SUBJECT TERMS	15. NUMBER OF PAGES
Efficiency, Forward-swept wing, Lift-drag, Lift-related drag, Aerodynamic cleaners, Transonic wave drag	60
	16. PRICE CODE: A04

17. SECURITY CLASSIFICATION OF REPORT	18. SECURITY CLASSIFICATION OF THIS PAGE	19. SECURITY CLASSIFICATION OF ABSTRACT	20. LIMITATION OF ABSTRACT
Unclassified	Unclassified	Unclassified	Unlimited

NSN 7540-01-280-5500

Available from the NASA Center for AeroSpace Information, 800 Elkridge Landing Road, Linthicum Heights, MD 21090; (301)621-0390

Standard Form 298 (Rev. 2-89)
Prescribed by ANSI Std. Z39-18
298-102